Chem Soc Rev

Recent Advancements of Pt and Pt-free Catalysts for Oxygen Reduction Reaction

Journal:	*Chemical Society Reviews*
Manuscript ID:	CS-REV-12-2014-000484.R1
Article Type:	Review Article
Date Submitted by the Author:	14-Dec-2014
Complete List of Authors:	Nie, Yao; Chongqing university, chemistry Li, Li; Chongqing university, chemistry Wei, Zidong; Chongqing university, chemistry

Journal Name

RSCPublishing

ARTICLE

ngsCite this: DOI: 10.1039/x0xx00000x

Recent Advancements of Pt and Pt-free Catalysts for Oxygen Reduction Reaction

Yao Nie, Li Li* and Zidong Wei*

Received 00th January 2012,
Accepted 00th January 2012

DOI: 10.1039/x0xx00000x

www.rsc.org/

Developing highly efficient catalysts for the oxygen reduction reaction (ORR) is a key to the fabrication of commercially viable fuel cell devices and metal-air batteries for future energy applications. Herein, we review the most recent advances in the development of Pt-based and Pt-free materials in the field of fuel cell ORR catalysis. This review covers catalyst material selection, design, synthesis, and characterization, as well as theoretical understanding of the catalysis process and mechanisms. The integration of these catalysts into fuel cell operations, and the resulting performance/durability, are also discussed. Finally, we provide insights into the remaining challenges and directions for future perspectives and research.

1. Introduction

Today, we are facing a severe challenge-global warming and climate change due to depletion of the traditional fossil fuels. The greenhouse gas emissions are mainly derived from the transportation sector and electricity power generation. Therefore, a global solution must involve a dramatic move to practical and environmentally sustainable energy sources. High-capacity energy systems, such as fuel cells, metal-air batteries, are highly desirable to meet the urgent requirement of electric vehicles and utilization of sustainable energies.[1, 2] Oxygen reduction reaction (ORR) is of utmost importance in these advanced electrochemical energy conversion technologies.[3-5] Nevertheless, our ability to control the reduction of oxygen gas electrocatalytically is still limited due to the sluggish ORR kinetics caused by the difficulties in O_2 adsorption on electrode surface, O-O bond activation/cleavage and oxide removal. The sluggish kinetics of ORR, on the one hand, demands high loading of precious metal-containing catalysts (e.g., Pt), which unfavourably increases the cost of these electrochemical energy conversion devices. For example, according to a United States Department of Energy's (DOE) study in 2007, 56% of the cost in a fuel cell stack comes from the platinum-based catalyst layers based on a projected cost for large scale fuel cell production.[6, 7] Therefore the cost of fuel cell is directly linked to the price of Pt in the volatile and highly monopolized precious metal market. An increase in the demand for fuel cell power systems is bound to drive up the already high price of Pt. At this juncture, the catalytic efficiency of the ORR electrocatalysts is required to be substantially improved so that the dependency on noble Pt can be significantly weakened or fully eliminated. On the other hand, the poor long-term stability of standard and advanced ORR electrocatalysts under the corrosive operating conditions is remaining a major obstacle. Fuel-cell vehicles in the test fleets monitored by DOE

Yao Nie *received her BE from Chongqing University in 2012. Now she is a Ph.D. candidate in Chongqing University. Her current research interests lie in the development of (i) low Pt materials with rational modification and (ii) non-precious metal for ORR in fuel cell application.*

Li Li *obtained her MSc and PhD in 2004 and 2010 from Chongqing University, China. Currently, she is a Professor of Chongqing University. Her main interests are in fundamental studies of electrochemical and electrocatalytic processes through the theoretical investigations. She uses density functional theory to explore the relationships between the catalytic activity and electronic structure of the catalysts, and understand the mechanism of enhanced catalytic activity and stability for different kind of materials.*

have used 0.4mg of Pt per square centimetre ($mg_{Pt}cm^2$) or more on the cathode, and in these vehicles the stability of the catalyst has still been short of durability target for industrialization.[8] At this juncture, how to reduce costs by reducing cathode Pt loadings without loss of performance or durability is the crucial subject of most currently electrocatalyst research.

In order to tackle above issues, numerous studies have been dedicated to screening more efficient ORR electrocatalytic materials that do not contain platinum (Pt-free) or contain only tiny amounts of this noble metal (low-Pt). Significant progress in rational designing and synthesising excellent Pt-based or Pt-free catalysts has been achieved due to the development of material science and nanotechnology in the past decades.[9-12] When the size of the catalysts is reduced to the nanoscale dimension, attractive physical and chemical properties that are not observed in bulk state can emerge, which affords new exciting opportunities to develop low-cost processes and address critical issues in real-world applications. Moreover, by virtue of advanced in situ characterization techniques, new insights into the nature of the active sites have been proposed, [13, 14] making the mode of developing catalysts gradually shift from the traditionally empirical trial-and-error methods to precise design and fabrication at molecular or atomic levels. In the case of developing superior ORR electrocatalysts, improved catalytic performance can be achieved by manipulating the atomic structure, especially the surface electronic structure of the catalysts based on the understanding of the ORR catalytic mechanism, which has proven to be the most crucial design principle. Many excellent reviews in fields of the design and synthesis of either Pt-based or non-Pt nanocatalysts for ORR have recently been published by several groups.[15-22] Most of these publications focused on discussing different approaches and strategies for preparation of a specific class of ORR catalysts (e.g., Pt-based core-shell catalysts, nanostructured Pt-alloy electrocatalysts and doped-carbon materials). In view of the rapid development of both Pt-based and Pt-free catalysts, there is a great need to provide timely updates of this field with emphasis on the new design concepts and significant breakthroughs of ORR catalysts covering Pt-based and Pt-free aspects.

In this paper, we provide an overview of the latest advances of efficient Pt-based and Pt-free catalysts for ORR at fuel cell cathodes rooting from the origin of their catalytic mechanisms. Current improved understanding of the mechanisms of ORR catalysts will be firstly introduced. Then, new understandings and developments in the synthesis and design of Pt-based catalysts are summarized. The insights into the structure and property relationship including facets/ geometric architectures/compositional profile effects and support effect on ORR performance will be highlighted to illustrate the origins and potentials of current developed Pt-based catalysts for practical applications. Next, the review will introduce the exciting new research push in developing Pt-free catalysts, especially centring on current tremendous progress in catalyst synthesis methodologies and the understanding of the mechanism of nitrogen-doped carbon (with or without transition metals) materials. The review will be concluded by providing the insights into the remaining challenges and research directions in order to shed light on the future development of ORR catalysts.

2. The Mechanisms for ORR

An atomic-level understanding of the ORR mechanism is still in its early stages because of the high complexity of ORR kinetics. What is known, however, is that the complete electrochemical ORR involves four net coupled proton and electron transfers (CPETs) to molecular oxygen at the cathode. There are several pathways for O_2 electroreduction:

(i) a "direct" four-electron reduction to H_2O (in acid media) or to OH- (in alkaline media);

(ii) a two-electron pathway involves reduction to hydrogen peroxide;

(iii) a "series" pathway with two- and four-electron reduction;

(iv) a "parallel" pathway that is a combination of (i)-(iii);

(v) an "interactive" pathway includes the diffusion of species from a "series" path into a "direct" path is possible.

(vi) an associative mechanism involves the adsorption of molecular O_2 and direct proton/electron transfer to it and to OOH, which breaks into O and OH.

(vii) a dissociative mechanism involves the splitting of the O-O bond in O_2 and the hydrogenation of atomic O to OH and to H_2O.

For transition metal catalysts, two-electron reduction was reported for less active metals such as Au and Hg. For the most active catalyst, Pt, four-electron reduction is generally believed. Based on above possible pathways, many researchers dedicated to find the rate determining step (RDS), and understand the sequence of electron transfer and proton transfer. Generally, the kinetic of ORR on metal catalysts is mainly obstructed by three steps: (1) the first electron transfer of ORR; (2) the hydration of oxygen; and (3) the desorption of the intermediates.

Numerous references mentioned that the first electron transfer is the RDS of ORR.[23-27] For example, Anderson's team calculated the activation energies of the elemental steps of ORR using reaction centre models and self-consistent ab initio calculations. They found that on Pt catalysts, the first electron transfer step has highest barrier; and proton transfer is involved in the RDS. Other researchers also obtained the same conclusion by different approaches in investigating the first electron transfer step.[28,29] However, Janik and Taylor et al. proposed a different opinion on the sequence of the electron and the proton transfer.[30-32]They indicated that the first electron transfer precedes the protonation of the adsorbed O_2 molecule, occurring with the proton formally residing as an H_3O^+ species

Zidong Wei *received his PhD from the Tianjin University in 1994. Currently, he is a full professor in Chongqing University. His research interests include electrocatalysis, computational study, electrochemical material and their applications in catalysis and energy storage. He has published over 160 papers with about 120 papers in peer-reviewed journals. He serves as the editorial board membership of more than 5 international journals. His works have been cited over 3000 times. He has been granted 26 patents associated with catalysis. He has served as an Editorial Board Member of 6 International and China-based journals.*

connected to the adsorbed O_2 molecule by hydrogen bonding through two additional water molecules.
Differently, Goddard indicated that the O_{ads} (adsorbed oxygen) hydration has highest barrier energy in spite in gas or solution through calculating the reaction pathways and barriers for the ORR on platinum in gas phase and in solution.[33]According to their results, it can be proposed that decreasing the barrier for O_{ads} hydration while providing hydrophobic conditions for the OH and H_2O formation steps could improve the efficiency of ORR catalysts.

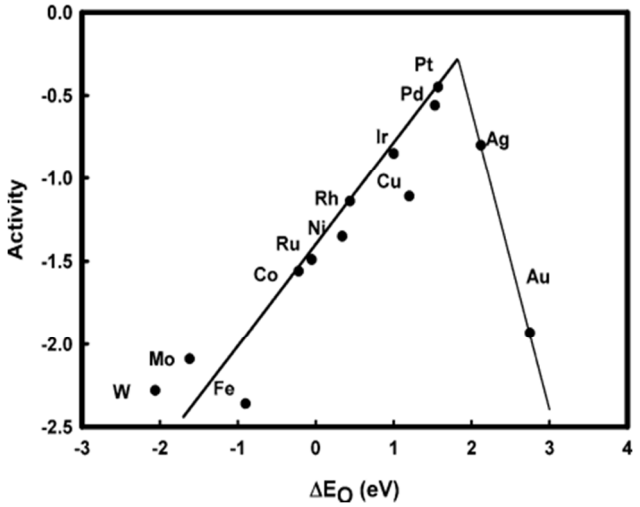

Figure 1. Trends in oxygen reduction activity (defined in the text) plotted as a function of the oxygen binding energy. Reprinted with permission from ref.34.Copyright © 2004, American Chemical Society.

Recently, it is widely accepted that the adsorption of intermediate species such as O, OH might be the crucial step of ORR on metal catalysts, as proposed by Nørskov et al.[34-36] Nørskov et al. introduced a method for calculating the free energy of all intermediates as a function of the electrode potential directly from density functional theory (DFT) calculations of adsorption energy for the surface intermediates of ORR. They showed that for Pt (111) as electrode adsorbed oxygen tends to be so stable at high potentials that the proton and electron transfer becomes impossible. By lowering the potential, the stability of the adsorbed oxygen decreases and the reaction may proceed. This is suggested to be the origin of the overpotential for Pt. They also made DFT calculations to get the bond energies of oxygen and hydroxyl for a number of interesting metals, as shown in Figure 1.[34] A nice volcano appeared and it showed that Pt and Pd are the best catalysts for ORR. For metals that bind oxygen too strongly, the rate is limited by the removal of adsorbed O and OH species. For metal surface that bind oxygen too weakly, the rate is limited by the dissociation of O_2, or more likely, the transfer of electrons and proton to adsorbed O_2. The volcano plot in Figure 1 indicates that there was some room for improvement. Metals with a somewhat lower oxygen binding energy than Pt should have a higher rate of ORR. A better electrocatalyst for the ORR should bind oxygen more weakly than Pt does by about 0.2eV. Based on previous thermodynamic activity volcano relationship, Nørskov et al. further developed a microkinetic model for ORR by calculating the activity on materials with a varying OH binding energy.[37,38]They found that the existence of a kinetic activity volcano which is in close agreement with the thermodynamic activity volcano derived earlier. For the reduction of O_2 to H_2O through a 4e- pathway, they identified an activity optimum at 0.1eV weaker OH binding than Pt (111). While the reduction of O_2 to H_2O_2 through a $2e^-$ pathway, they showed a similar correspondence between the thermodynamic and kinetic activity volcano with the activity optimum around 0.3eV weaker OH binding than Pt (111).
Furthermore, Nørskov et al. established the linear relationship between the oxygen-metal bond interactions with the position of the metal d states relative to the Fermi level, which called d-band centre. [34,35]The origin of this relationship is as follows: the variation in the oxygen-metal bond from one transition-metal surface to the next depends to a large extent on the strength of the coupling between the oxygen 2p states and the metal d states. In general, an upward shift of the d states relative to the Fermi level must therefore results in an upward shift of the anti-bonding states, leading to less filling and thus leading to a stronger bond. Then, they constructed a direct interaction between the catalytic activity and the electronic structure of metal catalyst. Therefore, it has become easier to screen new catalysts for the ORR, by looking for surfaces with a down shift of the Pt d-band centre relative to the Fermi level, such as alloying, varying the surface metal, modulating the alloy structure.[39-41]The approaches to tune the d-band centre or surface electronic structures of Pt are discussed in detail later on.
Developing non-precious metal-based ORR electrocatalyst has been stimulated extensively by the recent push for the commercialization of various energy conversion systems. One of the most promising non-precious metal electrocatalysts for ORR is transition metal-nitrogen-carbon (M-N-C) materials (M=Co, Fe, Ni, Mn, etc.), which have gained increasing attention due to their promising catalytic activity displayed towards the ORR, along with the utilization of abundant, inexpensive precursor materials. Since Jasinski and coworkers found that metal phthalocyanines featuring a metal-N_4 center are able to catalyze ORR under acidic conditions,[42] recent years have seen encouraging progress to immobilize the metal-N complex (mainly Fe-N) and also to improve its catalytic performance. Due to the complex nature of the catalysts, the atomic structure of the active site and the catalytic mechanism of these M-N-C catalysts remain largely elusive. The likely active-site structures have been summarized by Dodelet in a 2006 review of non-precious group metal catalyst litereature.[43] The sites include the following most frequently considered ones: (i) M-N_4 site,[44] since the metal macrocycles such as porphyrin and phthalocyanine are catalytically active for ORR, their basic structural motif, i.e. M-N_4, has been regarded to be the active centre in the heterogeneous environment; (ii) M-Nx sites, which was first proposed by Yeager and co-workers [45,46]and further developed by the Dodelet group and others;[43](iii) metal-free carbon structure, as originally proposed by Wiesener (with metal merely serving as a catalyst for the ORR active-site formation).[47]
In the case of Fe-based M-N-C catalysts, Dodelet et al. using Time of Flight Secondary Ion Mass Spectrometry detected FeN_4 species in the catalyst prepared using Fe acetate, Fe porphyrin and NH_3 as the precursor.[48] Several Fe-Nx species have also been proposed by Dodelet and Kramm, as shown in Figure 2.[49] Among these Fe-Nx species, only FeN_4/C sites and N-FeN_{2+2} /C sites were active for ORR.[49,50] Kramm et al.

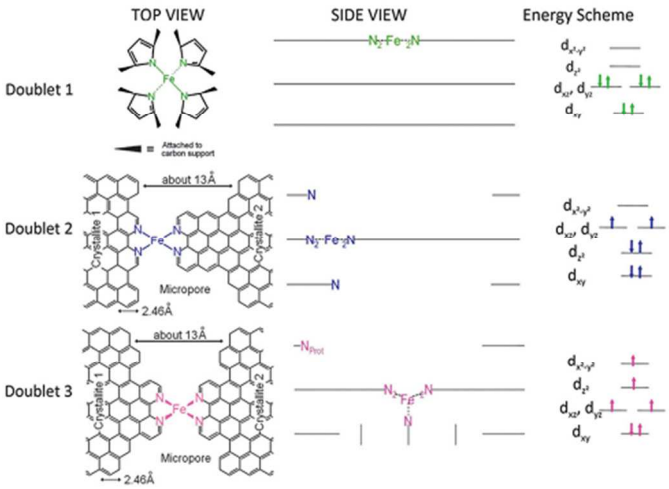

Figure 2. Side views and top views of the proposed structures of Fe-N_x species: (Doublet 1): the FeN_4/C catalytic site in heat-treated, macrocycle-based catalysts. (Doublet 2): the FeN_{2+2}-like micropore-hosted site found in the catalyst prepared with iron acetate and heat-treated in ammonia. The distance between the two nitrogen atoms belonging to the graphene planes above and below the FeN_{2+2}-plane is similar to that in crystaline iron phthalocyanine. (Doublet 3): the N-FeN_{2+2}-like composite site. The iron (II) ion in N-FeN_{2+2} is coordinated by five pyridinic nitrogen atoms, one of them belonging to a plane located at the vertical below the N_4-plane. This axial nitrogen coordination moves the iron (II) ion out of the N_4-plane towards the fifth coordinating nitrogen atom. Doublet 3 may exist as N–FeN_{2+2}/C or as a composite site N–FeN_{2+2}…N_{prot}/C, where N_{prot} is a protonable pyridinic nitrogen atom appearing at the edge of the upper plane in the side view of Doublet 3. In all side views, graphene planes are drawn as lines. Reprinted with permission from ref. 49.Copyright © 2012, Royal Society of Chemistry.

attributed the improved ORR kinetics of these Fe-N_4 centres to Fe-ion centres with higher electron densities.[51]Koslowski related the current density of ORR to the amount of in-plane FeN_4 centres using Mössbauer spectra and a linear correlation was identified.[52] Wang et al. calculated the adsorption energy of ORR species and the energetics (heats of reaction and activation energies) of all of the possible ORR elementary reactions on the modeled FeN_4 embedded grapheme to investigate the reaction pathways for ORR on this catalyst.[53] By using first-principles DFT calculations, they indicated that the O_2 molecule is only chemisorbed to the central transition metal Fe of the FeN_4 complex embedded in the graphene layer, implying that the existence of an N-chelated transition metal plays a pivotal role to initializing the ORR in this class of catalysts. The FeN_4 embedded graphene could promote a four-electron ORR via an OOH dissociation pathway and with catalytic activity for ORR comparable to (may even higher) that of Pt catalysts. They also showed that the rate-determining step on the modelled FeN_4 embedded grapheme is the O_2 dissociation reaction.

The presence of Co-Nx/C sites was also observed. Experimental studies on Co-based pyrolyzed porphyrins electrocatalysts in acidic medium showed that Co-N_4 centres promote a complete $4e^-$ reduction of O_2 to H_2O and Co-N_2 centres are responsible for the formation of H_2O_2 intermediate.[54] Later RRDE measurements on pyrolyzed Co-polypyrrole and Co-porphyrins derived electrocatalysts showed that Co-N_4 centres are responsible for the reduction of O_2 to peroxide and peroxide is further reduced on Co_xO_y/Co particles in both acidic and alkaline media supporting a dual site $2 \times 2e^-$ ORR mechanisms.[55, 56] However, the location of the Co-N_2 type site is ambiguous since it can be either graphitic or located at the edges of the carbon support. Previous computations have found weak binding of Co to graphite edge N atoms (which form a Co-N_2 edge defect) suggesting that Co will easily dissolve from the support.[57] This indicated that in the presence of Co the ORR activity was likely dominated by graphitic Co-Nx defects. A recent combined experimental and computational study on molecular Co-phthalocyanine carbon supported electrocatalysts (Co-N_4 active site) in alkaline medium has reported that peroxide is the main ORR product.[58] But, it remains unclear if these conclusions can be transferred directly to pyrolyzed Co-Nx/C electrocatalysts where the active sites are embedded in a carbon matrix.

Newly emerging evidence suggests that the metal-N_4 might not be exactly the active site: the chemical environment around this centre could also affect significantly the ORR activity. It was demonstrated that the presence of the porosity in the pristine carbon black during the pyrolysis (e.g. using disordered carbon) is important for achieving high catalytic activity.[59] This implies that the active site forms at/near the micropores of the nitrogenised graphite. Instead of the four-coordinated Fe centre, the five-coordinated Fe centre was also suggested by Jain et al.,[60] the structure of which mimics the Fe-porphyrin complex in biological systems for O_2 activation.[61,62]

Many other authors proposed a different opinion regarding the possible role of the transition metal towards the ORR active site. Instead of being a part of the active site structure, the metal-ion centres merely catalyze the formation of various nitrogen sites (e.g. pyridinic-N, pyrrolic-N).[63-65] Specifically, the ORR activity is attributed to the formation of graphitic nitrogen and/or pyridinic nitrogen functional groups, or the degree of edge plane exposure the latter represents. This further complicates the understanding of the exact nature of the catalytically active moieties with respect to ORR. Insight into active site formation mechanisms and structures of M-N-C catalysts is still insufficient at the current technology state. Further investigations of the exact ORR active site as well as the structures of the active site of M-N-C materials are required in order to boost the ORR performance of this group of catalyst.

Recently, the carbon-based materials with abundant free-flowing π-electrons and large surface area such as carbon nanotubes (CNT), nanofibers, and grapheme have received attention as alternative metal-free catalyst materials to platinum. However, these π-electrons are too inert to be used directly in the ORR. For N-doped electron-rich carbon nanostructures, carbon π-electrons have been shown to be activated through conjugation with lone-pair electrons from N dopants; thus, O_2 molecules are reduced on the positively charged C atoms that neighbour N atoms.[66-68] Generally, the carbon atoms that possess highest spine density are the electrocatalytic active sites.[69] If the negative value of spin density is small, the carbon atoms with large positive atomic charge may act as the active sites too. It was also found that, as long as the electroneutrality and the spine density of sp^2 carbon is broken, and charged and highest spin sites that favour O_2 adsorption are created, sp^2 carbon will be transformed into active metal-free ORR electrocatalysts regardless of whether the dopants are electron-rich (e.g., N) or electron-deficient (e.g., B).

For N-doped carbon materials, an ORR mechanism in acidic environment was proposed for carbon atoms adjacent to pyridinic N sites, on the basis of the reaction energies of every reaction step estimated by DFT calculations.[69] In this model, oxygen is assumed to adsorb through the end-on mode. [(1) and (2) are two different, neighbouring carbon atoms].

$O_2 + H^+ + e^- \rightarrow$ *OOH

*OOH + $H^+ + e^- \rightarrow$ *OH(1) + *OH(2)

*OH(1) + $H^+ + e^- \rightarrow H_2O$

*OH(2) + $H^+ + e^- \rightarrow H_2O$

When the second H atom is introduced into the system, the distance between the O atoms increased to 2.9Å, implying that the O-O bond would break. The four-electron pathway towards water with little or no hydrogen peroxide production will thus be followed for this type of active sites.[69]

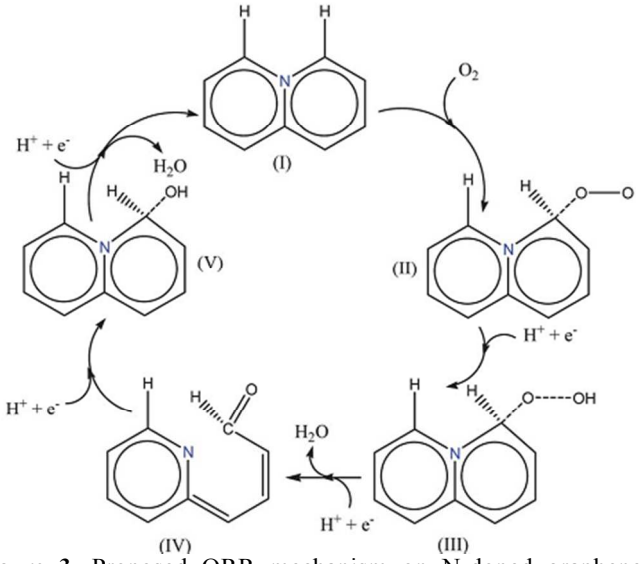

Figure 3. Proposed ORR mechanism on N-doped graphene nanoribbons. Reprinted with permission from ref.70. Copyright © 2011, Royal Society of Chemistry.

In another theoretical work based on DFT calculations, the most likely active site of N-doped graphene was proposed based on the adsorption energy of oxygen on carbon atoms and on the energy barrier for the first electron transfer, which was assumed to be the rate determining step of the ORR.[70]Carbon atoms located at a site on the edge and next to a valley graphitic N atom showed the lowest energy barrier for the first electron transfer, together with a low (though not the lowest) end-on oxygen adsorption energy. An ORR mechanism was then proposed based on the reaction energies of the various steps (Figure 3). Similarly, the four-electron pathway would be followed. When H_2O is released, the remaining adsorbed oxygen atom will cause the C-N bond to be cleaved (experimentally observed) producing a stable CHO group and a pyridinic N species. This mechanism thus suggests that both the graphitic and the pyridinic N configuration are important species for the four-electron reduction of oxygen to water.

Both of these proposals were made under the assumption that the ORR occurs under acidic conditions. A better (in situ) characterization and understanding of the reaction mechanism of these materials in alkaline conditions are the prerequisites for further development since it is known that N-doped carbon electro-catalysts perform better in alkaline medium.

3. Pt -Based Catalysts

Currently, platinum nanoparticles are the most used cathode electrode materials to catalyze the sluggish ORR.[71] However, the sky-rocketing price and scarcity of Pt are key obstacles for its broad deployment in all commercial technologies based on this precious metal.[72] In a sense, Pt should be considered as an industrial metal more than a precious one. Since most of its demand comes from auto-catalyst makers, its price has a direct correlation with economic expansion. To weaken its correlation with economic expansion, many efforts have been directed to developing the Pt-based catalysts with less precious metal loading and cost while preserving or achieving higher activity and durability during prolonged exposure to reaction conditions. It is widely believed that rational optimizing the intrinsic reactivity of Pt-involved active sites and maximizing their utilization based on the understanding of mechanism of ORR are crucial to develop effective Pt-based catalysts for ORR. ORR is very sensitive to the surface electronic properties and electronic surface atomic arrangement or coordination of the catalyst. Hence, engineering the surface properties, including the surface electronic structure and atomic arrangement of the catalysts, is believed to effectively tune catalytic properties of Pt catalyst, enabling enhancement in both activity and durability. Accordingly, altered electronic properties induce a change in adsorption behavior, specifically a shift of surface-oxide formation to higher potentials.[73] This adsorption behaviour is believed to be the origin of the high activity for ORR.[74] In general, there are four routes to manipulate the surface structure properties of Pt: (i) controlling the exposed facet (or the shape) of Pt nanocrystals and thus maximizing expression of the facets most active towards ORR. (ii) combining Pt with another metal to generate multimetallic nanocrystals with structures in the form of alloys, core-shells, branches or anisotropies. This strategy is attractive and practical because a bimetallic system is expected to display not only a combination of the properties associated with each distinct metal, but also new or unexplored properties due to a possible synergistic effect between each metal.[75,76] Furthermore, the reasonable selection of the alloy metals and the precise control of the size, compositional profile and inner structures of this Pt-based system can boost the final performance. (iii) modifying Pt nanoparticle surfaces with elaborately selected foreign species, such as metal clusters, molecules, ions, organic or inorganic compounds. Apart from improving the activity or stability of the resulting catalyst, this strategy, in some case, can also render catalysts with specific properties (e.g., hydrophilicity and electronic property) that are beneficial to their operation in ORR system due to the participation of the functional modification species. (iv) choosing an appropriate catalyst support with high corrosion resistance and with strong interactions with the supported metallic catalyst. It is also recognized that the selection of a robust non-carbon support can improve durability of the catalysts and, in some cases, introduce a synergistic cocatalytic effect between Pt-based nanoparticles and the support via support-metal interaction.[77-80] According to the discussion above, the recent development of Pt-based catalyst will be reviewed in this section.

3.1 Facet-Controlled Catalyst

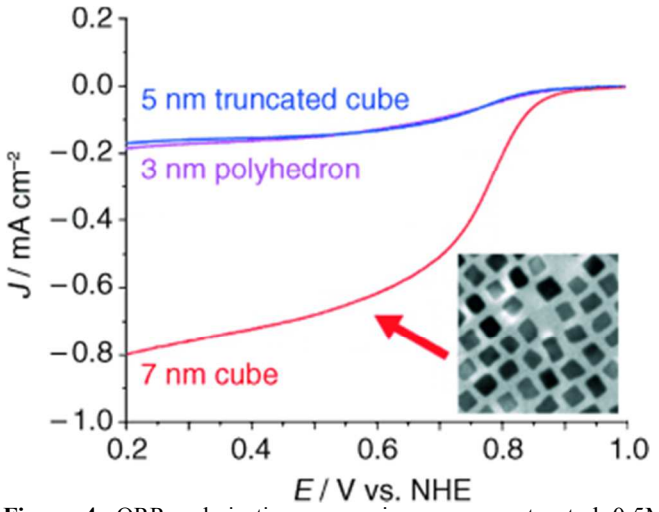

Figure 4. ORR polarization curves in oxygen saturated 0.5M H_2SO_4 as a function of potential for different Pt catalysts at the rotation speed of 1600 rpm. Reprinted with permission from ref. 94. Copyright © 2008 WILEY-VCH Verlag GmbH & Co. KGaA, Weinheim.

The facet-controlled synthesis of metal nanocrystals has received extensive attention owing to its fascinating role in tuning the catalytic performance of the nanocrystals.[81] Studies of single-crystal Pt electrodes revealed that the ORR activity varies at different crystal facets.[82-88] Structure sensitivity of ORR on the Pt low-index single-crystal surfaces in perchloric acid has been well established. In nonadsorbing $HClO_4$ electrolytes, single-crystal Pt (110), (111), and (100) surfaces were observed to have the activity for ORR following a descending order. [82] However, if H_2SO_4 was being used as an electrolyte, Pt {100} presented a higher ORR activity than Pt {111}.[89-91]This was mainly due to the adsorption and inhibiting effects of the bisulfate anion. The systematic investigations of the adsorption of bisulfate anions showed that bisulphate coverage on a Pt (100) electrode was less than one-third of the coverage on a Pt (111) electrode in the same concentration of sulfuric acid solution. Pt (111) could adsorb bisulfate anions much more strongly and in a wider potential range than Pt (100), due to the different properties of their respective facets. Following this work, it was further confirmed that a catalytic performance is dependent on the surface atom arrangement, that is, morphologic characteristics. Therefore, "transfer" the active catalytic surface from a single crystal to more practical nanophase by establishing a shape-control synthesis strategy is a promising route to boost Pt acticity towards ORR. Early research led by El-Sayed et al. shed light on promising directions in shape-controlled synthesis of single Pt nanocrystals, including {111}-bounded nanotetrahedra, {100}-terminated nanocubes, and "near spherical" nanocrystals containing a mixture of {111} and {100} facets.[92] Sun et al. reported a simple high-temperature organic phase synthesis of monodisperse {100}-terminated Pt nanocubes and studied their catalysis for oxygen reduction in H_2SO_4 electrolytes.[93] Electrochemical studies showed that the Pt nanocubes catalyzed oxygen reduction in a 1.5M H_2SO_4 aqueous solution with specific activity over 2-fold higher than that from the commercial Pt catalyst. Sun et al. also reported that in catalyzing ORR in H_2SO_4, the 7nm {100}-terminated Pt nanocubes were shown to be much more active than other shaped Pt NPs,[94]demonstrating that the shape-dependent ORR activity of Pt nanparticles was due to the different adsorptions of sulphate ions on Pt (111) and (100) facets as observed on single-crystal Ptn electrodes. As shown in Figure 4, the onset potential gain for 7 nm Pt nanocubes was nearly 50mV when compared to the rest of Pt NPs, and at half-wave potential (0.8 V), the current density generated from the 7 nm Pt NPs was about four times that of either the 3 or 5 nm.

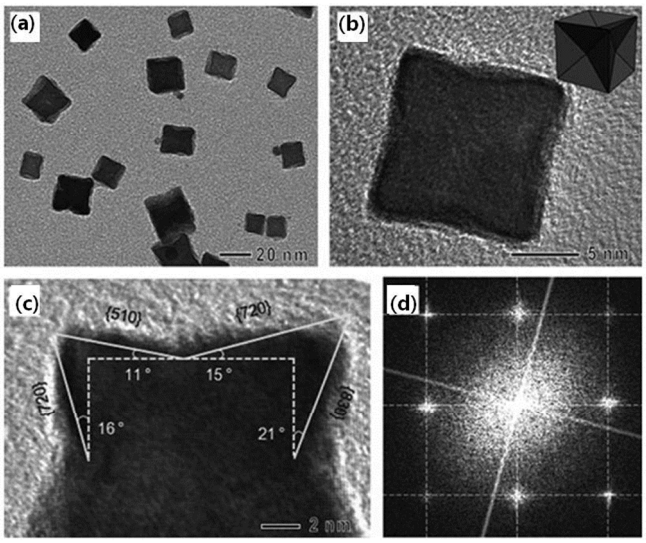

Figure 5. (a) TEM and (b), (c) HRTEM images of Pt concave nanocubes. d) FT pattern of the concave nanocube shown in (c) recorded along the [001] zone axis. Reprinted with permission from ref. 97. Copyright © 2011 WILEY-VCH Verlag GmbH & Co. KGaA, Weinheim.

Because of the high density of atomic steps, ledges, and kinks , high-index facets of face-cantered-cubic (fcc) metals with a generally exhibit significantly enhanced catalytic activity toward specific reactions as compared to the most common stable low-index planes.[95,96]Study of Pt was extended to the high index planes by Feliu et al.[83,84] Sun and co-workers have reported the synthesis of tetrahexahedral (THH) Pt nanocrystals with high-index facets, such as {730}, {210}, and {520}, by applying a square-wave potential to polycrystalline Pt microspheres supported on a glassy carbon electrode.[81] Xia et al. have demonstrated the synthesis of Pt concave nanocubes enclosed by high-index facets including {510}, {720}, and {830} by using a simple route based on reduction in an aqueous solution (Figure 5).[97] The Pt concave nanocubes exhibited substantially enhanced electrocatalytic activity per unit surface area towards ORR compared with those of Pt cubes, cuboctahedra, and commercial Pt/C catalysts that are bounded by low-index planes such as {100} and {111}. However, the mass activity of Pt concave cubes was still less than that of the Pt/C catalyst, presumably owing to their smaller ECSAs per unit weight of Pt associated with the relatively larger particle size.

Although these Pt nanocrystals have been shown to have high catalytic activity, detailed mechanisms for the enhanced performance from high-index plane are nevertheless still not clear. It is also recognised that the mass activity of such nanoparticles is lower than other highly active ORR catalysts, because the Pt nanocrystals with full-grown high-index planes tend to be quite large in size. Moreover, the surface structure of these well-faceted nanocrystals would be unstable during fuel

cell operations, especially those with high-index planes and unsaturated atomic steps, edges and kinks, all of which are active sites for crystal growth. Due to the morphological changes that Pt nanoparticles undergo during fuel cell operation, these facets may easily be deactivated, resulting in degradation of their catalytic activity and thus limiting their capability in practical application.

3.2 Multimetallic Nanocrystals with Structures in the Form of Alloys, Core-Shells, Branches or Anisotropies

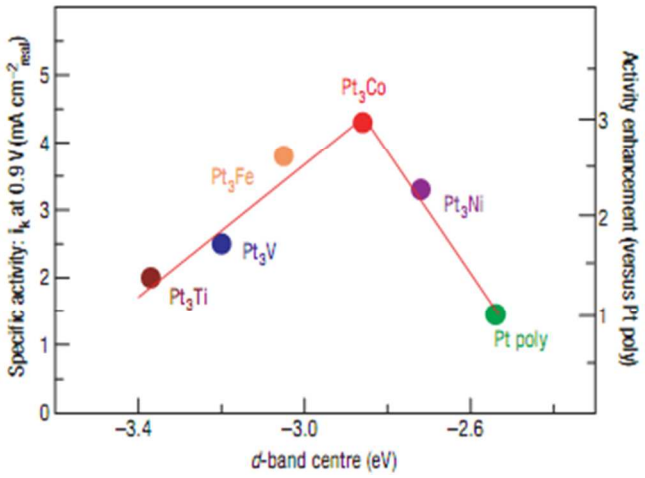

Figure 6. Relationships between experimentally measured specific activity for the ORR on Pt_3M surfaces in 0.1M $HClO_4$ at 333 K versus the d-band centre position. Reprinted with permission from ref. 124. Copyright © 2007, Rights Managed by Nature Publishing Group.

3.2.1 Pt Alloys Alloy catalysts with a lower content of expensive Pt metal can not only inherit the properties of the Pt constituent but also usually show a superior performance when compared with monometallic Pt. [98,99] In past years, many Pt-based alloy systems with a wide range of compositions, such as PtPd, PtAu, PtAg, PtCu, PtFe, PtNi, PtCo and PtW, have been studied and accordingly improved ORR activities of these alloy systems have been reported.[100-114] It was believed that the observed activity enhancement in the Pt alloy catalysts is mainly due to the modification to the surface electronic structure of Pt. Although it does not always describe the electronic structures precisely, DFT calculation provides important clues for the requirement of surface structures for enhanced performance in ORR. DFT works have shown that modified chemisorption properties for adsorbed oxygen species on a Pt alloy surface are largely caused by short-range electronic charge-transfer effects (ligand effects) and long-range geometric lattice strain (geometric effects). [115-118] These electronic and geometric effects result in a shift of the energetic centre of Pt-projected d-states affecting surface adsorbate bond strengths and thus lead to altered chemisorption of reactants, intermediates, and products. [35, 119-123] Stamenkovic and his co-workers studied polycrystalline alloy films of Pt_3M catalysts (M: Ni, Co, Fe, and Ti) to understand the role of 3d metals in the electrocatalytic ORR activity of Pt-alloys.[27]They found that the catalytic activity for the ORR on such alloys was dependent on the nature of the 3d metal. They also showed a fundamental relationship in electrocatalytic trends on Pt_3M (M: Ni, Co, Fe, Ti, V) surfaces between the experimentally determined surface electronic structure (the d-band centre) and activity for ORR,[124] as shown in Figure 6. This relationship exhibited a 'volcano-type' behaviour, where the maximum catalytic activity was governed by a balance between adsorption energies of reactive intermediates and surface coverage by spectator (blocking) species. A better ORR electrocatalyst should bind oxygen molecules more weakly than does Pt, to increase the removal rate of oxygen-containing intermediates, and the optimal ORR reactivity is depicted by weakness of the binding energy of oxygen-containing species of around 0.2eV compared to that of pure Pt.[34-36] In this aspect, Ni, Co, and Fe were found to be most effective alloying elements.[35,124]This electrocatalytic trends established for extended surfaces can be used to explain the activity pattern of Pt_3M catalysts as well as to provide an important guidance for researchers in choosing the most suitable alloy component to modulate the surface chemisorption property of Pt. By combining simulations with experiments in the quest for surfaces with desired activity, an advanced concept in nanoscale catalyst engineering was then developed. Stamenkovic et al. prepared homogeneous Pt_3M (where M=Fe, Ni, or Co) nanocatalysts with controllable particle size and composition by an organic solvothermal method and then supported on high surface area carbon to investigate their ORR performance(Figure 7a-c).[125] As shown in Figure 7h, the Pt_3M catalysts showed improvement factors of ~2-3 in specific activity versus Pt catalyst at 0.9V. Among the alloy catalysts, Pt_3Co/C had the highest activity, reaching 3.2mAcm^{-2}, versus 3.0 and 2.3mAcm^{-2} for Pt_3Ni and Pt_3Fe, respectively. The above volcano-type dependence of catalytic performance on the type of 3d transition metal was revealed in both specific activity and mass

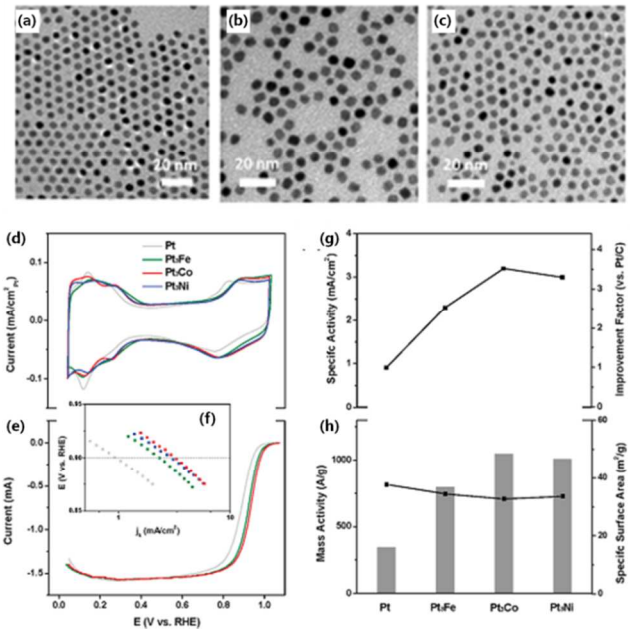

Figure 7. TEM images of the as-synthesized 5nm (a) Pt_3Fe, (b) Pt_3Co, and (c) Pt_3Ni NPs. Electrocatalytic results of the Pt_3M/carbon catalysts for the ORR. (d) CVs recorded at 50mV/s in Ar saturated 0.1M $HClO_4$ at 60ºC. (e) Polarization curves recorded at 20mV/s in O_2-saturated 0.1M $HClO_4$. (f) Tafel plots of the kinetic current densities depending on electrode potentials (RHE, reversible hydrogen electrode). (g) The dependence of specific activity, and (h) mass activity (columns, left axis) and specific surface area (filled squares, right axis) on the types of alloys. The electrocatalytic results were obtained by average of three independent measurements with an error margin of <10%. Reprinted with permission from ref.125.Copyright © 2011, American Chemical Society.

activity (Figure 7g, h). These findings undoubtedly confirmed that the highly homogeneous character of the nanoscale materials synthesized here was in line with their solid-solution nature and catalytic behaviour of corresponding well-defined extended surfaces. In contrast to the mainly reported Pt alloy ORR electrocatalysts which mostly have to be Pt-rich in total composition (Pt_3M), Chen et al .used first-principle theoretical calculations and experimental measurements to demonstrate that the strong surface segregation tendency of Pt in Pt-W alloys and the peculiar electronic effect of 5d transition metal W to Pt allow facile formation of stable Pt-enriched surfaces with likely better-than-Pt ORR activity at Pt-lean alloys such as PtW_2.[102] The prepared PtW_2 alloy catalysts exhibited a Pt mass activity nearly 4 times higher than the pure Pt catalysts and almost no changes in the activity and surface area in over 30,000 cycles of potential cycling under oxidizing conditions of ORR, in contrast to significant losses seen with the pure Pt catalyst (Figure 8). Significant progress has been made in preparation technologies for a wide range of Pt-M (M=ad-metal) alloy nanoparticles with controllable compositions and sizes.[101, 103, 125-132] These alloy nanoparticles are now routinely prepared either by decomposition/reduction of metal carbonyls and metal salts, or by coreduction of two metal salts.[133-143] Although the nearly precise control have been achieved on nanoparticle sizes and compositions, each of these previous syntheses is specific for one typical kind of Pt-M nanoparticles. Therefore, it is important to have a generalized synthetic process so that each kind of Pt-M nanoparticles can be prepared in a very similar reaction condition and their catalytic properties can be better controlled and compared. Sun et al. reported a simple, yet general, approach to monodisperse Pt-M (M: Fe, Co, Ni, Cu, Zn) nanoparticles by coreduction of $M(acac)_2$ and $Pt(acac)_2$ (acac: acetylacetonate) with oleylamine at 300 °C.[144] This general method will enable the detailed investigation of Pt-based alloy NPs for ORR catalytic applications.

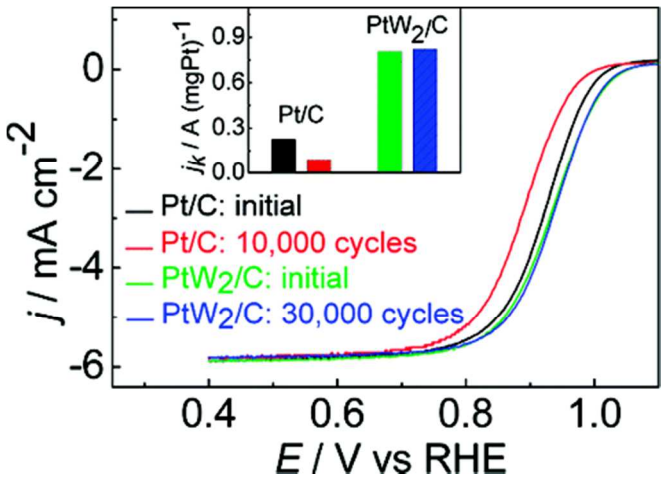

Figure 8. ORR polarization curves before and after 30,000 cycles of potential cycling for Pt/C and PtW_2/C catalysts in O_2-saturated 0.1 M $HClO_4$ at 1600 rpm. Reprinted with permission from ref.102.Copyright © 2011, American Chemical Society

Despite these recent achievements in both understanding of the enhancement mechanism and preparation technologies of Pt-based alloys, the realization of Pt alloy electrocatalysts that maintain their initial Pt mass based activity has remained a major barrier. A key reason for their activity degradation is the continuous leaching of the less-noble-metals during long-term stability test in acidic environment.[145-149] A clear understanding and a path forward to

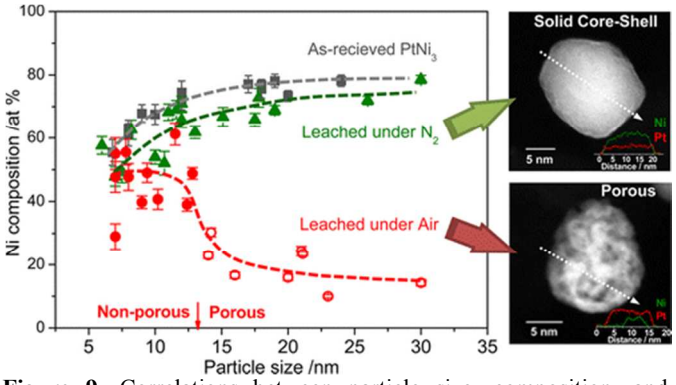

Figure 9. Correlations between particle size, composition, and porosity in the three catalysts ($PtNi_3$, $PtNi_3$ leached under N_2, $PtNi_3$ leached under air), where the horizontal dot lines represent the average compositions. Reprinted with permission from ref.160.Copyright © 2013, American Chemical Society.

suppress and control metal leaching are therefore believed to be critical to achieve high catalytic stability. Advanced electron microscopic and spectroscopic studies revealed that two distinctly different structures exist in dealloyed Pt bimetallic nanoparticle catalysts: on the one hand, solid core-shell nanoparticles with a Pt-rich shell of given thickness surrounding a nonporous Pt-poor alloy core (the core-shell structured Pt bimetallic nanoparticle willed be discussed in the next section in detail) and on the other hand nanoscale particles with nanoporosity characterized by highly irregular pores, pits, and voids in their interior (also called "spongy" or "swiss cheese" type particles).[150-156] Such porous nanostructures potentially can not only have high surface area to volume ratios and low density, but also supply enough active sites for all absorbed molecules involved over a close range. Meanwhile, the particular nanoporosity is in favour of O_2 mass transport through the metal surface, thus enhancing the ORR kinetics by confining O_2 near the active metal surface. Thus the deliberate introduction of nanoporosity in bimetallic alloys has always been reported and perceived to be an effective way to enhance the catalytic activity due to enhanced active surface area.[151,152,157-159] Recent studies have shown that nanoporosity forms spontaneously during the dealloying (leaching) of Pt alloy nanoparticles if and only if the particle size exceeds a critical value due to the competed surface atomic processes during dealloying (i.e., leaching of transition metals vs. surface diffusion of residual Pt atoms).[150, 152] For instance, Snyder et al. reported that in order to evolve fully formed porosity, $PtNi_3$ nanoparticle must have a minimum particle size of ca. 15 nm; [152] Oezaslan et al. reported a critical particle diameter of ca. 30nm in $PtCu_3$ and $PtCo_3$ nanoparticle for the pore formation.[150] However, molecular understanding of the impact of nanoporosity beyond increased surface areas, in particular its influence on the particle composition and surface lattice strain, and, related to these, the intrinsic ORR activity and stability of a nanoparticle electrocatalyst is needed to be explored. The findings of Strasser and his co-workers provided an explanation for the degradation of bimetallic particle ensembles.[160]They uncovered that nanoporosity formation in PtNi particles larger than ca. 10nm is intrinsically tied to a drastic dissolution of Ni and, as a result of this, a rapid drop in intrinsic catalytic activity during ORR testing, translating into severe catalyst performance degradation. In contrast, O_2-free acid leaching enabled the suppression of nanoporosity resulting in more solid core-shell particle architectures with thin Pt-enriched shells; surprisingly, such particles maintained high intrinsic activity and improved catalytic durability under otherwise identical ORR tests, as shown in Figure 9. Therefore, they suggested that catalytic stability could further

improve by controlling the particle size below ca. 10nm to avoid nanoporosity.

As discussed in previous section, the catalytic characteristics of the Pt nanocrystals can be further activated when the catalysts are bounded by active facets, which can be also applied for Pt bimetallic alloys. Stamenkovic et al. demonstrated that extended single crystal surfaces of Pt_3Ni (111) exhibit an enhanced ORR activity that is 10-fold higher than Pt (111) and 90-fold higher than the current state-of-the-art Pt/C catalysts.[98] To date, this is the most active cathode catalyst that has been developed. Consequently, it is not surprising that Zhang et al. found that {111}-terminated Pt_3Ni nano-octahedra were at least five times more active for ORR than {100}-terminated Pt_3Ni nanocubes.[110] Similarly, {111}-terminated nanotruncated Pt_3Co octahedra had been found to have higher activity than {100}-terminated Pt_3Co nanocubes.[161] In addition, {100}-terminated Pt-Mn nanocubes were reported to have higher ORR activity than the commercial catalyst.[162]

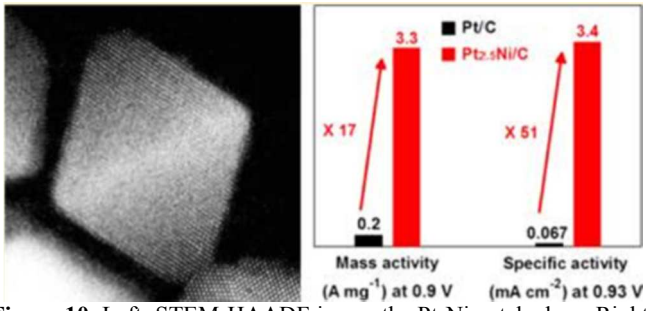

Figure 10. Left: STEM-HAADF image the Pt-Ni octahedron. Right: the mass activities at 0.9V and specific activities at 0.93V for Pt-Ni octahedron and commercial Pt/C. Reprinted with permission from ref.171.Copyright © 2013, American Chemical Society.

Like many other heterogeneous catalysis studies, a fundamental question is whether such a high activity observed on the extended single crystal surfaces can be obtained from nanometer-sized particles. Monte Carlo simulation suggested that {111}-facet-erminated Pt_3Ni nanoctahedra would be energetically stable and have a surface segregation profile similar to that of the extended Pt_3Ni surfaces.[98, 163] Thereafter, a number of research groups have made good progress by synthesizing octahedral Pt-Ni particles and reporting high ORR activity, which demonstrates that the strategy is very promising to solve the catalyst problems. Yang and co-workers reported the synthesis of truncated octahedral Pt_3Ni nanocrystals,[164] while Zhang et al. developed a synthesis and separation procedure to obtain a product of predominantly Pt_3Ni nanooctahedra.[101] However, the highest ORR activities (both specific and Pt mass) obtained from these catalysts were only 10-fold higher than the commercial Pt/C catalyst,[165] far below the values suggested by the work based on bulk single crystals. The difference in activity enhancement between bulk single crystals and nanoparticles may come from the surfactants chemically adsorbed on the surface of the as-synthesized octahedra, the deviation in shape, and the variation in elemental composition. In general, organic surfactants are usually employed to control the particle morphology, which contaminate the surface and require careful cleanings before the particles become catalytically active. Many approaches, such as UV-ozone, [162, 166] plasma,[101] potential cyling,[167] calcination,[168] and chemical treatment,[169,170] have been applied to remove the surfactants. The complex contaminants removal and synthetic procedures add much production cost and make these techniques economically unfeasible. Shao and Xia et al. reduced the surface coverage of surfactants on the Pt-Ni catalyst by using CO decomposed from $W(CO)_6$ as a capping agent for {111} facets in the presence of Ni.[171] The synthesised Pt-Ni octahedral exhibited a specific activity 51-fold higher than that of the state-of-the-art Pt/C catalyst for the ORR at 0.93 V, together with a record high mass activity of 3.3 Amg_{Pt}^{-1} at 0.9 V, as shown in Figure 10. Carpenter et al. reported a novel, simple method of synthesizing well-faceted PtNi nanoparticles without the use of capping agents. Specifically, they employed a facile solvothermal method in which N, N-dimethylformamide (DMF) functioned as both solvent and reductant.[172]The as-prepared well-faceted Pt_3Ni alloy nanoparticle catalysts showed specific activities greater than 1000 μAcm^{-2}_{Pt}, alloy catalysts prepared with a nominal composition of PtNi displayed activities close to $3000\mu Acm^{-2}_{Pt}$, or almost 15 times that of a state-of-the-art Pt/carbon catalyst. Despite the much progress has been achieved, the wet synthetic methods developed in above experiments have low scaling-up capacity and are thus not suitable for mass production of the octahedral Pt-Ni catalyst. Recently, Peng et al. reported a scalable, surfactant-free, and low-cost solid-state chemistry method for mass production of octahedral Pt-Ni alloy nanoparticles on carbon support (Pt-Ni/C) and demonstrate high ORR activity of the made catalyst.[173]The octahedral was prepared by simply impregnating both metal acetylacetonates onto a carbon support and reducing them at 200 °C in $120/5cm^3min^{-1}$ CO/H_2 for 1 h, as shown in Figure 11. ORR tests for as-prepared $Pt_{1.5}Ni$ catalyst showed much improved activity ($3.99mAcm^{-2}_{Pt}$ and $1.96Amg^{-1}_{Pt}$ at 0.9V vs. RHE) compared to the commercial Pt/C.

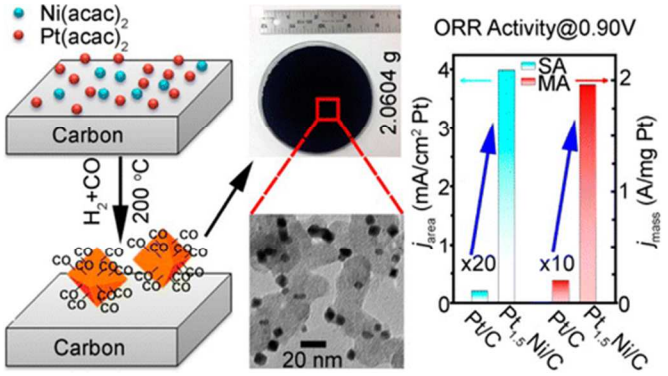

Figure 11. Schematic illustration of the solid-state chemistry-enabled scalable production of octahedral Pt-Ni alloy electrocatalyst for ORR. Reprinted with permission from ref.173.Copyright © 2014, American Chemical Society.

Engineering the near-surface composition and the inner structures of these Pt-Ni polyhedral nanocrystals can further perfect the ORR activity. Strasser et al. presented a facile and surfactant-free solvothermal method to synthesis shape and size-selective octahedral PtNi NPs, which shown an exceptional ORR made possible by their carefully tuned alloy particle surface composition.[165] They showed that the solvothermal reaction time correlates with the near-surface Pt atomic composition of the octahedra without affecting their size or shape. The reaction time could tune the surface Pt:Ni composition since the reaction time acted like an in situ annealing process, mainly smoothing out the near-surface compositional gradient by metallic interdiffusion,[174,175] The PtNi octahedra prepared with the longest reaction time reached a 10-fold surface area-specific (~3.14 $mAcm^{-2}_{Pt}$) as well as a 10-fold Pt mass based (~1.45 Amg^{-1}_{Pt}) activity gain over the state-of-art Pt electrocatalyst, approaching the theoretically predicted limits. As mentioned before, introducing porous to the inner of the nancrystals interior diminishes the number of buried non-functional precious metal atoms, and their uncommon geometry provides a pathway for tailoring physical and

chemical properties of Pt catalysts. Recently, Chen et al. presented a novel class of electrocatalysts that exploit structural evolution of bimetallic nanoparticles; specifically, the starting material, crystalline $PtNi_3$ polyhedra, transformed in solution by interior erosion into Pt_3Ni nanoframes with surfaces that offers three-dimensional molecular accessibility, as shown in Figure 12a.[176] Both the interior and exterior catalytic surfaces of this open-framework structure were composed of the nanosegregated Pt-skin structure, which exhibited enhanced ORR activity(Figure 12b). The Pt_3Ni nanoframe catalysts achieved a factor of 36 enhancement in mass activity and a factor of 22 enhancement in specific activity for ORR, respectively (relative to state-of-the-art Pt/C catalyst). More importantly, the stability of Pt_3Ni nanoframe was also impressive. After potential cycling durability test, they still maintained their morphology and activity, as shown in Figure 12c.

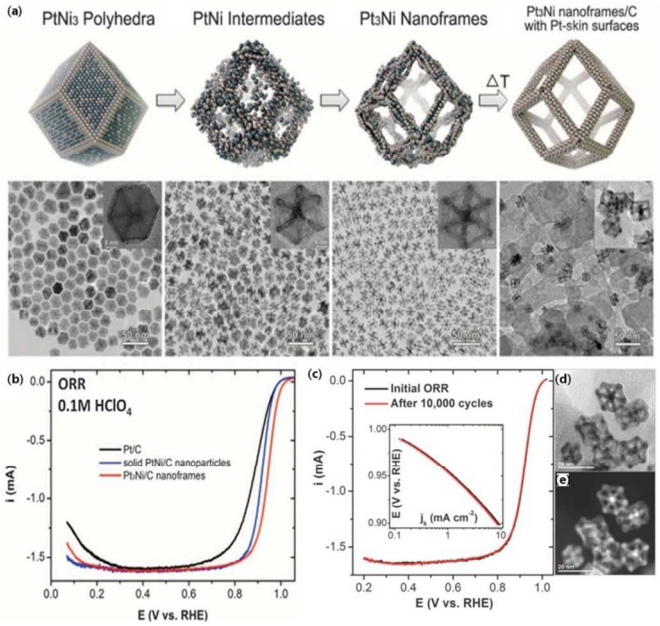

Figure 12. (a)Schematic illustrations and corresponding TEM images of the samples obtained at four representative stages during the evolution process frompolyhedra to nanoframes. (b) ORR polarization curves. The ORR activity (c) and TEM images of Pt_3Ni nanoframe before (d) and after (e) stability test. Reprinted with permission from ref.176.Copyright © 2014, American Association for the Advancement of Science.

Although the shape-controlled synthesis of monometallic nanocrystals with high-index facets has been studied extensively,[177-181] alloy nanocrystals bound by high-index facets have been little explored to date because of the difficulties in controlling high-energy surfaces in the presence of two metals with different nucleation and growth habits. Yang et al. described the synthesis of a set of Pt-M (M=Au, Ni, Pd) icosahedral nanocrystals based on the gas reducing agent in liquid solution method.[182] Among the Pt-M alloy icosahedral nanocrystals generated, Pt_3Ni had an impressive ORR specific activity of $1.83mAcm^{-2}_{Pt}$ and $0.62Amg^{-1}_{Pt}$. The area-specific activity of icosahedral Pt_3Ni catalysts was about 50% higher than that of the octahedral Pt_3Ni catalysts ($1.26\ mAcm^{-2}_{Pt}$), as shown Figure 13. DFT and molecular dynamics simulations indicated that this improvement may arise from strain-induced electronic efffects. Recently, Sun et al. has reported a new synthetic strategy that enables the one-pot fabrication of concave-nanocubic (CNC) and hexoctahedral (HOH) Pt-Ni alloy nanocrystals exclusively bound by high-index facets by simply adjusting the concentration of glycine.[183] They found that CNC Pt-Ni alloy nanocrystals were formed at a low concentration of glycine by self-assembly, which has never been observed previously in the synthesis of nanocrystals with high-index facets. While the HOH Pt-Ni alloy nanocrystals could be evolved at a high concentration of glycine by crystal growth control. The specific activities (at 0.90V vs. RHE) of the HOH ($1.08mAcm^{-2}$), nanocubic ($0.93mAcm^{-2}$), and CNC Pt–Ni alloy NCs ($0.44\ mAcm^{-2}$) were 5, 4, and 2 times, respectively, as high as that of Pt/C ($0.22mAcm^{-2}$).

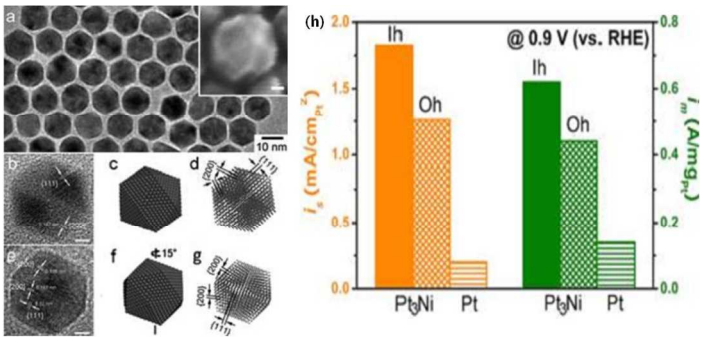

Figure 13. (a) TEM and SEM (inset) and (b-g) HRTEM micrographs, and 3D models of Pt_3Ni icosahedral nanocrystals at two different orientations, respectively. The scale bars correspond to 2 nm.(h) Mass- and area-specific activities of the Pt_3Ni icosahedral and octahedral nanocrystal and Pt reference catalysts at 0.9 V. Reprinted with permission from ref.182.Copyright © 2012, American Chemical Society.

3.2.2 Core-Shell structured Catalysts In all Pt alloy systems reviewed above, leaching or dissolution of the non-Pt metal from the alloy surface to the acidic solution would lead to instability of Pt bimetallic catalysts, compromising the advantages of Pt alloy catalysts. Generating a nanostructure in the form of a thin Pt shell on non-noble metal core can mitigate the dissolution of the inner non-Pt metals due to the protection of the outer Pt shell, thus resulting in highly enhanced durability. More importantly, since only the outmost few layers of Pt atoms in a catalyst are actually needed in facilitating a reaction while most atoms in the bulk are more or less wasted, this strategy is attractive and practical to make full use of every noble-metal atom and drive down the costs of catalysts greatly. “e” in Figure 14). This approach provides a controlled fabrication of monodisperse core-shell nanoparticles. Core-shell nanoparticle examples like Au@Pt,[184,185] AuCu@Pt,[186] Pd@Pt,[187,188] Cu@Pt,[189] and Ni@Pt,[190] are successfully fabricated via colloidal synthesis. Besides the colloidal synthesis, UPD is another recently developed technique for controlling the heterogeneous structures of bi- or multimetallic core-shell nanoparticles (route “f” in Figure 14).When Cu is used as the sacrificial layer, a Pt can be deposited on different metallic nanoparticles through the electrochemical replacement reaction. Adzic and co-workers described the design of a carbon-supported Pt mono-layer on Pd (Pt_{ML}/Pd/C) or Pd_9Au_1 (Pt_{ML}/Pd_9Au_1/C) nanoparticles synthesized by UPD and replacement reactions.[191] In addition， the physical vapor deposition method was also employed to prepare core-shell nanoparticles.[192-198](ii) (electro) chemical dealloying/leaching methods (route “a” and “b” in Figure 14) or (iii) thermal or adsorbate-induced segregation (route “c” and “d” in Figure 14). In general, to avoid the dissolution of non-Pt atoms from the topmost surface layers in the oxidizing and acidic environment of fuel cell, the mother Pt alloy is usually pretreated in an acidified solution or dealloyed by cyclic voltammetry. The dissolution of the non-noble 3d transition metal leaves behind an atomically rough

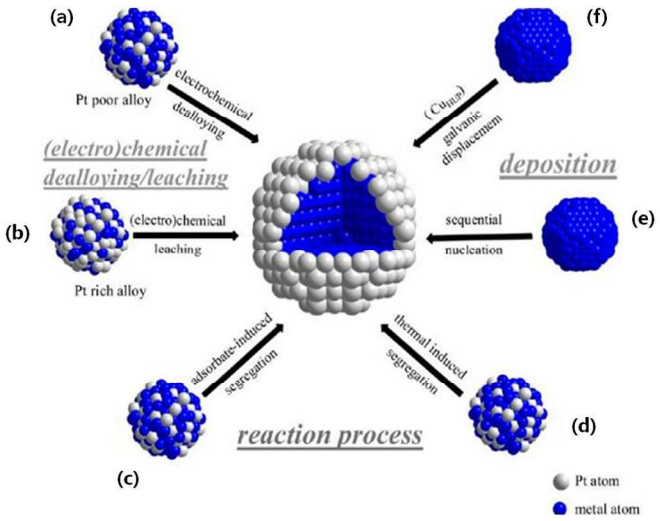

Figure 14. Illustration of basic synthesis approaches for the preparation of core-shell nanoparticle catalysts. Electrochemical (acid) dealloying/ leaching results in (a) dealloyed Pt bimetallic core-shell nanoparticles and (b) Pt-skeleton core−shell nanoparticles, respectively. Reaction process routes generate segregated Pt skin core−shell nanoparticles induced either by (c) strong binding to adsorbates or (d) thermal annealing. The preparation of (e) heterogeneous colloidal core−shell nanoparticles and (f) Pt monolayer core-shell nanoparticles is via heterogeneous nucleation and UPD followed by galvanic displacement, respectively. Reprinted with permission from ref.15.Copyright © 2013, American Chemical Society.

surface composed of Pt atoms with low/no lateral coordination.[29] This nanostructure, first discovered by Toda et al., [29,199] is currently referred to as a "Pt-skeleton" and maintains favourable catalytic properties toward the ORR if the Pt-shell is thin enough. [29,200,201] Another approach to form a pure Pt surface layer (one monolayer thick) is to thermally anneal the mother alloy, leading to the so-called "Pt-skin" nanostructure. As stressed by Stamenkovic et al. [124, 201] from measurements on single crystal surfaces and Toda et al.[29] on nanocrystallites, the thermal annealing restructured the near-surface region of the catalyst (it reduced the number of low coordination surface atoms), yielding the formation of (111) domains and compositional oscillations (the first and third monolayer (ML) become Pt-rich, while the second one enriches in M). Overall, these effects contributed to a better ORR activity of the Pt-skin over the Pt-skeleton nanostructure and the mother alloy. The formation and reversibility of Pt-skeleton and Pt-skin nanostructures is illustrated in Figure 15.[202] Early studies performed by Chen et al.[190] have shown that the Pt-skin and Pt-skeleton nanostructures can be tailored at the nanometer scale. Durst and Maillard et al. have outlined the reversibility of the Pt-skin nanostructure toward the Pt-skeleton nanostructure during acid treatment.[203]This reversibility caused a large decrease of the overall Co content (by more than 30% in the present case) but no release of the lattice strain of the core material. Furthermore, the use of reactive gases is a rather unique way to engineer the core-shell structures of nanoparticles (adsorbate-induced segregation).[204-206] For instance, after CO annealing, the Pt_3Co alloy resulted in nanoparticles with a Pt-enriched surface and a Pt_xCoy alloy core due to the strong binding of CO on Pt surface atoms and reduced total surface energy.[207] Jang and his co-workers demonstrated that reversible surface segregation of Pt in Pt_3Au/C catalysts was accomplished through a heat treatment under a CO or Ar atmosphere, which resulted in surface Pt segregation and reversed

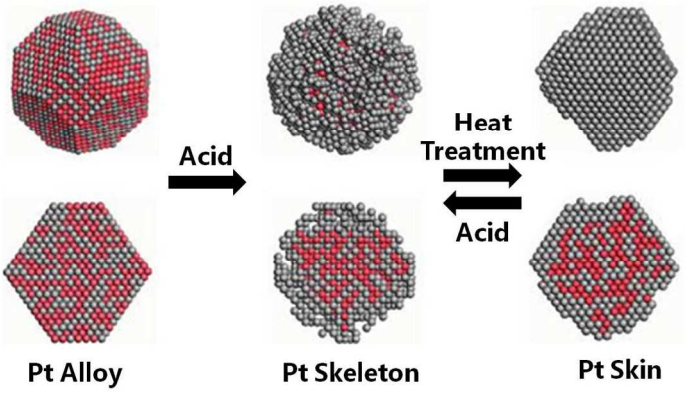

Figure 15. Schematic illustration of the formation and reversibility of Pt-skeleton and Pt-skin nanostructures. Reprinted with permission from ref. 202.Copyright © 2011, American Chemical Society.

segregation respectively, as shown in Figure 16.[208] The Pt-segregated Pt_3Au/C exhibited a significantly improved ORR activity ($227mA/mg_{metal}$) compared to that of commercial Pt/C ($59mA/mg_{metal}$). The DFT calculations revealed that the binding energy for Pt-segregated Pt_3Au (111) surfaces was 0.1eV lower than that for Pt (111) surfaces, which was previously mentioned to exhibit the optimum OH binding energy for ORR.

Advanced preparation techniques for core-shell nanocatalysts offer experimental parameters to control the nanoscale structure and composition, including Pt shell coverage/thickness, composition of the core, particle size, and particle shape. Optimizing these critical characteristics can result in considerable activity and durability benefits. For example, Chen et al. showed that the ORR electrocatalytic properties of the precious metal shell can be tuned by varying its surface coverage.[190] They synthesized carbon-supported Ni@Pt core-shell nanoparticle catalysts (Ni@Pt/C) with a series of Pt coverages by depositing different amounts of Pt on Ni nanoparticles ca.5 nm in size. It was found that Pt approximately forms an extended layer on Ni particles as its coverage does not exceed that required for a monolayer formation. The ORR electrocatalytic properties of the Ni@Pt/C catalysts exhibited a volcano type of dependence on Pt coverage, with the apex occurring near the monolayer, as shown in Figure 17.

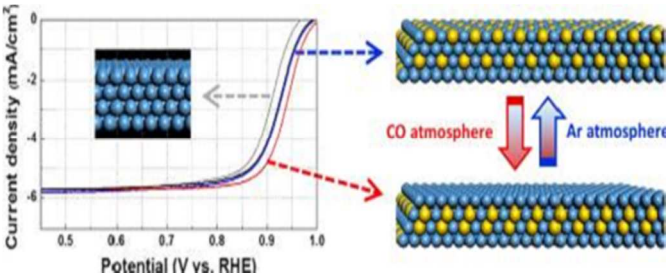

Figure 16. The ORR performance obtained in O_2-saturated 0.1M $HClO_4$ with a scan rate of 5mV/s. Reprinted with permission from ref.208. Copyright © 2013, American Chemical Society.

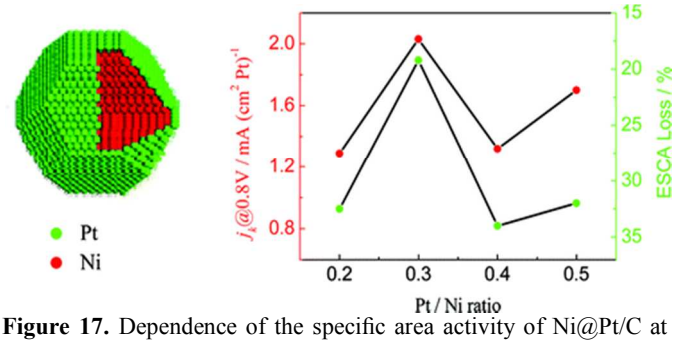

Figure 17. Dependence of the specific area activity of Ni@Pt/C at 0.8 V and the loss of the ECSA of Pt after the degradation test of repeating potential cycling. Reprinted with permission from ref.190.Copyright © 2011, American Chemical Society.

Recently, Xia et al. reported a versatile route to the conformal deposition of ultrathin shells of Pt on Pd nanocrystals with control on the atomic scale (Figure 18).[209] The introduction of the Pt precursor at a relatively slow rate and high temperature allowed the deposited Pt atoms to spread across the entire surface of a Pd nanocube to generate a uniform shell. The number (n) of Pt atomic layers on each Pd cubic seed could be precisely controlled from a monolayer to multiple layers by simply adjusting the amount of Pt precursor introduced into the reaction solution. Compared to a commercial Pt/C catalyst, the Pd@Pt_{nL} (n=1-6) core-shell nanocubes showed enhancements in specific activity and durability toward ORR. A volcano-type relationship between the ORR specific activity and the number of Pt atomic layers was observed and the ORR specific activity was maximized for the catalysts based on Pd@Pt_{2-3L} nanocubes. The influence of different preparation techniques for core-shell nanocatalysts and various experimental parameters on the final ORR activity and durability were systemic reviewed by Strasser and Oezaslan.[15]

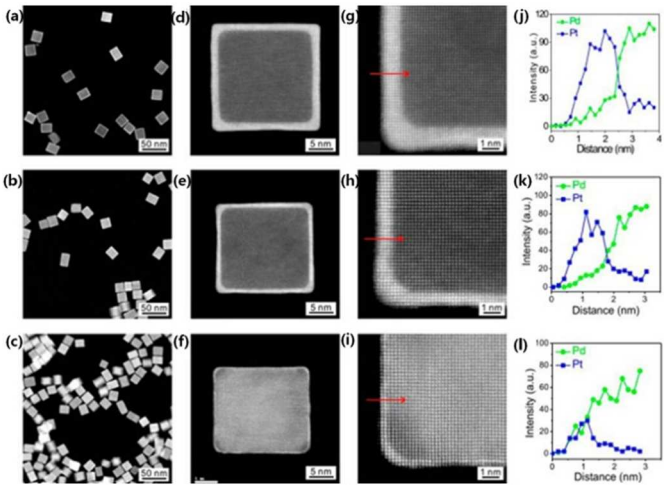

Figure 18. Controlling the number of Pt atomic layers. (a-c) Low-magnification HAADF-STEM images showing a large number of (a) Pd@Pt_{6L}, (b) Pd@Pt_{4L}, and (c) Pd@Pt_{1L} nanocubes; (d-f) HAADF-STEM images of individual (d) Pd@Pt_{6L}, (e) Pd@Pt_{4L}, and (f) Pd@Pt_{1L} nanocubes; (g-i) atomic-resolution HAADF-STEM images taken from the (g) Pd@Pt_{6L}, (h) Pd@Pt_{4L}, and (i) Pd@Pt_{1L} nanocubes, revealing the numbers of Pt atomic layers; (j-l) EDX line scan analyses of the (j) Pd@Pt_{6L}, (k) Pd@Pt_{4L}, and (l) Pd@Pt_{1L} nanocubes along the red arrows marked in (g-i). Reprinted with permission from ref.209.Copyright © 2014, American Chemical Society.

The origin of activity benefits of core-shell nanoparticles is found in altered electronic and geometric properties associated with beneficial chemisorption properties of surface atoms for the minimization of free-energy barriers, as metioned before. Compressive lattice strain in the Pt shells induced by Pt-Cu alloy particle cores, for instance, lowers the bonding strength of oxygenated adsorbates and causes ORR activity increases. [73,210] Based on combining computational and experimental study, Zhuang et al. have found that a Pt skin (1~2 monolayers thick) on a AuCu intermetallic substrate, would be an ideal structure, on which the oxygen adsorption energy can be decreased, relative to that on Pt (111), to an extent close to 0.2eV.[186] Additionally, as for core-shell nanostructured catalysts, the core can usually stabilize the Pt shell and result in superior stability in ORR operations. In these Pd- or Pd_9Au_1-supported Pt monolayer core/shell nanoparticles presented by Adzic et al.,[191] the core increased the stability of the shell by shifting positively its oxidation potential, and by preventing the cathode potential reaching values at which Pt dissolution takes place. The latter was realized by the slow oxidation of the Pd core that impedes excursions of the cathode potentials to high values. The Pt mass activity of the $Pt_{ML}/Pd_9Au_1/C$ electrocatalyst after 200000 potential cycles from 0.7 to 0.9V decreased about 30%, while the mass activity of commercial Pt/C catalyst showed a terminal loss below 50 000 cycles.

Overall, Pt in the form of a thin shell on non-noble metal core leads to enhanced catalyst utilization, better efficiency, and higher catalytic activity and durability, thus giving immense scope for validating the techno-commercial prospects of fuel cell by utilizing this class of materials. The ability to scalable fabricate core-shell particles with uniform shell thickness, controllable composition, and uniform dispersion on a support is need to be further improved.

3.2.3 Anisotropic Catalysts The Pt-based catalysts mentioned above are zero-dimensional (0-D) Pt nanoparticles and usually supported on the high surface area carbon blacks. These 0-D nanoparticles undergo serious migration, aggregation, and Ostwald ripening due to their high surface energy, which leads to a significant loss of electrochemical surface area (ECSA).[211-214] On the other hand, the problem of carbon corrosion accompanied with the detachment of nanoparticles occurs in all above systems.[215-218] These drawbacks motivated researchers to explore high surface area self-supported catalysts with anisotropic nanostructures, such as nanowires,[219-221] nanotubes,[222,223] branched nanoflower[224-225] and nanodendrites.[226-227] These materials not only exhibit maximum catalytic performance by their high surface area but also utilise fully their inherent potential because of the presence of highly reactive edges, corners and stepped atoms on their surface. Furthermore, their high surface area and anisotropic properties make them more make them less vulnerable to dissolution, migration, Ostwald ripening, and aggregation compared to the 0-D Pt nanoparticles, and in some cases the potential to eliminate corrosion of the catalyst support. Pivovar et al. synthesized PtNi nanowires with a diameter of 150-250 nm and a length of 100-200μm. The PtNi nanowires produced a peak mass activity of 917mAmg_{Pt}^{-1}, which is 3 times greater than carbon-supported Pt/C and 2.1 times greater than the U.S. Department of Energy target for proton-exchange membrane fuel cell activity.[228] Wang and Lou et al. prepared 3-D Interconnected Pt nanoassemblies via a one-pot method and its specific ORR activity was 2.2- and 1.7-times of that of commercial Pt and Pt/CB catalysts, respectively.[229] After an accelerated durability test, the self-supported interconnected Pt nanoassemblies lost only 16% of the initial Pt ECSA, while the commercial Pt black and Pt/C catalysts lost 85% and 95% of their initial ECSA.

Because of the attractive advantages of such anisotropic nanostructures, a substantial research focus has been devoted to establishing facile and well-defined protocols for the synthesis of these nanostructured catalysts, which has been systematic reviewed by Zhang et al.[21] However, the practical application of these anisotropic structures in fuel cell system is limited due to the loss of nanoparticle morphology.

3.3 Surface Modified with Selected Foreign Species Apart from modulating exposed facets of Pt nanocrystals and combining Pt with other metals to generate bimetallic nanocrystals with structures in the form of alloys, core-shells branches or anisotropies, modifying Pt nanoparticles surfaces with metal clusters, molecules, ions, organic or inorganic compounds can also lead to an optimized Pt electronic structure which is beneficial to ORR operation.[230-239] For example, as for metal clusters, modifying Pt nanoparticles with Au clusters has been already proved to be efficient in stabilizing Pt against dissolution under harsh fuel cell work environment, as demonstrated by Zhang et al.[230] More importantly, there were no leakage issues on Au. There were insignificant changes in the activity and surface area of Au-modified Pt over the course of cycling, in contrast to sizable losses observed with the pure Pt catalyst under the same conditions, as shown in Figure 19. In situ x-ray absorption near-edge spectroscopy and voltammetry data suggested that the Au clusters confer stability by raising the Pt oxidation potential.

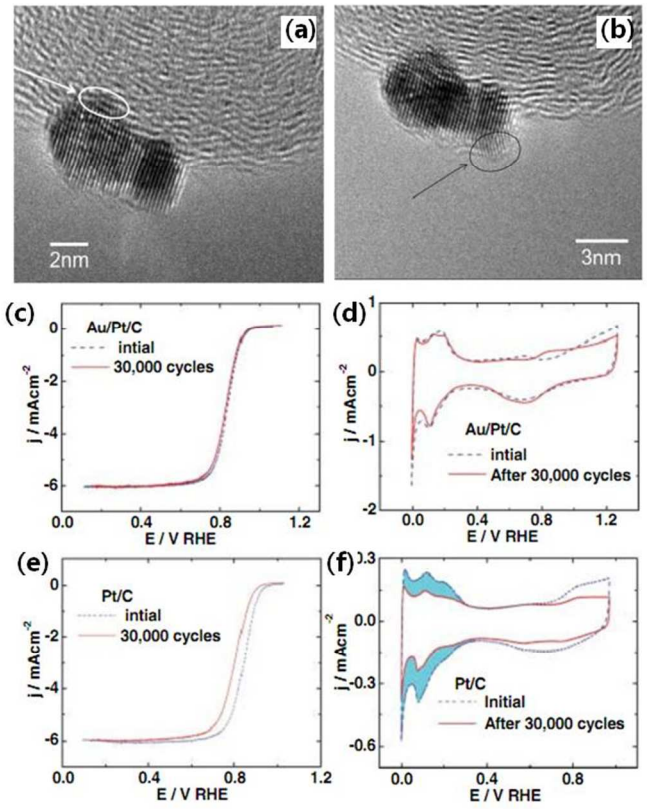

Figure 19. Electron micrographs of a Au-modified Pt/C catalyst made by displacement of a Cu monolayer by Au. High-resolution images (a) and (b) show atomic rows with spacings that are consistent with the Pt(111) single-crystal structure. A different structure in the areas indicated by the arrows is ascribed to the Au clusters. Polarization curves for the O_2 reduction reaction on Au/Pt/C (c) and Pt/C (e) catalysts on a rotating disk electrode, before and after 30,000 potential cycles. Sweep rate, 10mV/s; rotation rate, 1600 rpm. Voltammetry curves for Au/Pt/C (d) and Pt/C (f) catalysts before and after 30,000 cycles; sweep rate, 50 and 20mV/s, respectively. The potential cycles were from 0.6 to 1.1V in an O_2-saturated 0.1M $HClO_4$ solution at room temperature. The shaded area in (f) indicates the lost Pt area. Reprinted with permission from ref.230.Copyright © 2007, American Association for the Advancement of Science.

Although the conventional opinion is that the use of a "capping agent" in a wet-chemistry route undermines the overall catalytic activity of the metal nanoparticles because of the lack of "clean" surface active sites, at present, chemical functionalization of the metal surface is becoming a new trend in designing electrocatalysts. This is based on the modication of the metal surface by non-metallic molecules or compounds that can block the adsorption of poisoning species or influence the hydrophilicity and electronic property of the metal.[240-243] For example, Markovic's group demonstrated that the ORR activity on the cyanide functionalized Pt {111} facets showed a 25-/10-fold increase in H_2SO_4/H_3PO_4 electrolytes compared to the naked Pt {111} facets, where cyanide adsorbed on the Pt surface indeed acted as a third body and consequently selectively blocked the adsorption of sulfuric and phosphoric acid anions.[242,243] Miyabayashi and Miyake et al. successfully modified a Pt NP surface with a controlled ratio of octylamine (OA) and pyrene group (PA) by convenient two-phase liquid reduction procedures.[232]The modification of the Pt NP surface with OA and PA significantly improved the electrocatalytic activity such as area specific and mass specific activities. It seems that the high ORR electrocatalytic activity was originated from a change of the adsorption kinetics of reaction intermediates and/or concentration of oxygen adjacent to the Pt NP surface. Erlebacher et al. reported the synthesis of a hydrophobic, protic ionic liquid (IL, [MTBD][beti])-encapsulated Ni/Pt nanoporous nanoparticle catalyst supported on carbon.[233]The high O_2 solubility of the [MTBD][beti], in conjunction with the confined environment within the pores, biases reactant O_2 toward the catalytic surface, consistent with an increased residence time and enhanced attempt frequencies, resulting in improved reaction kinetics. The half-cell specific activity of this catalyst architecture was found to be an order of magnitude higher than that of commercial Pt/C.

In some case, decorating Pt NPs surface with carbon[234] or silica layer[235, 236] can suppress the migration, agglomeration and dissolution of Pt NPs to some extent and resulted in excellent stabilities. However, the ORR activity of these catalysts was only slightly improved as the outside coating might prevent the facial diffusion of the reactants involved in ORR into the inner Pt active sites. Wei et al. reported the design and synthesis of a Pt/C@PANI core-shell structured catalyst and demonstrated that the activity for the oxygen reduction reaction strongly depends on the thickness of the PANI shell.[237]The greatest enhancement in catalytic properties for Pt/C@PANI occurred at a PANI thickness of 5nm. In particular, the Pt/C@PANI catalysts showed super stability. Pt/C@PANI (30%) catalyst decreased by only ~30% after 1500 CV cycles, whereas the Pt/C catalyst lost ~83% of its initial ECSA, as shown in Figure 20a, b. The long-term durability of the PANI@Pt/C and Pt/C catalysts was also examined in a single cell using an AST protocol. The polarization curves obtained after every 1000 cycles of the AST protocol with single cells incorporating the PANI@Pt/C and Pt/C cathode catalysts are shown in Figure 20c, d. The initial performance of the cell in which the Pt/C

catalyst was used was similar to that of the cell in which the PANI@Pt/C catalyst was used. However, after the AST test was performed, the performance of the cell with the PANI@Pt/Ccathode catalyst showed significantly better durability than the cell with the Pt/C cathode catalyst. The analysis from X-ray photoelectron spectroscopy (XPS) of Pt 4f peak showed that the Pt $4f_{7/2}$ peak of the Pt/ C@PANI catalyst was shifted to a higher binding energy (72.05eV) relative to the Pt $4f_{7/2}$ peak of the Pt/C catalyst, indicating that the improved activity and stability could be attributed to the novel PANI-coated core-shell structure, which resulted in electron delocalization between the Pt d-orbitals and the PANI π-conjugated ligand and in electron transfer from Pt to PANI. The DFT calculationsdisclosed that the number of holes in PANI increased with the electrons transfer from PANI to support C, which cause partial oxidation of PANI and thus strengthening the electric conductivity of PANI.[238] According to Figure 20e, the system energy decreased markedly with the coverage of PANI on the Pt/C, which meant that the Pt/C@PANI was more stable than Pt/C. The lifted HOMO energy level and lowered d-band centre of Pt/C@PANI compared with Pt/C were beneficial to the electron transfer between Pt/C@PANI and O_2 due to the reduced gap between the Pt/C@PANI HOMO and the oxygen LUMO, and the desorption of intermediate species on the surface of the catalysts and releasing fresh catalytic sites for the subsequent reaction. This result strongly supported the experimental observation of the improved ORR activity and stability.

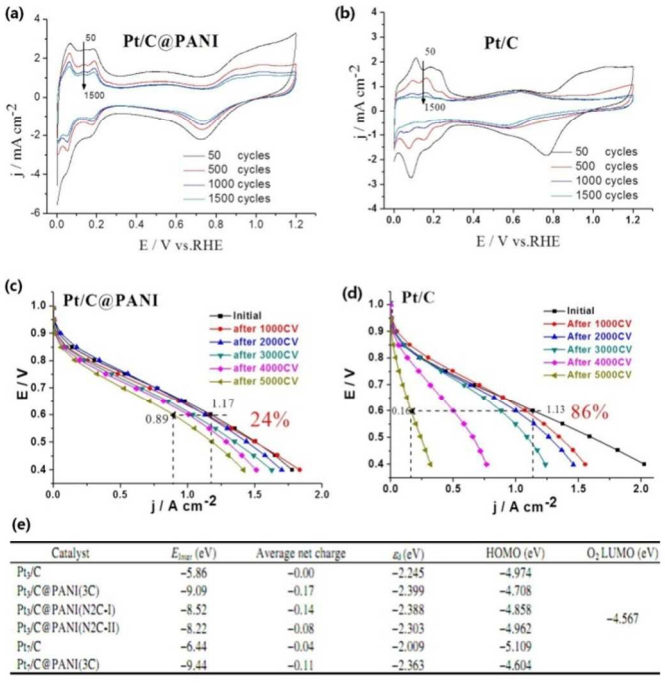

Catalyst	E_{Int} (eV)	Average net charge	ε_d (eV)	HOMO (eV)	O_2 LUMO (eV)
Pt_3/C	-5.86	-0.00	-2.245	-4.974	
Pt_3C@PANI(3C)	-9.09	-0.17	-2.399	-4.708	
Pt_3/C@PANI(N2C-I)	-8.52	-0.14	-2.388	-4.858	-4.567
Pt_3/C@PANI(N2C-II)	-8.22	-0.08	-2.303	-4.962	
Pt_3/C	-6.44	-0.04	-2.009	-5.109	
Pt_3/C@PANI(3C)	-9.44	-0.11	-2.363	-4.604	

Figure 20. CV curves of electrodes made from (a) Pt/C@PANI and (b) Pt/C catalysts at different CV cycles in N_2-purged 0.5M H_2SO_4 solution at a 50mV/s scan rate. Polarization curves of single PEM fuel cells with cathodes fabricated from (c) PANI@Pt/C and (d) Pt/C catalysts after the indicated numbers of CV cycles. (e) Interaction energy between PANI, Pt and C; average net charge, d-band centre, HOMO energy level for Pt/C and Pt/C@PANI; LUMO energy level for O_2. Reprinted with permission from ref.237.Copyright © 2012, American Chemical Society.

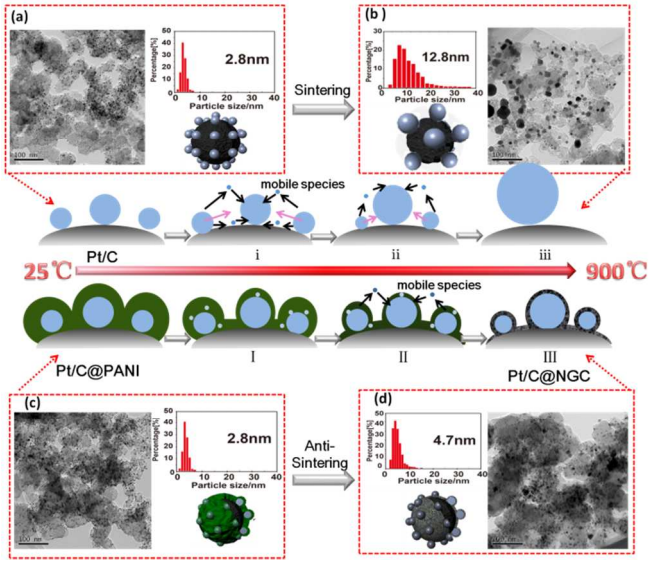

Figure 21. The synthetic strategy of Pt/C@NGC. Reprinted with permission from ref.239.Copyright © 2014, Royal Society of Chemistry.

More interestingly, the ORR activity could be further improved after subjecting Pt/C@PANI to a high temperature heat treatment due to the formation of a more active coating shell: nitrogen-doped graphitic carbon (NGC) (The NGC is usually employed as an ameliorative carbon support or a promising Pt-free ORR catalyst).[239] It is worthy to point out that the confinement effect of the PANI could render Pt NPs with an anti-sinter capability and the size of Pt nanoparticle in Pt/C@NGC catalyst were only 4.7nm even after 900ºC heat treatment, thus guaranteeing the feasibility of the design concept of the Pt/C@NGC (Figure 21). The Pt/C@NGC catalyst exhibited a specific activity of 0.308mAcm^{-2} and a mass activity of 163mAmg$^{-1}_{Pt}$ at 0.9 V, which was 2.5 times and 1.7 times greater than those of Pt/C respectively.

The strategy of modified with Pt or Pt alloy surface with elaborately selected foreign species blazes a new path to boost the ORR electrocatalytic performance of Pt-based catalysts.

3.3 **Support-Enhanced Catalysts**

Currently, the carbon black is the most commonly used support for ORR catalyst.[244, 245] Although the carbon support materials used in commercially available catalysts have reasonable performance, carbon corrosion at high electrode potentials in the presence of oxygen results in the separation of Pt particles from the carbon support and consequent performance loss.[246-250]Additionally, the predominance of weak interactions between the carbon support and the catalytic metal nanoparticles can not substantially modify the electronic structure of Pt and anchor Pt tightly to the carbon support, leading to migration and aggregation of supported Pt nanoparticles and a consequent decrease in the active surface area with long-term operation (a continuing problem in vehicle applications).[251, 252] To solve these issues, several recent studies have concentrated on developing highly graphitic carbon materials, such as carbon nanofibers, nanotubes, nanohorns and graphenes.[253] These carbon materials with a higher graphitic character are far more resistant toward degradation, given the relatively small number of edge plane sites, which act as reactive centres for carbon oxidation.[254,255] The abundant π sites on the graphitized carbon surface interact strongly

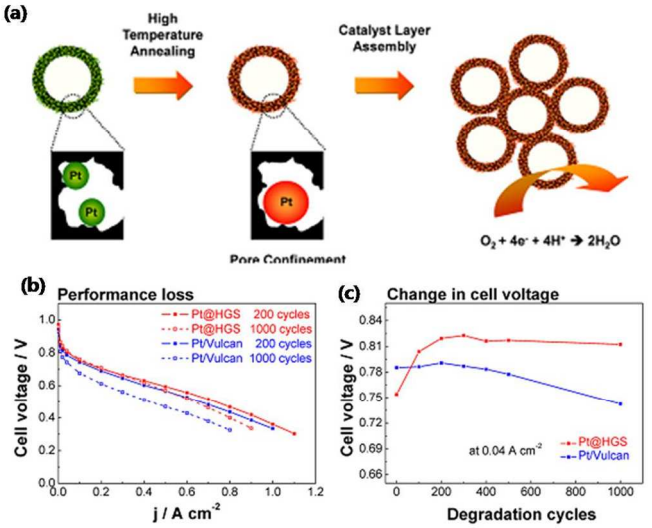

Figure 22. (a) Schematic model of Pt encapsulation by pore confinement.(b) Fuel cell performance curves at 80 °C before and after degradation test under start-stop conditions. (d) Comparison of cell voltage change in the kinetic region for Pt@HGS and Pt/Vulcan during the in situ degradation tests at 0.04Acm^{-2} (with 0.18 and 0.36mg$_{Pt}$cm^{-2}loading at anode and cathode, respectively). Reprinted with permission from ref.260. Copyright © 2012, American Chemical Society.

with Pt, as demonstrated by XPS and electron-spin resonance studies.[254,255] The Pt-C interactions are partially covalent, due to the electron delocalization between the carbon π sites and the Pt d-orbital, and also partially ionic due to the electron transfer from Pt to carbon.[256]These strong metal support interactions may help topartially inhibit Pt oxidation and dissolution during potential cycling. Further engineering the nanostructure of these highly graphitic carbon materials offers the possibility of controlling and improving several properties at the same time. Recently, several new nanostructured carbon supports, like colloid-imprinted carbon (CIC) supports,[257]ordered hierarchical nanostructured carbon (OHNC), [258] ordered graphitic mesoporous carbon (OMC) [259] have been introduced as robust carbon-based supports for ORR. Mayrhofer and Schüth et al. reported a mesostructured graphitic carbon support in the form of hollow graphitic spheres (HGS).[260] The specific surface area of the HGS exceeded 1000m^{2}g^{-1} and the precisely controlled pore structure in HGS was specifically developed to overcome the long-term catalyst degradation, while still sustaining high activity. The synthetic pathway (Figure 22a) leaded to Pt nanoparticles of approximately 3 to 4nm size encapsulated in the HGS pore structure that were stable at 850°C and, more importantly, during simulated accelerated electrochemical aging. Moreover, the high stability of the cathode electrocatalyst was also retained in a fully assembled polymer electrolyte membrane fuel cell. As presented in Figure 22c, the cell voltage for Pt/Vulcan gradually decreased and resulted in an overall loss of about 50mV after 1000 start-stop cycles. This was further reflected in the complete down shift of the performance curve after 1000 start-stop cycles in Figure 22b. On the contrary, the cell voltage of Pt@HGS remained almost unaffected and significantly higher than in the case of Pt/Vulcan, demonstrating the superiority of the HGC support.

On the other hand, modifying these highly graphitic carbon support surface with elaborately selected functional groups may induce a unique effect.[261-265] Wei et al. found a strong interaction formed between Pt nanoparticles and thiolated carbon supports (Pt/SH-CNTs), resulting in markedly enhanced tolerance against Pt dissolution at high potentials.[261] The durability test showed that the Pt ECSA of Pt/SH-CNTs catalyst only decreased approximately 22.3% after 1500 CV cycles, whereas the Pt/pristine-CNTs and Pt/COOH-CNTs catalysts lost about 48.1% and 81.3% of their initial ECSA, respectively. The CV curves clearly showed that the oxidation of the Pt NPs on the SH-CNTs starts as late as ca. 0.90 V vs. RHE but as early as ca. 0.75 V vs. RHE on OH-CNTs, indicating that Pt/SH-CNTs have a higher oxidation resistance than Pt/OH-CNTs (Figure 23a). The strong interaction between Pt NPs and SH-CNTs was further evidenced by the shift in the Pt 4f$_{7/2}$ peak to a higher binding energy (72.7eV) as compared with that for the Pt/pristine-CNTs (71.9eV) and Pt/COOH-CNTs (71.5eV) catalysts (Figure 23b). This shift in binding energy could be attributed to the strong ligand effect between Pt NPs and SH-CNTs. The DFT calculations strongly supported the above results.[262] In order to investigate the Pt-Pt interaction, a Pt cluster with 5 Pt atoms was simulated. Figure 23c-d shows the dissolution and migration of a single Pt atom on the Pt$_5$ cluster. The dissolution and migration processes on SH-SWCNTs and OH-SWCNTs were endothermic processes, and the endothermic energy on SH-SWCNTs was larger than on OH-SWCNTs. The migration active energy on SH-SWCNTs (57kcal/mol) was greater than that on OH-SWCNTs (36kcal/mol), which confirms that SH-SWCNTs can restrict the dissolution and migration of the Pt cluster in comparison to OH-SWCNTs. DFT calculations also suggested that the enhanced stability of the Pt/SH-CNTs originates from the increased interaction between Pt and SH-CNTs and the depressed d-band centre of the Pt NPs. Thus, the development

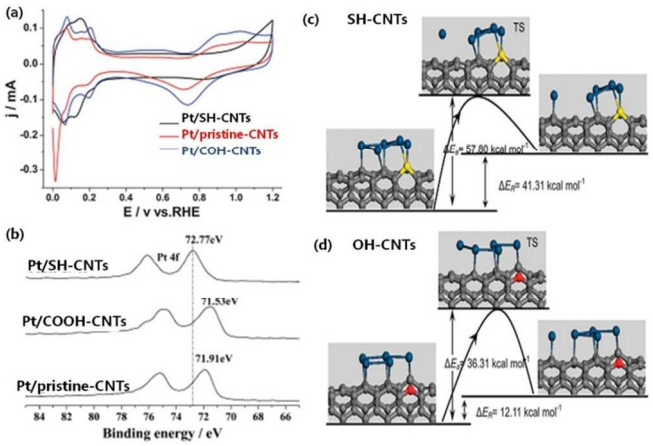

Figure 23. (a) Normalized Pt ECSA of electrodes made with Pt/SH-CNTs, Pt/pristine-CNTs and Pt/COOH-CNTs catalysts in N_2-purged 0.5M H_2SO_4 at room temperature (0-1.2V vs. RHE, sweep rate 50mV/s). (b) Pt_{4f} XPS spectra of Pt/SH-CNTs, Pt/COOH-CNTs and Pt/pristine-CNTs catalysts. Reaction energy diagrams for the migration of a Pt cluster on (c) SH-SWCNTs and (d) OH-SWCNTs. The gray, blue, yellow, and red atoms are carbon, platinum, sulfur, and oxygen, respectively. Reprinted with permission from ref.261.Copyright © 2011, Royal Society of Chemistry and from ref.262. Copyright © 2012, Royal Society of Chemistry.

of surface functional groups on carbon-based support is a promising methodology that can drastically increase the Pt tolerance against harsh ORR work environment.

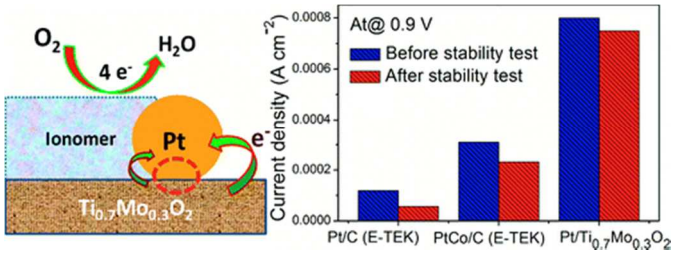

Figure 24. Stability characterization of $Pt/Ti_{0.7}Mo_{0.3}O_2$ and commercial Pt/C (E-TEK) and PtCo/C (E-TEK) catalysts at 0.9 V before and after stability by 5000 potential cycles. The electrode rotation rate was kept at 1600 rpm, with a sweep rate of 1mV/s in 0.5M H_2SO_4. Reprinted with permission from ref. 280.Copyright © 2011, American Chemical Society.

Although the above nanostructured carbon materials show a several fold lower intrinsic corrosion rate, they still do not prevent irreversible carbon oxidation at high electrode potentials. Recently, the electrocatalytic systems based on Pt NPs supported on non-carbonaceous materials such as WC,[266-268] WO_x,[269-271] TiO_2,[272, 273] TiC,[274] ITO[275, 276] RuO_2-SiO_2[277] and TaB_2[278] have been studied by several research groups. Their results indicated that the electrocatalytic activities of Pt could be significantly improved due to the strong metal/support interaction (SMSI) between Pt NPs and the supporting materials. It is widely recognized that SMSI can drastically cause the electronic states or Fermi level of the Pt nanoparticles to shift up or down, thereby affecting the activity and durability of the catalyst.[279,280] For example, Hwang et al. used noncarbon $Ti_{0.7}Mo_{0.3}O_2$ as a novel functionalized cocatalytic support for Pt.[280] The novel nanostructure $Ti_{0.7}Mo_{0.3}O_2$ support with "electronic transfer mechanism" from $Ti_{0.7}Mo_{0.3}O_2$ to Pt could modify the surface electronic structure of Pt, owing to a shift in the d-band centre of the surface Pt atoms, as shown in Figure 24. Furthermore, Pt/ $Ti_{0.7}Mo_{0.3}O_2$ exhibited much higher stability than commercial Pt/C after potential cycling, which was attributable to the SMSI between Pt and $Ti_{0.7}Mo_{0.3}O_2$. Albeit many non-carbonaceous materials appear promising for making highly efficient electrocatalytic systems of ORR, some obstacle issues (such as small specific surface area and limited conductivity) are still under further investigations. The elaborately functionalized Ti_3AlC_2 support material (Figure 25a) reported by Wei et al. owed excellent electric conductivity comparable to carbon black, as shown in Figure 25b.[281,282]Electronic structure changes of Pt NPs was also found in Pt/Ti_3AlC_2, as clarified by DFT calculations. The catalytic activity of the Pt/e-TAC, assessed by the half-wave potential, showed no significant decrease after durability test (Figure 25c).

All the potential routes detailed above offer new perspectives on the ORR at fuel cell cathodes based on Pt-containing catalysts. They have the advantage of preferable facets, optimal surface chemisorption properties, robust structures, large surface areas, or the opportunity to eliminate or alleviate catalyst aggregation and recombination problems.

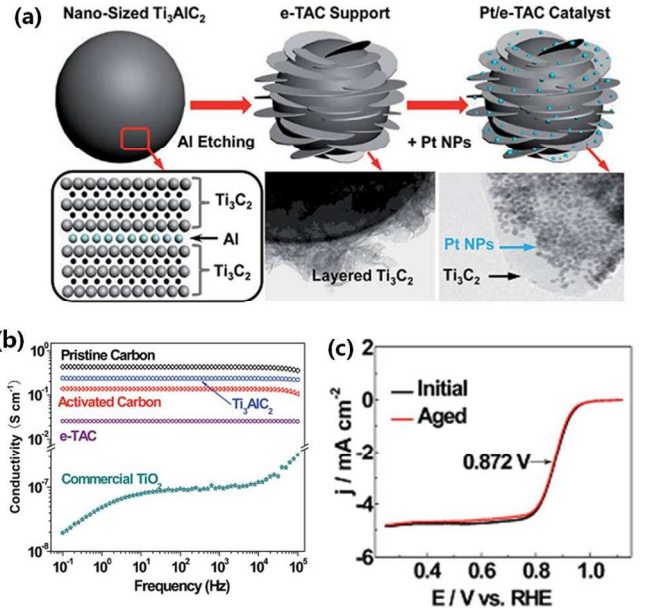

Figure 25. (a) Schematic of Pt/e-TAC catalyst formation. (**b**) Electrical conductivity of pristine carbon, activated carbon, commercial TiO_2, pristine Ti_3AlC_2 and the e-TAC support.(c) ORR polarization curves for Pt/e-TAC before and after the ADT cycling (recorded in O_2-saturated 0.1M $HClO_4$ at 1600 rpm and with a scan rate of $10mVs^{-1}$). Reprinted with permission from ref.282.Copyright © 2014, Royal Society of Chemistry.

4. Pt-free catalysts

4.1 Cheaper Noble Metal Catalysts

Palladium (Pd)[283], Iridium (Ir)[284], Ruthenium (Ru)[285]and Silver (Ag)[286] based catalysts have been widely investigated as alternatives to Pt. Among them, Pd has received considerable attention in comparison with other metal catalysts because of its relatively high ORR activity, stability, abundance, and low cost.[287-289] With a much lower price for Pd ($654.1/Oz.) as compared to Pt ($1796.9/Oz.), the cost of fuel cells could be considerably lowered by switching from Pt- to Pd-based catalysts.[290] However, the ORR activity of conventional Pd nanoparticles is at least five times lower than that of their Pt counterparts, preventing their direct used as an efficient ORR catalyst.[290,291] Similar to the case of Pt-based electrocatalysts, improved catalytic performance for Pd-based can be achieved via appropriate modification of its electronic structure. One way to modify the electronic structure of Pd is to add foreign metals to Pd.[292] Studies on energetics of oxygen dissociative adsorption on 1nm Pd shells with a series of core metals have shown that tuning charge redistribution and surface strain can change the d-band centre of the Pd shell and, thus, oxygen dissociative adsorption energy. For this reason, core/shell Cu/Pd, Co/Pd, and Mo/Pd systems may be similar to Pt in catalyzing ORR.[293] Using DFT calculations, Lu and Sun et al. predicted that core/shell M/CuPd (M = Ag, Au) NPs with a 0.8 or 1.2nm $CuPd_2$ shell have similar but optimal surface strain and composition and may surpass Pt in catalyzing ORR, as shown in Figure 26.[294] The synthesized $Ag/Cu_{37}Pd_{63}$ and $Au/Cu_{40}Pd_{60}$ catalysts with 0.75 and 1.1 nm shells were more efficient catalysts than the commercial Pt catalyst, with their mass activity reaching 0.20A/mg of noble metal at -0.1V vs.

Ag/AgCl; this was over 3 times higher than that from the commercial Pt. Koenigsmann and co-workers fabricated Pd_9Au nanowires with superior catalytic performance for ORR, compared with commercial Pt nanoparticles.[295]

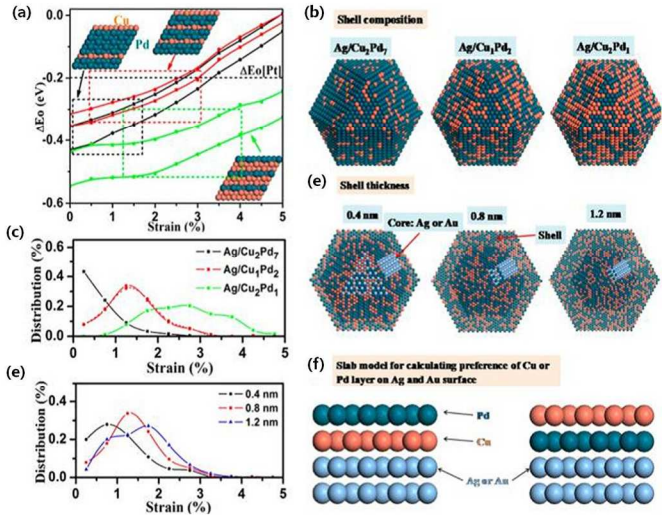

Figure 26. (a) ΔE_O as a function of strain and composition. Black, red, and green curves represent Cu/Pd atomic ratios of 2/7, 1/2, and 2/1, respectively. Several curves in each color correspond to various fcc hollow sites for O adsorption. ΔE_O on the Pt(111) surface is indicated by the dashed horizontal line. Black, red, and green boxes outline the possible ΔE_O values on Ag/Cu2Pd7, $Ag/CuPd_2$, and Ag/Cu_2Pd NPs, respectively. (b),(c) Models of core/shell NPs for various shell compositions with a shell thickness of 0.8 nm (b) and evaluated distribution of surface strain on these core/shell NPs (c). The dashed curve in (c) indicates $Au/CuPd_2$ NPs. (d, e) Models of core/shell NPs for various shell thickness with a composition of $CuPd_2$ (d) and evaluated distribution of surface strain on these core/shell NPs (e). (f) Slab models for calculation of Pd|Cu|M (left) and Cu|Pd|M (right) interfacial energies. Reprinted with permission from ref.294.Copyright © 2014, American Chemical Society.

Facet engineering would be able to drastically enhance the activity of Pd nanocrystals and thus lead to the development of Pd-based catalysts for ORR. A recent study by Kondo et al. demonstrated that the ORR activity on Pd single crystals followed a trend opposite to that of Pt, i.e., Pd (110) <Pd(111)<Pd(100), suggesting that the Pd(100) surface offers the most active sites for ORR.[296] However, Xiao et al. proposed that the Pd(110) is more active than other sites based on their theoretical calculations.[297] Shao and Xia et al. thoroughly studied the structure dependence of ORR activity for shape-controlled Pd nanocrystals with a particle size ~6 nm.[298] The Pd cubes enclosed by {100} facets were one order of magnitude more active than Pd octahedral enclosed by {111} facets towards ORR, as shown in Figure 27. Their results demonstrated that the ORR activity was strongly dependent on the atomic structure on the surface of a Pd nanocatalyst, guiding the design of more active catalysts for ORR and other applications.

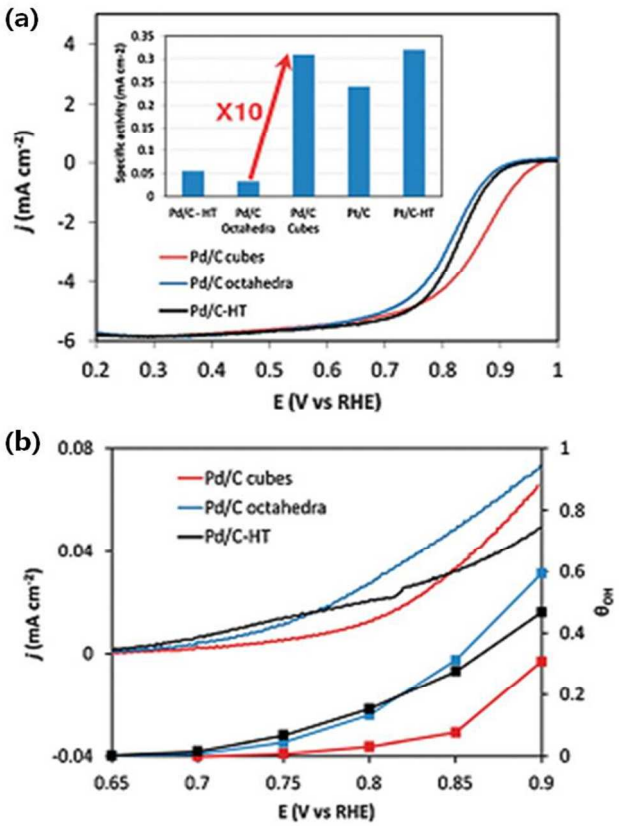

Figure 27. (a) ORR polarization curves for Pd cubes and octahedra supported on carbon black in 0.1M $HClO_4$. Inset: Comparison of specific activities for Pd/C cubes, Pd/C octahedra, Pd/C-HT, Pt/C, and Pt/C-HT at 0.9V. (b) Anodic polarization curves in $0.1MHClO_4$ and coverage of OH of Pd/C cubes, Pd/C octahedra, and Pd/C-HT after subtracting the double layer current density. The currents were normalized to the electrochemical active area. Reprinted with permission from ref.298.Copyright © 2011, Royal Society of Chemistry.

The third approach to modify the electronic structure of Pd to find proper supports that can promote the reactivity of Pd and Pd-based catalysts via strong electron coupling between Pd and support. Chen strongly coupled Pd tetrahedron/tungsten oxide nanosheet hybrid nanomaterials ($Pd/W_{18}O_{49}$) by using organopalladium (I) complexes containing palladium−palladium bonds as precursors.[299]The authors found that although supportless Pd nanoparticles or $W_{18}O_{49}$ alone has low catalytic activity toward ORR, their hybrids exhibited not only surprisingly high ORR activity but also superior stability to Pt in alkaline solutions. The unusually high catalytic activity could be attributed to the strong chemical interaction and electronic coupling effects between the Pd nanocrystals and $W_{18}O_{49}$ nanosheets, which can weaken the interaction between Pd and the nonreactive oxygenated species and thus provide more active sites for O_2 adsorption and activation. Wei et al. showed that the activity and stability of Pd toward ORR could be enhanced by Pd-O-oxide covalent bonding when Pd was supported on exfoliated montmorillonite (ex-MMT) nanoplatelets.[300] As shown in Figure 28a, b, the Pd d-state shifted to lower energy after the Pd has been loaded onto a support. The downshift was greater for Pd on ex-MMT than for Pd on C, indicating that the Pd d-states on Pd_{13}/ex-MMT were closer to the Pt d-states on Pt_{13}. The thin PdO_x layer or the Pd-O

junction between Pd NPs and ex-MMT was experimentally observed and also confirmed by DFT calculations (Figure28c). Figure 28c showed that considerable overlap near the Fermi level exists between the Pd d-states and the $O(AlO_6)$ p-states, suggesting that the Pd d-states and $O(AlO_6)$ p-states share matching energies and enable electrons to transfer between them to form Pd-$O(AlO_6)$bonds. Upon the formation of the Pd-$O(AlO_6)$ bonds, the Pd 4d-states and the $O(AlO_6)$ p-states shifted toward lower energies. The lowered d-state energy indicated a larger gap exists between the d-orbital of Pd and the p orbital of O_{ads}. Thus, the bonding strength of O_{ads} on Pd was weakened. This diminished bonding strength allowed ORR on Pd/ex-MMT to proceed via an efficient pathway, similar to that on Pt. This newly developed Pd/ex-MMT catalyst showed excellent catalytic activity toward ORR, and the activity was comparable to that of commercial Pt/C catalysts. Furthermore, Pd/ex-MMT catalyst showed almost no degradation after the stability test. This investigation showed that the exfoliated montmorillonite nanoplatelets can efficiently modify the electronic structure of Pd NPs and therefore lead to enhanced catalytic activity and stability for ORR.

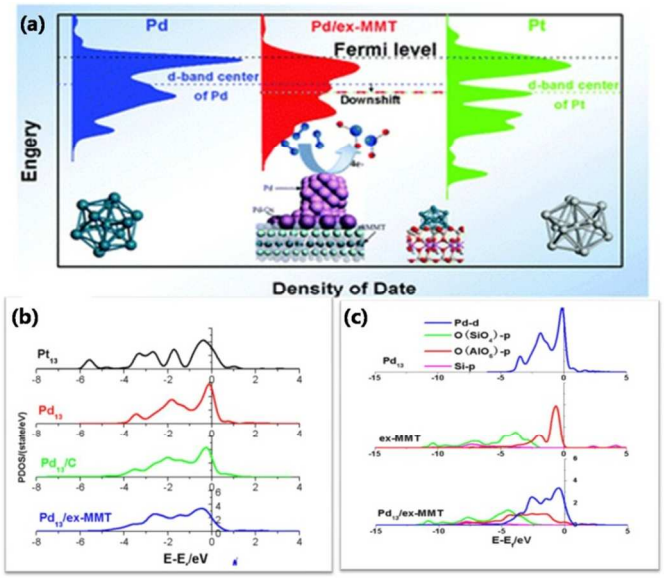

Figure 28. (a) the Ferml level for Pt_{13}, Pd_{13} and Pd_{13}/ex-MMT. (b) the PDOS of d-states for Pt_{13}, Pd_{13}, Pd_{13}/C, and Pd_{13}/ex-MMT.(d) the PDOS of the d-state and the p-state for Pd_{13} (without or on ex-MMT) and for the O and Si from the ex-MMT (with or without Pd_{13}), respectively. Reprinted with permission from ref. 300.Copyright ©2014, Royal Society of Chemistry.

Despite much progress has been achieved for Pd-based catalyst, the best activities reported for Pd are barely equivalent to typical Pt/C, with the best use of Pd appearing to be in combination with Pt as in the core-shell configurations discussed above. In any case, replacement of most of the Pt by Pd may not significantly address the cost issue, owing to demand/price fluctuations.[301]

4.2 Non-Precious Metal Catalysts

4.2.1 Transition Metal-Nitrogen-Carbon Catalysts Among various non-precious metal ORR catalysts, transition metal-nitrogen-carbon (M-N-C) complexes or composites are the most promising candidates due to their low price, high activity, durability and resistance to the methanol cross-over effect.[302]Research into M-N-C complexes for ORR started in 1964 when Jasinski et al. discovered that cobalt phthalocyanine showed ORR activity.[42] Later Yeager et al. reported the first M-N-C composites for ORR by the pyrolysis of non-N_4-marcrocycles precursors.[304]After that numerous efficient ORR catalysts based on different metal/N/C sources have been developed. Besides metal-N_4 macrocycles,[305,306] inorganic nitrogen sources (ammonia gas, sodium azide),[307-309] small organic molecules (acetonitrile, pyrrole, 1-methylimidazole etc.) [310-313]and nitrogen-containing polymers (melamine resin, PANI, poly-dopamine, etc.)[314-319] are commonly used N precursors. Compared with other nitrogen sources, the N-containing polymers which are more ordered than the small-molecule precursors, could possibly template the formation of a more ordered and thus more stable carbon-based active layer during heat treatment. Polypyrrole was used initially, but it was soon found that polyaniline-derived catalysts were more active and durable.[320]Zelenay group used polyaniline as a template in the preparation of a catalyst incorporating iron and cobalt (Figure 29).[314]They found that the polyaniline-Fe-C catalyst exhibits higher ORR activity than the polyaniline-Co-C catalyst. The best-performing catalyst in fuel cell testing, with an excellent combination of high ORR activity and long-term performance durability, was the mixed-transition-metal catalyst polyaniline-FeCo-C, The most active catalyst, polyaniline-FeCo-C, catalyzed the ORR at potentials within ~60mV of that delivered by state-of-the-art carbon-supported platinum, combining their high activity with remarkable performance stability for non–precious metal catalysts (700 hours at a fuel cell voltage of 0.4 volts) as well as excellent four-electron selectivity (hydrogen peroxide yield <1.0%). Recently, Dodelet group used a metal-

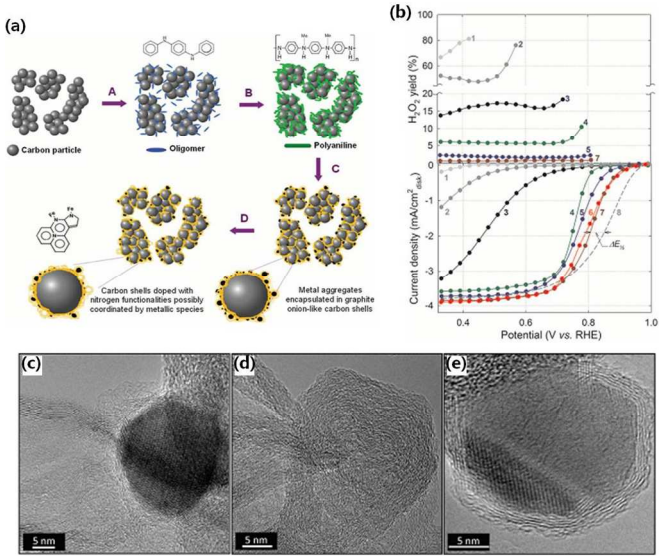

Figure 29. (a)Schematic diagram of the synthesis of PANI-M-C catalysts. (b) ORR polarization plots (bottom) and H_2O_2 yield plots (top) measured with different PANI-derived catalysts and reference materials: 1, Ketjen black EC-300J; 2, heat-treated carbon black; 3, heat-treated PANI-C; 4, PANI-Co-C; 5, PANI-FeCo-C(1); 6: PANI-FeCo-C(2); 7, PANI-Fe-C; 8, E-TEK Pt/C (20 $mg_{Pt}cm^{-2}$).(c) (d) (e) HRTEM image of PANI-FeCo-C. Reprinted with permission from ref.314.Copyright © 2011, American Association for the Advancement of Science.

organic framework consisting of zeolitic Zn imidazolate (ZIF-8) as the host for Fe and N precursors [iron(II) acetate and 1,10-phenanthroline (Phen)].[310]The prepared Fe/Phen/ZIF-8 catalyst exhibited a volumetric activity of 230Acm^{-3} at 0.8V (i_R-free).

Although above breakthroughs were attained by the careful selection of suitable nitrogen/transition-metal precursors and carbon supports as well as optimization of the synthetic conditions, achieving comparable activity and durability of the M-N-C catalysts with the state-of-the-art Pt/C catalyst remains a challenge. Two crucial factors govern the performance of M-N-C catalysts, as follows:
(I) the elemental composition and the interactions between different components, which determine the intrinsic nature of active sites. Currently, no consensus has yet been reached regarding the exact identity of the catalytic active sites in M-N-C catalysts, as discussed in section two. Two preponderant lines of thought in the research community are:(i) that nitrogen functionalities on the surface of the carbon-based catalysts are directly responsible for their ORR activity,[321-324] and (ii) that N-groups act as the coordinating environment for Fe- or Co-ions where the ORR takes place.[325-328] Despite the uncertain active sites, it is still believed that the ORR performance of M-N-C catalysts is strongly dependent on the carbon support, the source of metal and nitrogen, and the thermal treatment conditions. Many research efforts have been dedicated to correlate the final ORR activity with the experimental parameters.[329-332] With regard to the type of transition metals in the precursors, Fe and Co lead to the formation of the active centres with higher activity towards the ORR, when compared to other transition metals (e.g., Zn, Ni, Mn, Cu, Cr).[333]Furthermore, this two metals likely play different roles in contributing to the active-site formation during the synthesis. For instance, in Co-N-C catalysts derived from ethylene diamine (EDA) or polyaniline (PANI),[318]Co species appear to generate the active sites that have the electrochemical properties (e.g., onset potential, Tafel slope) similar to those exhibited by metal-free N-C catalysts. That means Co species may just assist in the nitrogen doping into carbon lattice, but do not directly participate in the active sites. Unlike for Co, there is increasing evidence to support an assumption that Fe species are able to be directly involved in the active sites stabilized by coordinating nitrogen and carbon, similar to a Fe-N_x moiety.[307,329] Furthermore, by simultaneously taking advantage of the catalytic properties of Co and Fe, it was found that bimetallic CoFe-based catalysts exhibit improved activity and performance durability for the ORR.[314,318,334] Xia and Sun et al. used DFT calculations to confirm that for the polyaniline-derived M/N/C system, the catalytic activities decrease in the sequence CoFe-PANI > Fe-PANI > Co-PANI.[335] This was due to a synergistic effect between heterogeneous metal atoms in CoFe-PANI, which facilitates additional electron donation from the active sites to the adsorbed oxygen reduction intermediates. The doping with cobalt might also decrease the HOMO (highest occupied molecular orbital)-LUMO (lowest unoccupied molecular orbital) gap in CoFe-PANI, making it more active. A better (in situ) characterization and understanding of the reaction mechanism for M-N-C catalysts is of utmost importance for further development.

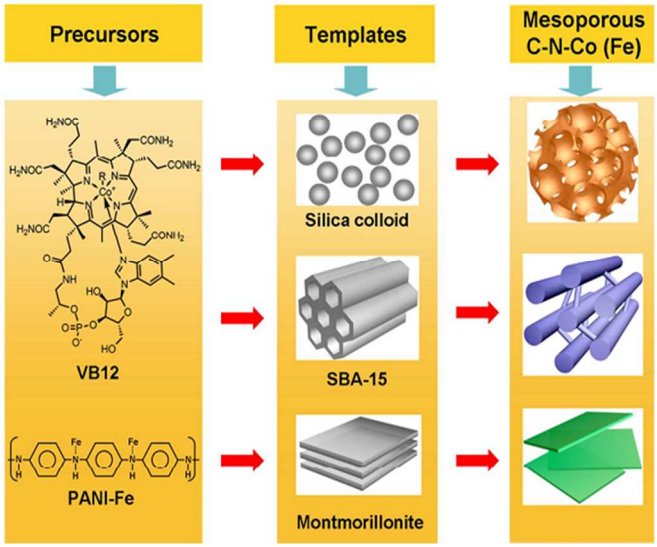

Figure 30. Templating synthesis of mesoporous C-N-Co (Fe) catalysts for ORR. Reprinted with permission from ref.336. Copyright © 2013, American Chemical Society.

(II) specific surface area and porous structure, which determine the accessible part of active sites and the transport properties of ORR-relevant species. The traditional method for preparing M/N/C catalysts involves direct pyrolysis of the mixture of nitrogen, carbon, and transition-metal precursors and frequently fails in controlling the porous structure, thus leading to limited exposure of the ORR active sites and relatively poor transport properties. Introducing well-defined nanoporous structures is an effective way to solve this problem. Müllen and Feng et al. prepared a family of mesoporous nonprecious metal catalysts for ORR in acidic media, including cobalt-nitrogen-doped carbon (C-N-Co) and iron-nitrogen-doped carbon (C-N-Fe), by employing vitamin B_{12} (VB_{12}) and the polyaniline-Fe (PANI-Fe) complex as precusors.[336] Silica nanoparticles, ordered mesoporous silica SBA-15, and montmorillonite were used as templates for achieving mesoporous structures (Figure 30). The most active mesoporous catalyst was fabricated from VB_{12} and silica nanoparticles and exhibited a remarkable ORR activity in acidic medium (half-wave potential of 0.79 V, only ~58mV deviation from Pt/C, high selectivity (electron-transfer number>3.95), and excellent electrochemical stability (only 9mV negative shift of half-wave potential after 10 000 potential cycles). The outstanding ORR performance of the prepared catalysts was strongly associated with their well-defined mesoporous structures, high BET surface area, and homogeneous distribution of numerous metal/nitrogen active sites.

In addition, the M-N-C catalysts prepared by pyrolysis as reviewed above are known to contain metal-rich particles encapsulated in graphitic carbon shells.[321] And it is assumed that the encapsulation phases contribute little to the ORR activity.[337]However, as reported by Bao and co-workers in a series of studies, [338,339] when metal nanoparticles are confined inside carbon nanotubes (CNTs), a unique host-guest electronic interaction changes the local work function of the CNT walls. As a result, catalytic functionalities can be achieved on the outside surface of the CNTs. For example, metallic iron nanoparticles confined within Pod-like CNTs showed enhanced

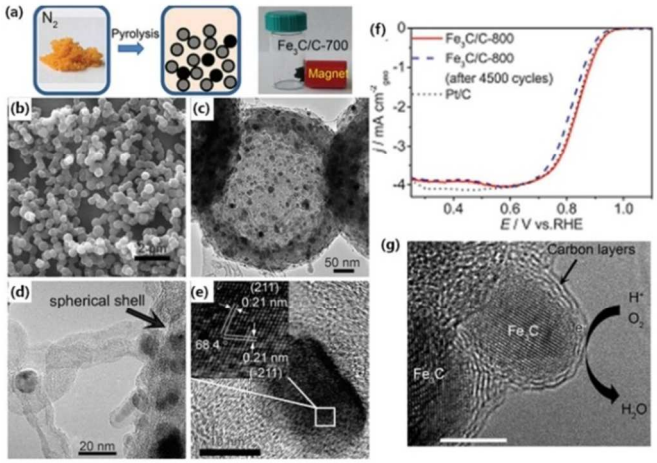

Figure 31. (a) Synthesis of Fe_3C/C hollow spheres. (b) SEM image of Fe_3C/C-700. (c) TEM image of one typical hollow catalyst sphere of Fe_3C/C-700. (d) TEM image of bamboo-like carbon nanotubes grown on the surface of the hollow spheres. (e) HRTEM image of a Fe_3C nano particle in Fe_3C/C-700 and the index crystal plane shown in the inset. (f) LSVs of Fe_3C/C-800 and Pt/C at 900rpm in O_2-saturated 0.1m KOH before and after 4500 potential cycles. Potential cycling was carried out between 0.6 and 1.0 V in N_2-saturated 0.1m KOH. (g) Oxygen reduction process on Fe_3C/C, the scale bar is 5nm. Reprinted with permission from ref. 340.Copyright © 2014 WILEY-VCH Verlag GmbH & Co. KGaA, Weinheim.

ORR activity compared to that of the pristine CNTs.[308] Recently, in an attempt to prepare the M-N-C-type catalyst under high pressure, Li and Xing et al. instead obtained a novel type of ORR catalyst in form of hollow spheres comprising uniform Fe_3C nanoparticles encased by graphitic layers with a negligible amount of nitrogen or metal on the surface (Figure 31).[340] The Fe_3C/C catalyst exhibited excellent ORR activity and stability in both acidic and alkaline media. Despite the fact that the encased Fe_3C nanoparticles were not in direct contact with the electrolyte, they still played a key role in the catalysis. This role was most likely defined by the synergetic interaction between the carbide and protective graphitic layers. In other words, the encased carbide nanoparticles activated the surrounding graphitic layers, making the outer surface of the carbon layer active towards ORR (as schematically illustrated in Figure 31g), which was similar to the situation of iron encapsulated within carbon nanotubes reported by Bao et al.. More importantly, even with negligible surface nitrogen or iron functionalities, the catalyst still exhibited excellent ORR activity, which provides a unique model material for probing the ORR active sites of this type of encapsulation catalysts.

4.2.2 Transition Metal Oxides, Chalcogenides, Nitrides and Oxynitrides Transition metal oxides, in particular manganese and cobalt oxides, [341-343] are another class of promising non-precious metal catalyst for ORR in alkaline solution. Manganese oxides (MnO_x), including MnO, MnO_2, Mn_3O_4, MnOOH, Mn_2O_3, and Mn_5O_8, have all been identified as high active ORR catalysts.[344-349] Since MnO_x can effectively catalyze the disproportionation reaction of HO_2^- to H_2O, it is possible for MnO_x to catalyze 4-electron reduction of oxygen in combination with another material active for 2-electron reduction of oxygen to peroxide.[350,351] Previous studies have revealed that the oxygen defects in crystalline MnO_x influence their catalytic activity for the ORR in alkaline conditions.[352] However, their potential for application in practical fuel cells is limited due to their poor electrical conductivity (10^{-6}~10^{-5} Scm^{-1}).[353] These problems can be solved by coating MnO_x onto functional materials with high conductivity. Ketjenblack carbon-supported amorphous MnO_x nanowires have been shown to be highly active electrocatalysts for ORR in alkaline solution, due to the abundant active sites for oxygen adsorption, together with other microscopic features (e.g. high density of surface defects). [354] The MnO_x-doped carbon nanotubes prepared by a simple electrochemical deposition method showed a remarkable ORR electrocatalytic activity, long-term stability and excellent resistance to crossover effects compared to a conventional Pt/ C catalyst. [355] Jaramillo et al. reported glassy carbon (GC)-supported Mn_3O_4 electrocatalysts for ORR, confirming that MnO_x sites contribute to all steps in ORR.[356] In the case of cobalt-based oxides, Dai et al. showed that covalent hybridization of cobalt oxide (e.g., Co_3O_4, CoO) with graphene oxide or CNT could lead to drastically improved ORR activity of cobalt oxide.[342, 357] The high catalytic activity of supported oxide nanoparticles was thought to be facilitated by the strong coupling between oxide nanoparticles and the highly graphitic carbon support, which however cannot be easily achieved, for example, by impregnation or precipitation methods. They also found that the strongly coupled CNT hybrid materials afforded a higher ORR performance than did the graphene counterpart, as shown Figure 32.[357]

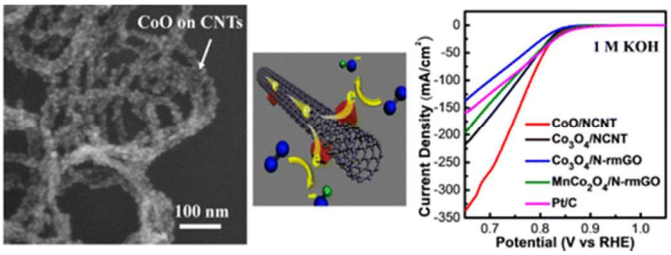

Figure 32. TEM of CoO/CNTs and polarization curves of various different catalysts. Reprinted with permission from ref. 357.Copyright © 2012, American Chemical Society.

Mixed valence oxides of transition metals with a spinel structure are regarded as an important class of metal oxides. In particular, substituted Co_3O_4 with Ni, Cu, and Mn have shown high activity and stability towards ORR.[358,359] Dai et al. developed a $MnCo_2O_4$/N-doped graphene hybrid material as a highly efficient ORR electrocatalyst in alkaline conditions.[343] A strongly covalent coupling between spinel oxide nanoparticles and graphene oxide sheets was also verified in $MnCo_2O_4$/N-doped graphene hybrid. Mn substitution was found to increase the activity of catalytic sites of the hybrid materials, further boosting the ORR activity compared with the pure Co_3O_4/N-rmGO hybrid. At the same mass loading, the $MnCo_2O_4$/N-rmGO hybrid could outperform Pt/C in ORR current density at potential <0.75V vs. RHE with stability superior to Pt/C. As demonstrated by Dai group, when some early transition metal oxide nanoparticles are supported on graphene or carbon nanotube, they can exhibit a promising ORR activity in alkaline media. But their activity drops significantly when these nanoparticles are supported on conventional carbon supports. Recently, Sun et al. reported that M(II)-substituted magnetite $M_xFe_{3-x}O_4$ (M = Mn, Fe, Co, Cu) nanoparticles (sub-

10nm)supported on conventional carbon support were catalytically active for ORR.[360] They also found that these $M_xFe_{3-x}O_4$ nanoparticles loaded on conventional carbon support showed the M(II)-dependent ORR catalytic activities with $Mn_xFe_{3-x}O_4$ being the most active followed by $Co_xFe_{3-x}O_4$,$CuxFe_{3-x}O_4$, Fe_3O_4. The ORR activity of the $Mn_xFe_{3-x}O_4$ was further tuned by controlling x and $MnFe_2O_4$ NPs were found to be as efficient as the commercial Pt in catalyzing ORR.

Other metal oxides, such as TiO_2,[361] NbO_2[362]and Ta_2O_5 [363]have also been found to be catalytically active for ORR. In recent years, great attention has been directed towards a different class of oxides, namely the perovskite family with the general formula ABO_3. The potential of these materials was shown already in the early 1970s,[364] but recent findings have sparked new interest in perovskite catalysts, as indicated by the increasing number of publications.[365] Given the easy tailoring of perovskite compositions by cation substitutions, a potential for promising catalytic properties exists. $Ba_{0.5}Sr_{0.5}Co_{0.8}Fe_{0.2}O_{3-\delta}$ (BSCF5582)-based complex perovskite oxide is being spotlighted as a competitive candidate of bifunctional catalyst in ORR and oxygen evolution reaction (OER) catalysis.[366] As a mixed electronic and ionic conductor, BSCF5582 exhibits fast oxygen exchange kinetics and ionic conductivity, facilitating the movement of oxygen anions through oxygen vacancies, which enables it to be proper for such diverse applications as oxygen membranes and intermediation temperature solid oxide fuel cell (IT-SOFC) cathode materials. [367-368] Shao-Horn et al. reported that any transition-metal oxide perovskite, which has an e_g-filling (σ*-orbital occupation) close to 1, shows the maximum ORR activity, on the base that the B-site transition-metal-oxygen covalency between metal-3d and oxygen-2p works as a criterion in determining catalytic activity.[366] A recent publication about double perovskites has shown that when the B site of the ABO_3 perovskite structure was partially occupied by Fe instead of Co, lower ORR activity was observed and the reaction mainly followed a 2-electron process.[369] Furthermore, previous studies on perovskites having the B site fully occupied by Co cations have reported a 4-electron process for ORR.[370-372] The investigation conducted by Fabbri et al. revealed that BSCF catalyzes the ORR at potentials lower than ~0.77V vs. RHE leading to a parallel formation of $HO2^-$ (2-electrons transferred) and OH- (4 electrons transferred) (in their case, the B site of BSCF is occupied by 80at% Co and 20at% Fe cations).[373] One possible explanation for the large ORR overpotential and hydroperoxide generation could be the insufficient availability of the active sites or partially blocked active sites on the surface. Recently, Shao-Horn et al. used pulsed laser deposition to fabricate well-defined surfaces composed of BSCF on thin-film $La_{0.8}Sr_{0.2}MnO_{3-\delta}$(LSMO) grown on (001)-oriented Nb-doped SrTiO3 (NSTO) and discussed their bifunctionality for both ORR and OER.[374] The combined overpotentials from both OER and ORR kinetics on BSCF|LSMO|NSTO could be as low as 0.7V, which rivals the intrinsic activities of state-of-the-art catalysts in the literature. Moreover, BSCF decoration enhanced the surface stability for ORR relative to LSMO|NSTO.

In the past decade, transition-metal chalcogenides (M-X, where M=Co, Ru, Re, or Rh and X=S, Se, or Te) have been studied as ORR catalysts. [375-380] Alonso-Vante et al. advanced the synthesis, electrochemical, and spectroscopic characterizations of these materials. Some of these compounds showed good activity toward ORR in acid. Cobalt sulfides have been investigated as ORR catalyst with the highest activity among all chalcogenides in acidic solution. Theoretical studies predicted that the electrocatalytic activity of Co_9S_8 is similar to that of Pt via a four-electron ORR pathway and S^{2-} provides an adsorption site for O following O-O bond scission.[377] Wu et al. developed a Co_9S_8-N-C catalyst for ORR in alkaline media.[376] The ORR activity of Co_9S_8-N-C catalysts was much higher than that of the-sate-of-the-art Pt/C 0.1M NaOH solution. Dai et al. synthesized a $Co_{1-x}S$/ reduced graphene oxide (RGO) hybrid material by a mild solution-phase reaction followed by a solid-state annealing step.[375] Strong electrochemical coupling of the RGO support with the $Co_{1-x}S$ nanoparticles and the desirable morphology, size, and phase of the $Co_{1-x}S$ nanoparticles mediated by the RGO template rendered the hybrid with a high ORR catalytic performance in acid.

Transition-metal nitrides and oxynitrideshave been also investigated for ORR catalysis applications as they have good electrical conductivities and corrosion resistance. The formation of nitrides favourably modifies the catalyst electronic structure so that the contraction of d-bands in Group 4–6 nitrides results in a greater electron density near Fermi level. This facilitates the donation of electrons to adsorbates such as oxygen.[381] Therefore, the formation of nitrides on the surface may make it easier for the catalytically active metal to reduce oxygen. Previously, ORR activities of monometallic nitrides/oxynitrides of Group 4-6 have been studied in acidic solution for fuel-cell applications. [381-385] ZrO_xNy and TaO_xNy were found to show moderate ORR activities and excellent chemical stabilities in sulphuric acid.[384,385] Studies on MoN and Mo_2N demonstrated that they had comparatively good ORR activities and the ORR proceeded through a nearly four-electron process.[382,383] Compared to monometallic oxynitrides, bimetallic oxynitrides are potentially better ORR catalyst candidates since their catalytic properties can be enhanced by the combination of multiple active species or by the tuning of electronic states. Indeed, bimetallic Co-W-O-N catalysts supported on carbon were found to have an onset potential of 0.749V in 0.5M H_2SO_4, an activity substantially higher than monometallic W and Co oxynitrides.[386] Recently, Khalifah et al. reported that the $Co_xMo_{1-x}O_yN_z$ catalysts synthesized by a solution impregnation method followed by ammonolysis exhibit moderate ORR activity in acidic conditions and superb activity in alkaline conditions, which is only 0.1 V away from the performance of Pt/C.[387]

The rise of alkaline polymer electrolyte membrane fuel cell and the significant progress in developing alkaline polymer electrolyte membrane[388] render these transition metal oxides, chalcogenides, nitrides and oxynitrides as very competitive candidates for ORR. However, the current ORR activity of these catalysts is still far lower than that of Pt. Inherent low conductivity and poor stability in acid medium are the important drawbacks that limit their application as ORR cathodes in fuel cell. Future improvement of their ORR activity and stability via optimizing and controlling their size, phase, and morphology is necessary.

4.3 Metal-Free Catalysts

Although Pt alloys or non-noble metals have been developed as substitute catalysts for ORR, they still suffer from multiple disadvantages, such as low stability under fuel cell conditions, vulnerability to fuel crossover, and harmfulness to the environment.[389] Thus, the ongoing search for metal-free catalysts for ORR has attracted much attention. Metal-free

catalysts typically consist of various carbon-based materials such as graphite, graphene, carbon nanotubes and ordered mesoporous carbon. With the progress in tuning intrinsic property of these carbon material with a series of heteroatoms, such as B,[390] N,[391-396] S,[397] Se,[397] P,[398,399] and F[400], plenty of doped carbon-based catalysts, including dual-doped[401-403] and trinary-doped[404] carbon materials, have been reported. However, the catalytic mechanism of different doped carbon catalysts is complicated and still remains unrevealed. Dai et al. [391] proposed that the high activity of nitrogen-doped carbon (NC) catalysts may be attributed to the larger electronegativity of N (electronegativity of nitrogen: 3.04) with respect to C atoms (electronegativity of carbon: 2.55), and the creating of positive charge density on the adjacent C atoms. These factors may result in the very favorable adsorption of O_2. While this explanation is not suitable for other carbon materials doped with the low electronegative atoms such as P-doped (electronegativity of phosphorus: 2.19) and B-doped (electronegativity of boron: 2.04) carbon materials, which have also shown pronounced catalytic activity. Recently, theoretical studies using simulation calculations have confirmed that breaking the electroneutrality of graphitic materials to create charged sites favorable for O_2 adsorption is a key factor in enhancing ORR activity, regardless of whether the dopant is electron-rich (e.g. , N) or electron-deficient (e.g. P, B).[390] When sulphur or selenium, whose electronegativities are similar to the carbon (electronegativity of sulfur: 2.58, electronegativity of selenium: 2.55), is used as dopant species, another explanation for the enhanced ORR activity has to be proposed. Very recently, Zhang et al. reported that the spin density should be more important in determining the catalytic active sites through using DFT calculation, compared to atomic charge density.[69] Zhang's theory may be appropriate for explaining the enhancement effect of S and Se doping. The detailed mechanisms for various different dopants need to be further investigated.

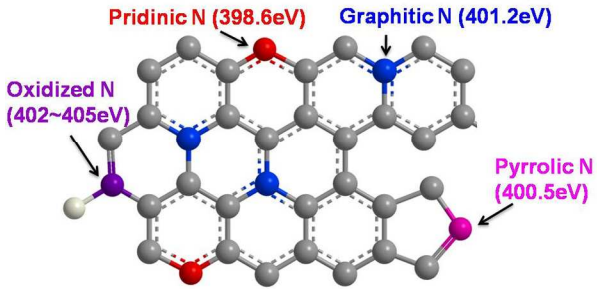

Figure 33. Schematic representation of the common N bonding configurations. Reprinted with permission from ref.429. Copyright © 2013 WILEY-VCH Verlag GmbH & Co. KGaA, Weinheim.

Among above various dopant, N dopnant is most popular. In NC-based catalyst, the molecular structure of nitrogen seems to be a critical role in affecting the properties of the N-doped nanocarbon materials. A schematic representation of the common N bonding configurations is illustrated in Figure 33. Pyridinic N and pyrrolic N atoms are located at edge or defect sites; they do not increase the number of electrons in the delocalized π-system. Graphitic N atom substitutes carbon atom within the graphitic structure. Therefore, they have the same configuration as graphitic carbon atoms but they introduce extra electrons in the delocalized π-system. Pyridinic N can also be present in its oxidized form. These different N-functionalities are often coexisting and their concentrations are practically adjustable.[405,406] Among these N functionalities, pyridinic, pyrrolic, and graphitic N are generally believed to contribute to the ORR catalytic activity. However, the exact contribution of single N functionality for the ORR is still a matter of debate. Some researchers assume that pyridinic N is involved in the ORR activity,[407,408] while others propose graphitic N.[409,410] A recent study suggested that both sites might be equally important for the ORR since it was proposed that graphitic and pyridinic N sites can interconvert during the ORR.[411] Besides the type of nitrogen site, it has also been observed that other properties, such as the amount of carbon edge sites (e.g. influenced by the type of metal catalyst used in the synthesis of carbon nanotubes), the total N content, the surface area and the degree of graphitization, can influence the resulting ORR activity.[412]

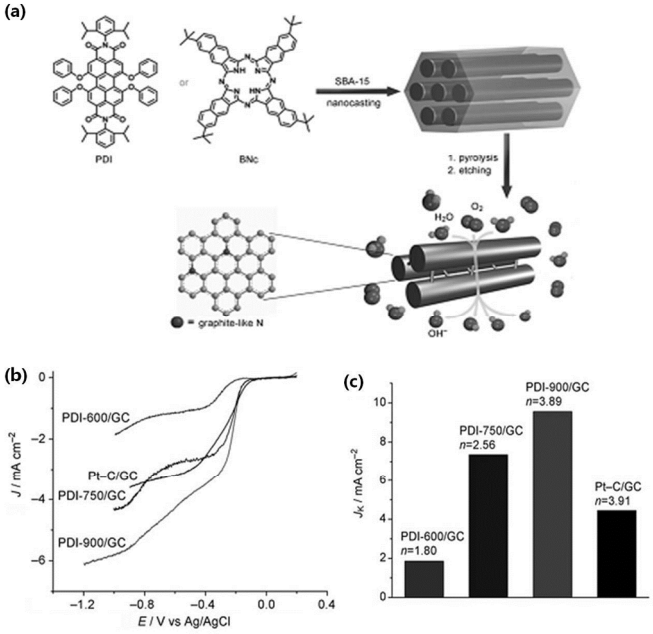

Figure 34. Preparation of nitrogen-doped ordered mesoporous graphitic arrays as metal-free catalysts for the ORR. Reprinted with permission from ref.395. Copyright © 2010 WILEY-VCH Verlag GmbH & Co. KGaA, Weinheim.

In general, NC is prepared mainly through three different routes. First route is in-situ introduction of nitrogen atom into carbon framework upon the formation of graphitic plane via processes like chemical vapor deposition (CVD).[413-415] This approach is often able to make high nitrogen content in carbon materials, but is not practicable for mass production of the catalysts for genuine application. Second one is post-heating graphitic carbon, including carbon nanotubes (CNTs), graphene and fullerene, with nitrogen-containing substances.[416, 417] Because of incorporation resistance from pre-existing graphitic structure, the nitrogen fraction is usually too insufficient to make enough catalytic sites. The last approach is direct pyrolysis of organic nitrogen-rich precursors with well-defined uniform N-containing structures, such as graphitic carbon nitride,[418] melamine foam[419] and polymer framework.[420,421] The last approach is the most popular method used nowadays due to its facile-managed preparation technology. However, direct pyrolysis of the nitrogen precursors at high temperature frequently leads to remarkable loss of active N species and fails

in controlling the inner porous structure, thus leading to limited formation of the ORR active sites and relatively poor transport properties. Previously, mesoporous-alumina-assisted and mesoporous-silica-template-assisted nitrogen incorporation, which can improve the surface area of the NC via introducing nanoporous structures and preserve a high content of N in synthesized NC materials, have been reported.[418]For instance, Müllen and Feng et al. fabricated nitrogen-doped ordered mesoporous graphitic arrays (NOMGAs) on the basis of using ordered mesoporous silica (SBA-15) as the template (Figure 34).[395]The unique features of the resulting NOMGAs, including a high surface area and a graphitic framework with a moderate nitrogen content, led to high electrocatalytic activity, excellent long-termstability, and resistance to crossover effects for ORR. These properties were superior to those observed for the commercially available catalyst Pt/C. However, these template-assisted methods require complicated synthesis procedures, thus hindering their scalable production. Recently, metal-organic frameworks (MOFs) and covalent-organic materials (COMs) have been used as precursors to yield highly nanoporous carbons due to their diverse structures, high surface area, large pore volume and various pore sizes.[422-425] Cao et al. fabricated zeolitic imidazolate frameworks (ZIF, a sub-family of MOFs, consist of transition metal ions, such as Zn^{2+} and Co^{2+}, and imidazolate linkers, which can form 3D tetrahedral frameworks resembling zeolite topologies) derived in situ nitrogen-doped porous carbon materials (ZIF-derived carbons) by carbonizing the ZIF-7/glucose composites.[426]This nanoporous NC showed comparable ORR electrocatalytic activity to commercial 20% Pt/C in 0.1M KOH. Owing to the versatility of MOF structures, the MOF-derived porous carbons would significantly broaden the family of nanoporous carbons with novel structures and multifunctional properties in the future.

Despite the improved surface area and total N contents, the ORR activities of the resulting porous NC materials as mentioned above were still significantly lower than that of Pt/C in acid environment, even when the total N content was as high as 10.7atm%.[427] In fact, excessively high N content leads to low electronic conductivity due to the interruption of π-π conjugation of doped carbon materials, which is unfavourable for electrochemical process. When the total N content reaches to an appropriate point, the total amount of nitrogen species may not be as important for inducing the ORR activity as the relative distribution of the N species with respect to each other. With regard to different types of nitrogen, the nitrogen incorporated into quaternary N in tetrahedral sp^3 hybridization with a 3D structure, which is quite different from the nitrogen incorporated into pyridinic and pyrrolic N in planar sp^2 hybridization due to the different torsion angle of the C-N bond (i.e., 0° for planar sp^2 and 60° for tetrahedral sp^3 nitrogen),[428] would interrupt the π-π conjugation of doped carbon materials and thus generating an intrinsic barrier that impairs a continuous pathway for electron transport along them. Recently, Wei et al. presented a novel strategy for the selective synthesis of pyridinic- and pyrrolic-nitrogen-doped grapheme (NG) by the use of layered montmorillonite (MMT) as a quasi-closed flat nanoreactor (Figure 35a).[429]The confinement effect of MMT extensively constrained the formation of quaternary N because of its 3D structure but facilitated the formation of pyridinic and pyrrolic N. The final content of planar N sites was inversely proportional to the interspace width (δ) of the MMT. Furthermore, the confinement effect of MMT could also mitigate serious loss of N species during the high temperature heat treatment. According to the results, the final content of planar N sites reached a maximum of 90.27% with the MMT interspace width at 0.46 nm. While the content of quaternary and oxidized N was restricted to less than 9.7% because of steric hindrance. Planar N doped graphene exhibited a low electrical resistance and high electrocatalytic activity (Figure 35b, c). The half-wave potential of ORR was less than that of state-of-the-art carbon-supported platinum by only 60 mV in an acidic electrolyte (Figure 35c). This synthetic method with elaborately designed procedures provides a simple but efficient and versatile approach to the low-cost mass production of NC materials.

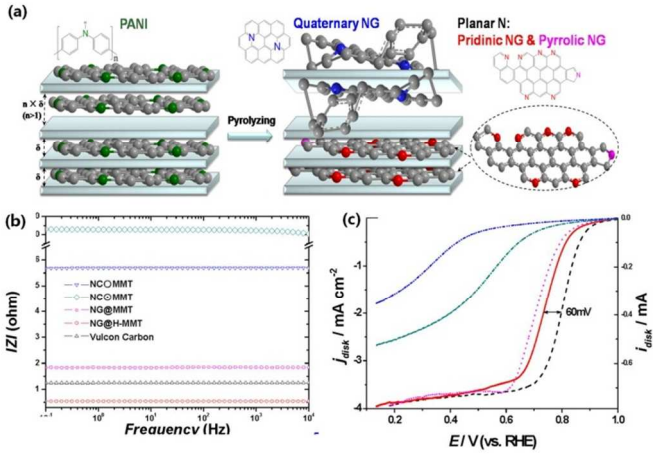

Figure 35. (a) Schematic representation showing the selectivity inside and outside of MMT during NG synthesis. (b) Bode spectra obtained through the application of a sine wave with an amplitude of 5.0mV from 10mHz to 10kHz for different catalysts (c) ORR polarization for different catalysts in O_2-saturated 0.1M $HClO_4$. Reprinted with permission from ref. 429.Copyright © 2013 WILEY-VCH Verlag GmbH & Co. KGaA, Weinheim.

Other carbon-based catalysts with novel nanostructures have been also investigated.[430-434] For instance, as both CNT and graphene can be doped with nitrogen in a controlled way, integrating their benefits simultaneously may provide a new opportunity to develop advanced metal-free carbon catalysts.[430,433] Most recently, Wei et al. demonstrated the synthesis of novel N-doped graphene/single-walled CNT hybrids (NGSHs) by a facile and cost-favorable one-step CVD method.[433] Layered double hydroxides (LDHs), which are a kind of hydrotalcite-like materials composed of positively-charged layers and charge-balancing interlayer anions, are employed as the bifunctional catalysts for NGSH formation (Figure 36). The FeMo-MgAl LDHs derived bifunctional catalysts embedded with thermally stable Fe NPs not only served as an efficient catalyst for the growth of N-doped SWCNTs, but also supplied a lamellar substrate for the templated deposition of N-doped graphene. The as-fabricated NGSHs possessed not only large surface area with high porosity but also high graphitic degree. They demonstrated a high ORR activity, much superior to two constituent components and even comparable to the commercial 20 wt% Pt/C catalysts with much better durability and resistance to crossover effect. Thus, a synergistic effect between graphene and CNT to enhance electrochemical activity is very likely.

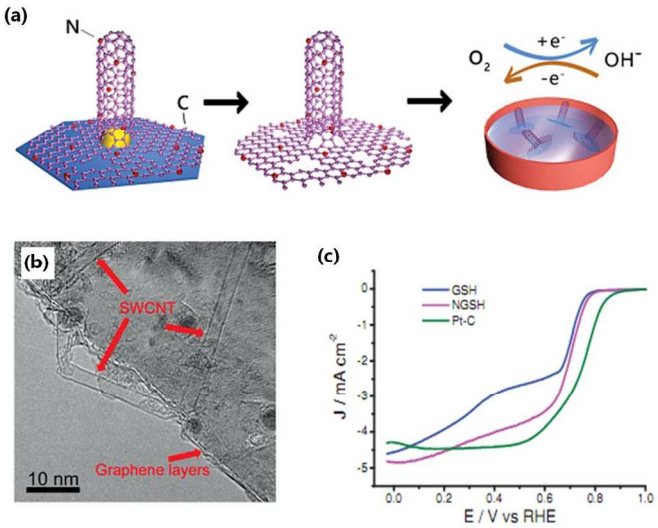

Figure 36. (a) Schematic illustration of the preparation of the nitrogen doped graphene/carbon nanotube hybrids (NGSHs). (b) TEM image of the NGSHs. (c) ORR polarization for graphene/SWCNT hybrids (GSHs), NGSHs and Pt/C supported on GC electrodes at a rotating rate of 1225 rpm. Reprinted with permission from ref.433.Copyright © 2014 WILEY-VCH Verlag GmbH & Co. KGaA, Weinheim.

It is worthy to point out that while such studies of the ORR on non-metallic heteroatom-doped carbon are advertised as "metal-free", there is typically no sufficient effort to characterize the doped materials to verify that they are indeed free of any trace metal. The effect of "trace metal" should not be ignored especially when those "metal-free" materials are prepared by using some metals during the synthesis process, such as production of graphene oxide by Hummers method and carbon nanotube by catalytic CVD method, or employing biomass or natural materials as precursors or templates. Recently, Masa et al. reported that the trace metal residues were responsible for the electrocatalytic effect in ORR at amorphous carbon surfaces.[435] They found that the metal-free catalysts that were synthesized without the involvement of any metal precursors over the entire synthesis cycle did not show as high ORR activity as the catalysts that were prepared by deliberate addition of trace metal precursors, or via synthesis routes that involved the use of metal precursors. In particular, adding Fe to a metal-free nitrogen-doped carbon catalyst in concentrations as low as 0.05% had significant influence on the ORR activity and selectivity of the catalyst. With regard to the preparation of graphene, a well-known "metal-free" catalyst, the Hummers oxidation method is usually applied. This process involves the use of permanganate oxidant to obtain an intermediate material, graphite oxide, prior to a reduction /doping step to give graphene.[436] It is known for decades that graphite contains large varieties of metallic impurities with a contribution up to 2wt%of the material.[437-445] These impurities consist of Fe, Ni, Co, Mo, Mn, V,and Cr. It has been previously shown by Compton and others that these metallic impurities within sp^2 carbon nanomaterials dramatically influence the electrocatalytic properties of the nanomaterials and that they can, in some cases, dominate the electrochemistry of the materials even when present at only trace levels.[446-450] Very recently there was an important report made by Pumera et al. arguing that the claimed "metal-free" electrocatalysis of ORR on heteroatom-doped graphene is caused by trace metallic impurities presented within the graphene materials.[451] In order to highlight the profound influences of residual manganese-based metallic impurities on ORR performance, they employed the Hummers oxidation method (the product was denoted as G-HU) and the Staudenmaier oxidation method (using a chlorate oxidant to produce hydrazine-reduced graphene, denoted as G-ST) to prepare two different graphene materials. The amount of metallic impurities present in the graphite starting material as well as in the graphene products were determined by inductively coupled plasma mass spectrometry (ICP-MS) analysis and summarized in Figure 37. To better understand the electrocatalytic behavior of the graphene materials, initial investigations on the electrochemistry of metal oxide nanoparticles (e.g., Fe_3O_4, NiO, Co_3O_4 and MnO)-modified glassy carbon electrodes (GC) towards ORR in KOH electrolyte solution were carried out. They found that the ORR onset potentials using these metal oxides were practically indistinguishable from that obtained with the bare GC with the striking exception of MnO_2. MnO_2-modified GC electrodes showed, in fact, a significant onset potential shift of 173mV, which indicated a clear catalytic behavior of MnO_2 for ORR.

Table 1: Content of metallic impurities (ppm) in the starting natural graphite and the graphene materials prepared by Hummers method (G-HU) and Staudenmaier method (G-ST) as determined by ICP-MS analysis.

Impurity	Graphite	G-HU	G-ST
Fe	4224	927.6	1685.9
Co	3.3	0.3	7.1
Ni	33.7	18.0	13.8
Mn	24.9	8311.3	17.9

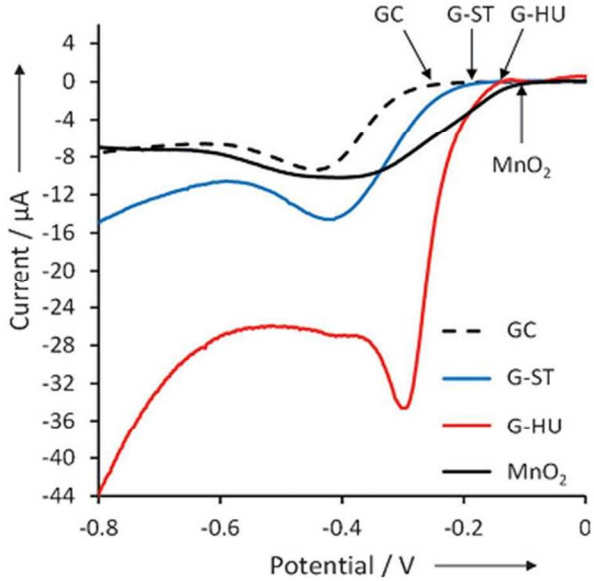

Figure 37. Linear sweep voltammograms recorded in air-saturated 0.1M KOH solution using a bare glassy carbon electrode (black-dashed line) and a GC electrode modified with G-HU (red line), and G-ST (blue line) graphene materials. Scan rate: 0.1V/s. Reprinted with permission from ref.451.Copyright © 2013 WILEY-VCH Verlag GmbH & Co. KGaA, Weinheim.

Thereafter, they investigated the behavior of the prepared graphene materials. As seen from Figure 37, G-HU rich in Mn-based impurities (>8000ppm) showed an onset potential at ~134 mV, which has the largest potential shift of about 133mV as compared to the GC. The graphene prepared by the Staudenmaier method, consisting of a very low content of Mn-based impurities (about 18ppm), gave an onset potential at ~183 mV, which was about 50mV more negative than that recorded for G-HU. These results suggested that the presence of Mn-based impurities in graphene causes a catalytic effect towards ORR and a catalytic effect is evident even for the G-ST which despite a Mn content as low as 18ppm (0.0018wt%) showed a potential shift of about 80mV in comparison to the bare GC electrode. This is a clear indication that even a slight trace of Mn metallic impurities in grapheme materials is sufficient to alter or dominate their electrocatalytic properties towards ORR. In light of these findings, they advocated that for all "metal-free" catalytic reactions, elemental analysis of metal contents should be provided to support the "metal-free" claims.

Despite tremendous effort has been made for development of Pt-free catalysts, a large majority of these Pt-free catalysts only exhibit comparable ORR performances to Pt/C in alkaline media. Developing a non-precious metal ORR catalyst with high activity, practical stability, and good four-electron selectivity in acidic media still remains a challenge.

5. Conclusions

In the present review, the significant potential of ORR catalyst for fuel cell applications was exhibited. The design of a new catalyst for oxygen reduction is closely related to the development of either new Pt-based systems to improve catalytic efficiency or Pt-free structures. The recent search for advanced catalysts has led to some exciting advances in our understanding of the catalytic nature, allowing more rational tuning of the catalytic properties via controlled synthesis. For Pt-based catalyst, highly active Pt-based catalysts have been prepared by rationally manipulating the surface chemiadsorption property of the Pt-based catalysts via tuning the exposed facets or alloying Pt with other transition metals. Further modulating the size, compositional profile and morphology can boost the catalytic characteristics of the Pt-based catalysts. Although tangible gains have been achieved in the continued development of these Pt-based nanocatalyst systems, generating viable, permanent solutions to many inherent performance issues (for example, the specific activity of commercial Pt catalysts is considerably lower than that of bulk Pt) continues to remain elusive. Significant advances have been achieved in the preparation technologies of nanoparticles with well-defined size, shape, compositional profile and morphology, as mentioned in the review, however, how to scale up the synthesis and bridge the gaps between the research studies in the lab and industrial applications to obtain the nanoparticles in large quantities while maintaining uniformity and precise control of their sizes and shapes still remain as a serious challenge. In addition, the preservation of structural integrity of these Pt-based systems is still a difficulty, due to the deformation and leaching of non-precious metal specieses or detachment of nanoparticles from the support under long-term harsh working conditions. Modifying Pt-based nanoparticles with elaborately selected organic or inorganic matters and choosing a robust support can not only improve the activity of the catalyst due to the optimized Pt surface electronic structure but also achieve superior stability in some case, which provides another practical direction to address both activity and stability issues in the future. Obviously, there is still a lot to explore, in terms of their applications as commercial entities.

With regard to Pt-free catalysts, various other noble metal based catalysts (i.e. Pd, Ru) have been investigated as alternatives to Pt. These metals have minimal applicability; however, as it involves replacing one expensive metal catalyst with another less expensive metal with diminished performance. Non-precious metal and metal-free catalysts eliminate the dependency on noble metals completely and have recently shown dramatic ORR activity improvements. Among the many approaches being explored, nitrogen-doped carbon-based catalysts with or without transition metal involvement (M/N/C or NC) have received considerable attention. Although a vigorous debate is ongoing regarding whether metal atoms participate directly in active sites or merely catalyze their formation, the presence of nitrogen-dopants in carbon structures is indispensable for yielding much improved ORR activity, relative to pristine carbon materials. Despite metal-free carbons with nitrogen doping are capable of yielding high activity for the ORR, the presence of transition metal is essential to in situ generate highly graphitized carbon nanostructures, resulting in more active and durable catalysts. It is noteworthy that although these Pt-free catalysts are capable of efficiently catalyzing the ORR in alkaline media, they still suffer from the low activity and poor durability in acid. At this juncture, fundamentally understandings of the nature of the active sites and their relationship with catalyst active site structures and composition using both theoretical calculations (molecular/electronic level modeling) and experimental approaches are urgently needed to be proposed for tailoring new non-precious metal catalyst structures and ORR activity levels. Further optimizing the catalyst synthesis conditions in order to achieve high active density or utilization of the active sites may boost the ORR performance.

Although the current obtained catalysts are not able to cope with the significant challenges of clean energy technologies, the exploration and improvement in rational design of various nanostructured ORR catalysts (including the control of size, shape, composition, structure, and interface/surface engineering), and providing insights into the nature of the catalytic activity will have important technologies implications in not only ORR, but also in other important catalytic reactions.

Acknowledgements

This work was financially supported by China National 973 program (2012CB215500 and 2012CB720300), by NSFC of China (Grant Nos. 21436003, 21376283, 21376284, 21276291, 21176271 and 20936008) and by the Fundamental Research Funds for the Central Universities (CDJZR12228802).

Notes and references

The State Key Laboratory of Power Transmission Equipment & System Security and New Technology, School of Chemistry and Chemical Engineering, Chongqing University, Chongqing

1 W. Vielstich, A. Lamm, H. Gasteiger, Handbook of Fuel Cells: Fundamentals, Technology and Applications; Wiley: New York, 2003.

2 P. G. Bruce, S. A. Freunberger, L. J. Hardwick, J. M. Tarascon, *Nat. Mater*, 2012, **11**, 19.

3 F. T. Wagner, B. Lakshmanan, M. F. Mathias, *J. Phys. Chem. Lett.* 2010, **1**, 2204.
4 H. A. Gasteiger, S. S. Kocha, B. Sompalli, F. T. Wagner, *Appl.Catal. B* 2005, **56**, 9.
5 W. Yu, M. D. Porosoff, J. G. Chen, *Chem. Rev.* 2012, **112**, 5780.
6 B. James, J. Kalinoski, in DOE-EERE Fuel Cell Technologies Program-2009 DOE Hydrogen Program Review (www.hydrogen.energy.gov/pdfs/review09/fc_30_james.pdf).
7 J. Sinha, S. Lasher, Y. Yang, in DOE-EERE Fuel Cell Technologies Program-2009 DOE Hydrogen Program Review (www.hydrogen.energy.gov/pdfs/review09/fc_31_sinha.pdf).
8 K. Wipke, Controlled Hydrogen Fleet and Infrastructure Analysis: 2011 DOE Hydrogen Program Annual Merit Review and Peer EvaluationMeeting(http://www.hydrogen.energy.gov/pdfs/review11/tv001_wipke_2011_o.pdf)
9 A. T. Bell, Science, 2003, 299, 1688.
10 Y. Li, G. A. Somorjai, *Nano Lett.*, 2010, **10**, 2289.
11 F. Zaera, *Catal. Lett.*, 2012, **142**, 501.
12 F. Zaera, J. Phys. *Chem. Lett.*, 2010, **1**, 621.
13 G. A. Somorjai, H. Frei, J. Y. Park, *J. Am. Chem. Soc.*, 2009, **131**, 16589.
14 B. M. Weckhuysen, *Nat. Chem.*, 2009, **1**, 690.
15 P. Strasser, *J. Phys. Chem. Lett.*, 2013, **4**, 3273.
16 S. Palacin, *Energy Environ. Sci.*, 2011, **4**, 1238.
17 F. Jaouen, G. Wu, P. Zelenay, *Energ. Environmen. Sci.,* 2011, **4**, 114.
18 I. E. L. Stephens, I. Chorkendorff, *Energ. Environmen. Sci.,* 2012, **5**, 6744.
19 D. Wang, D. S. Su, Energ. Environmen. Sci., 2014, **7**, 576.
20 I. Katsounaros, K. J. J. Mayrhofer, *Angew. Chem. Int. Ed.*, 2013, **53**, 102.
21 Y. Bing, H. Liu, L. Zhang, J. Zhang, *Chem. Soc. Rev.*, 2010, **39**, 2184.
22 H. Zhang, Y. Xia, *Chem. Soc. Rev.*, 2012, **41**, 8035.
23 T. Zhang, A. B. Anderson, *Electrochim Acta*, 2007, **53**, 982.
24 A. B. Anderson, J. Roques, V. Stamenkovic, *J Phys Chem B*, 2005, **109**, 1198.
25 T. V. Albu, A. B. Anderson, *Electrochim Acta.*, 2001, **46**, 3001.
26 A. B. Anderson, T. V. Albu, *J. Electrochem. Soc.*, 2000, **147**, 4229.
27 A. B. Anderson, T. V. Albu, *Electrochem Commun.*, 1999, **1**, 203.
28 C. Hartnig, M. T. M. Koper, *J. Electroanal. Chem.*, 2002, **532**, 165.
29 T. Toda, H. Igarashi, H. Uchida, M. Watanabe, *J. Electrochem. Soc*, 1999, **146**, 3750.
30 M. J. Janik, C. D. Taylor, M. Neurock, *J Electrochem Soc*, 2009, **156**, B126.
31 K. Y. Yeh, M. J. Janik, *Journal of Computational Chemistry*, 2011, **32**, 3399.
32 S. A. Wasileski, M. J. Janik, *Phys. Chem. Chem. Phys*, 2008, **10**, 3613.
33 Y. Sha, T. H. Yu, B. V. Merinov, P. Shirvanian, W. A. Goddard, *J. Phys. Chem. Lett.*, 2011, **2**, 572.
34 J. K. Nørskov, J. Rossmeisl, A. Logadottir, L. Lindqvist, J. R. Kitchin, T. Bligaard, H. Jonsson, *J. Phys. Chem. B*, 2004, **108**, 17886.
35 V. Stamenkovic, B. S. Mun, K. J. J. Mayrhofer, P. N. Ross, N. M. Markovic, J. Rossmeisl, J. Greeley, J. K. Nørskov, *Angew. Chem. Int. Edit.*, 2006, **45**, 2897.
36 V. Tripkovic, E. Skulason, S. Siahrostami, J. K. Nørskov, *J.* Rossmeisl, *Electrochim Acta*., 2010, **55**, 7975.
37 V. Viswanathan, H. A. Hansen, J. Rossmeisl, J. K. Nørskov, *J. Phys. Chem. Lett.*, 2012, **3**, 2948.
38 H. A. Hansen, V. Viswanathan, J. K. Nørskov, *J. Phys. Chem. C*, 2014, **118**, 6706.
39 J. Rossmeisl, J. K. Nørskov, *Surf. Sci.*, 2008, **602**, 2337.
40 J. Greeley, J. K. Nørskov, *J. Phys. Chem. C*, 2009, **113**, 4932.
41 G. A. Tritsaris, J. Greeley, J. Rossmeisl, J. K. Nørskov, *Catal. Lett*, 2011, **141**, 909.
42 R. Jasinski, Nature, 1964, **201**, 1212.
43 J. P. Dodelet, 3-Oxygen Reduction in PEM Fuel Cell Conditions: Heat-Treated Non-Precious Metal-N4Macrocycles and Beyond. In N_4-Macrocyclic Metal Complexes; Eds.; Springer: New York, 2006, 83-147.
44 H. A. Colijn, *Electrochim. Acta*, 1988, **33**, 801.
45 D. A. Scherson, E. B. Yeager, *Electrochim. Acta* 1983, **28**, 1205.
46 D. Scherson, E. B. Yeager, *Electrochim. Acta* 1986, **31**, 1247.
47 K. Wiesener, *Electrochim. Acta* 1986, **31**, 1073.
48 M. Lefèvre, J. P. Dodelet, P. Bertrand, *J. Phys. Chem. B*, 2002, **106**, 8705.
49 U. I. Kramm, J. P. Dodelet, *Phys. Chem. Chem. Phys.*, 2012, **14**, 11673.
50 U. I. Kramm, J. P. Dodelet, *J. Phys. Chem. Lett.* 2014, **5**, 452.
51 U. I. Kramm, *J. Electrochem. Soc.*, 2011, **158**, B69-B78.
52 U. I. Koslowski, I. Abs-Wurmbach, S. Fiechter, P. Bogdanoff, *J. Phys. Chem. C*, 2008, **112**, 15356.
53 S. Kattel, G. Wang, *J. Mater. Chem. A*, 2013, **1**, 10790.
54 J. M. Ziegelbauer, T. S. Olson, *J. Phys. Chem. C*, 2008, **112**, 8839.
55 T. S. Olson, S. Pylypenko, P. Atanassov, K. Asazawa, K. Yamada, *J. Phys. Chem. C*, 2010, **114**, 5049.
56 T. S. Olson, S. Pylypenko, J. E. Fulghum, *J. Electrochem. Soc.*, 2010, **157**, B54.
57 E. Vayner, A. B. Anderson, *J. Phys. Chem. C*, 2007, **111**, 9330.
58 R. R. Chen, H. X. Li, D. Chu , G. F. Wang, *J. Phys. Chem. C*, 2009, **113**, 20689.
59 J. Herranz, J. P. Dodelet, *J. Phys. Chem. C*, 2007, **111**, 19033.
60 M. Jain, S. h. Chou, A. Siedle, *J. Phys. Chem. B*, 2006, 110, 4179.
61 S. Chatterjee, K. Sengupta, S. Samanta, P. K. Das, *Inorg. Chem.,* 2013, **52**, 9897.
62 L. Capece, M. A. Marti, A. Crespo, F. Doctorovich, *J. Am. Chem. Soc.*, 2006, **128**, 12455.
63 S. Maldonado, K. J. Stevenson, *J. Phys. Chem. B*, 2004, **108**, 11375.
64 P. H. Matter, U. S. Ozkan, *Catal. Lett.*, 2006, **109**, 115.
65 P. H. Matter, E. Wang, J. M. M. Millet, U. S. Ozkan, *J. Phys. Chem. C,* 2007, **111**, 1444.
66 D. Yu, Q. Zhang, L. Dai, *J. Am. Chem. Soc.*, 2010, **132**, 15127.
67 L. Qu, Y. Liu, J. B. Baek, L. Dai, *ACS Nano*, 2010, **4**, 1321.
68 S. Chen, J. Bi, Y. Zhao, L. Yang, C. Zhang, Y. Ma, Q. Wu, X. Wang , Z. Hu, *Advanced Materials*, 2012, **24**, 5593.
69 L. Zhang, Z. Xia, *J. Phys. Chem. C*, 2011, **115**, 11170.
70 H. Kim, K. Lee, S. I. Woo, Y. Jung, *Phys. Chem. Chem. Phys.*, 2011, **13**, 17505.
71 N. M. Markovic, P. N. Ross, *Surf. Sci. Rep.,* 2002, **45**, 121.
72 http://www.platinum.matthey.com
73 P. Strasser, S. Koh, T. Anniyev, J. Greeley, K. More, C. Yu, Z. Liu, S. Kaya, D. Nordlund, H. Ogasawara, *Nat. Chem.,* 2010, **2**, 454.
74 J. R. Kitchin, J. K. Norskov, M. A. Barteau, J. G. Chen, *J. Chem. Phys.,* 2004, **120**, 10240.
75 C. T. Campbell, *Annu. Rev. Phys. Chem.*, 1990, **41**, 775.
76 J. A. Rodriguez, *Surf. Sci. Rep.*, 1996, **24**, 225.
77 S. J. Tauster, S. C. Fung, R. T. K. Baker, J. A. Horsley, *Science*, 1981, **211**, 1121.
78 T. Schalow, B. Brandt, D. E. Starr, M. Laurin, S. K. Shaikhutdinov, S. Schauermann, J. Libuda, H. J. Freund, *Angew. Chem., Int. Ed.*, 2006, **45**, 3693.
79 A. Wieckowski, E. R. Savinova, C. G. Vayenas, Catalysis and Electrocatalysis at Nanoparticle Surface; Marcel Dekker: New York, 2003.
80 J. A. Horsley, *J. Am. Chem. Soc.*, 1979, **101**, 2870.
81 N. Tian, Z. Y. Zhou, S. G. Sun, Y. Ding, Z. L. Wang, *Science*, 2007, **316**, 732.
82 N. M. Markovic, R. R. Adzic, B. D. Cahan, E. B. Yeager, *J. Electroanal. Chem.*, 1994, **377**, 249.
83 M. D. Macia, J. M. Campina, E. Herrero, J. M. Feliu, *J. Electroanal. Chem.*, 2004, **564**, 141.
84 A. Kuzume, E. Herrero, J. M. Feliu, *J. Electroanal. Chem.*, 2007, **599**, 333.
85 B. D. Cahan, H. M. Villulas, *J. Electroanal. Chem.*, 1991, **307**, 263.
86 T. Abe, G. M. Swain, K. Sashikata, K. Itaya, *J. Electroanal. Chem.*, 1995, **382**, 73.
87 N. Hoshi, M. Nakamura, A. Hitotsuyanagi, *Electrochim. Acta*, 2013, **112**, 899.
88 A. Hitotsuyanagi, M. Nakamura, N. Hoshi, *Electrochim. Acta*, 2012, **82**, 512.
89 P. Zelenay, M. G. Aldeco, G. Horanyi, A. Wieckowski, *J. Electroanal. Chem.*, 1993, **357**, 307.
90 K. Varga, P. Zelenay, A. Wieckowski, *J. Electroanal. Chem.*, 1992, **330**, 453.

91 M. E. G. Aldeco, E. Herrero, P. Zelenay, A. Wieckowski, *J. Electroanal. Chem.*, 1993, **348**, 451.
92 R. Narayanan, M. A. El-Sayed, *J. Phys. Chem. B*, 2005, **109**, 12663.
93 C. Wang, S. Sun, *J. Am. Chem. Soc.*, 2007, **129**, 6974.
94 C. Wang, H. Daimon, T. Onodera, T. Koda, S. Sun, *Angew. Chem. Int. Ed.,* 2008, **47**, 3588.
95 Y. Xia, P. Yang, Y. Sun, Y. Wu, B. Mayers, B. Gates, Y. Yin, F. Kim, H. Yan, *Adv. Mater.*, 2003, **15**, 353.
96 J. Chen, B. Lim, E. P. Lee, Y. Xia, *Nano Today*, 2009, **4**, 81
97 T. Yu, Y. Xia, *Angew. Chem. Int. Ed.*, 2011, **50**, 2773.
98 V. R. Stamenkovic, B. Fowler, B. S. Mun, G. F. Wang, N. M. Markovic, *Science*, 2007, **315**, 493.
99 J. Greeley, I. E. L. Stephens, A. S. Bondarenko, T. P. Johansson, H. A. Hansen, T. F. Jaramillo, J. Rossmeisl, I. Chorkendorff, J. K. Nørskov, *Chem. Rev.*, 2009, **1**, 552.
100 J. B. Wu, A. Gross, H. Yang, *Nano Lett.*, 2011, **11**, 798.
101 J. Zhang, J. Y. Fang, *J. Am. Chem. Soc.*, 2009, **131**, 18543.
102 Y. Dai, S. Chen, *J. Phys. Chem. C*, 2011, **115**, 2162.
103 J. Kim, Y. Lee, S. H. Sun, *J. Am. Chem. Soc.*, 2010, 132, 4996.
104 D. Xu, Z. P. Liu, *Angew. Chem. Int. Edit.*, 2009, **48**, 4217.
105 J. Y. Chen, B. Wiley, Y. J. Xiong, Z. Y. Li, Y. N. Xia, Nano Lett., 2005, **5**, 2058.
106 Z. M. Peng, H. Yang, *J. Am. Chem. Soc.*, 2009, **131**, 7542.
107 L. Wang, Y. Nemoto, Y. Yamauchi, *J. Am. Chem. Soc.*, 2011,**133**, 9674 .
108 X. W. Teng, M. Feygenson, Q. Wang, J. Q. He, W. X. Du, A. I. Frenkel, W. Q. Han, M. Aronson, *Nano Lett.*, 2009, 9, 3177.
109 H. A. Esfahani, L. Wang, Y. Nemoto, Y. Yamauchi, *Chem. Mater.,* 2010, 22, 6310 .
110 J. Zhang. H. Z. Yang, J. Y. Fang, S. Z. Zou, *Nano Lett.*, 2010, **10**, 638.
111 J. B. Wu, J. L. Zhang, Z. M. Peng, F. T. Wagner, H. Yang, *J. Am. Chem. Soc.*, 2010, **132**, 4984.
112 Y. E. Wu, S. F. Cai, D. S. Wang, W. He, Y. D. Li, *J. Am. Chem. Soc.*, 2012, **134**, 8975.
113 K. A. Kuttiyiel, K. Sasaki, Y. M. Choi, D. Su, P. Liu, R. R. Adzic, Nano Lett., 2012, 12, 6266.
114 K. Sasaki, H. Naohara, Y. M. Choi, Y. Cai, W. F. Chen, P. Liu, R. R. Adzic, *Nat. Comm.,* 2012, **3**, 1115.
115 J. R. Kitchin, J. K. Nørskov, *Phys. Rev. Lett.*, 2004, **93**, 156801/1.
116 T. Bligaard, J. K. Nørskov, *Electrochim. Acta.*, 2007, **52**, 5512.
117 J. Wu, L. Qi, H. You, A. Gross, J. Li, H. Yang, *J. Am. Chem. Soc.*, 2012, **134**, 11880.
118 P. Strasser, S. Koh, T. Anniyev, J. Greeley, K. More, C. F. Yu, S. Kaya, D. Nordlund, H. Ogasawara, A. Nilsson, *Nat. Chem.*, 2010, **2**, 454.
119 V. Stamenkovic, T. J. Schmidt, *J. Phys. Chem. B* 2002, **106**, 11970.
120 M. T. Paffett, K. A. Daube, S. Gottesfeld, C. T. Campbell, *J. Electroanal. Chem.*, 1987, **220**, 269.
121 U. Bardi, B. C. Beard, P. N. Ross, *J. Vac. Sci. Technol. A,* 1988, **6**, 665.
122 M. T. Paffett, J. G. Beery, S. Gottesfeld, *J. Electrochem. Soc.*, 1988, **135**, 1431.
123 B. Hammer, J. K. Nørskov, *Surf. Sci.*, 1995, **343**, 211.
124 V. R. Stamenkovic, B. S. Mun, M. Arenz, K. J. J. Mayrhofer, C. A. Lucas, G. Wang, P. N. Ross, N. M. Markovic, *Nat. Mater.*, 2007, **6**, 241.
125 C. Wang, N. M. Markovic, V. R. Stamenkovic, *ACS Catal.*, 2011, **1**, 1355.
126 N. Poudyal, G. S. Chaubey, C. Rong, J. P. Liu, *J. Appl. Phys.*, 2009, **105**, 07A749.
127 S. J. Guo, S. Zhang, S. H. Sun, *Angew. Chem., Int. Ed.*, 2013, **52**, 8526.
128 Q. Liu, Z, Yan, N. L. Henderson, E. R. Schaak, *J. Am. Chem. Soc.,* 2009, **131**, 5720.
129 Y. Kang, J. B. Pyo, X. Ye, T. R. Gordon, B. C. Murray, *ACS Nano*, 2012, **6**, 5642.
130 C. Wang, M. N. Markovic, V. Stamenkovic, *J. Am. Chem. Soc.*, 2011, **133**, 14396.
131 C. Wang, M. N. Markovic, V. Stamenkovic, *Nano Lett.*, 2011, **11**, 919.
132 S. J. Guo, S. Zhang, D. Su, S. H. Sun, *J. Am. Chem. Soc.,* 2013, **135**, 13879.
133 J. Kim, S. H. Sun, *Chem. Mater.*, 2008, **20**, 7242.
134 J. Kim, S. H. Sun, *Adv. Mater.,* 2009, **21**, 906.
135 V. E. Shevchenko, V. D. Talapin,L. A. Rogach, A. Kornowski, M. Haase, H. Weller, *J. Am. Chem. Soc.*, 2002, **124**, 11480.
136 T. Pellegrino, A. Fiore, E. Carlino, L. Manna, *J. Am. Chem. Soc.*, 2006, **128**, 6690.
137 D. C. Lee, A. Ghezelbash, B. A. Korgel, J. *Phys. Chem. B*, 2006, **110**, 20906.
138 Y. J. Kang, C. B. Murray, *J. Am. Chem. Soc.*, 2010, **132**, 7568.
139 K. Ahrenstorf, H. Weller, *Small*, 2007, **3**, 271.
140 K. Ahrenstorf, H. Weller, *Adv. Funct. Mater.*, 2008, **18**, 3850.
141 H. Y. Zhu, S. H. Sun, *J. Am. Chem.Soc.*, 2013, **135**, 7130.
142 M. Chen, E. D. Nikles, *Nano Lett.*, 2002, **2**, 211.
143 H. Wang, *Chem. Mater.,* 2013, **25**, 2450.
144 Y. Yu, S. Sun, *Nano Lett.*, 2014, **14**, 2778.
145 L. Dubau, F. Maillard, E. Rossinot, *J. Electrochem. Soc.*, 2010, **157**, B1887.
146 L. Dubau, Maillard, E. Rossinot, *Electrochim. Acta.,* 2010, **56**, 776.
147 S. Chen, H. A. Gasteiger, *J. Electrochem. Soc.*, 2010, **157**, A82.
148 L. Dubau, Maillard, E. Rossinot, *Electrochim. Acta*., 2011, **56**, 10658.
149 L. Dubau, Maillard, E. Rossinot, *Appl. Catal. B,* 2013, **142**, 801.
150 M. Oezaslan, P. Strasser, *J. Am. Chem. Soc.*, 2012, **134**, 514.
151 D. Wang, Y. Yu, H. D. Abruna, *Nano Lett.*, 2012, **12**, 5230.
152 J. Snyder, J. Erlebacher, *J. Am. Chem. Soc.,* 2012, **134**, 8633.
153 S. Chen, *J. Phys. Chem. C* 2009, **113**, 1109.
154 Z Yu, F. T. Wagner, *J. Phys. Chem. C*, 2012, **116**, 19877.
155 I. Dutta, N. P. Irish, *J. Phys. Chem. C* 2010, **114**, 16309.
156 Z. Liu, F. T. Wagner, *J. Electrochem. Soc.* 2012, **159**, F554.
157 R. Y. Wang, Y. Ding, *Energy Environ. Sci.*, 2012, **5**, 5281.
158 J. I. Shui, J. C. M. Li, *Adv. Funct. Mater.*, 2011, **21**, 3357.
159 D. Wang, P. Zhao, Y. Li, *Sci. Rep.,* 2011, **1**, 37
160 L. Gan, P. Strasser, *Nano Lett.* 2013, 13, 1131.
161 T. Yu, Y. Xia, *Angew. Chem., Int. Ed.*, 2011, **50**, 2773.
162 Y. Kang, C. B. Murray, *J. Am. Chem. Soc.*, 2010, **132**, 7568.
163 B. Fowler, V. Stamenkovic, N. M. Markovic, *Electrochem. Acta*., 2008, **53**, 6076.
164 J. Wu, F. T. Wagner, *J. Am. Chem. Soc.,* 2010, **132**, 4984.
165 C. Cui, P. Strasser, *Nano Lett.*, 2012, **12**, 5885.
166 M. C. Quesada, J. M. Andanson, A. Yarulin, B. Lim, Y. Xia, *Langmuir* 2011, **27**, 790.
167 J. S. Gullon, V. Montiel, A. Aldaz, J. Clavilier, *J. Electroanal. Chem.*, 2000, **491**, 69.
168 I. Lee, R. Morales, M. A. Albiter, F. Zaera, *Proc. Natl. Acad. Sci. U.S.A.* 2008, **105**, 15241.
169 Y. H. Lee, G. Lee, H. Song, J. T. Park, *Chem. Mater.*, 2006, **18**, 4209.
170 V. Mazumder, S. Sun, *J. Am. Chem. Soc.,* 2009, **131**, 4588.
171 M. Shao, Y. Xia, *Nano Lett.* 2013, **13**, 3420.
172 M. K. Carpenter, *J. Am. Chem. Soc.*, 2012, **134**, 8535.
173 C. Zhang, Z. Peng, *J. Am. Chem. Soc.* 2014, **136**, 7805.
174 W. Chen, Q. Peng, Y. Li, *Angew. Chem., Int. Ed.*, 2010, **49**, 2917.
175 H. G. Tompkins, M. R. Pinnel, *J. Appl. Phys.*, 1977, **48**, 3144.
176 C. Chen, P. Yang, V. Stamenkovic, *Science*, **343**,1339.
177 Y. Yu, Q. Zhang, B. Liu, J. Y. Lee, *J. Am. Chem. Soc.,* 2010, **132**, 18258.
178 N. Tian, Z. Y. Zhou, N. F. Yu, L. Y. Wang, S. G. Sun, *J. Am. Chem. Soc.,* 2010, **132**, 7580 .
179 X. Huang, Z. Zhao, J. Fan, Y. Tan, N. Zheng, *J. Am. Chem. Soc.*, 2011, **133**, 4718
180 J. W. Hong, S. U. Lee, Y.W. Lee, S. W. Han, *J. Am. Chem. Soc.,* 2012, **134**, 4565 .
181 J. Xiao, S. Liu, N. Tian, Z. Y. Zhou, H. X. Liu, B. B. Xu, S. G. Sun, *J. Am. Chem. Soc.,* 2013, **135**, 18754.
182 J. Wu, H. Yang, *J. Am. Chem. Soc.*, 2012, **134**, 11880.
183 X. Xu, X. Zhang, S. G. Sun, *Angew. Chem. Int. Ed.*, 2014, **53**, 12522.
184 D. Zhao, B. Xu, *Angew. Chem., Int. Ed.,* 2006, 45, 4955.
185 D. Zhao, B. Xu, *Phys. Chem. Chem. Phys.* 2006, 8, 5106
186 G. Wang, L. Xiao, L. Zhuang, *J. Am. Chem. Soc.*, 2014, **136**, 9643.
187 Y. Wang, N. Toshima, *J. Phys. Chem. B* 1997, 101, 5301.
188 Y. Lim, S. J. Yoo, P. Kim, Nanoscale, 2014, **6**, 4038.
189 S. Zhou, *Angew. Chem., Int. Ed.,* 2005, **44**, 4539.

190 Y. Chen, S. Chen, *J. Phys. Chem. C* 2011, **115**, 24073.
191 K. Sasaki, H. Naohara, Y. Cai, Y. M. Choi, P. Liu, M. B. Vukmirovic, J. X. Wang, R. R. Adzic, *Angew. Chem. Int. Ed.*, 2010, **49**, 8602.
192 S. Tenney, W. He, J. Ratliff, D. Mullins, D. Chen, *Top. Catal.*, 2011, **54**, 42.
193 S. Tenney, W. He, J. Ratliff, D. Mullins, D. Chen, *J. Phys. Chem. C*, 2011, **115**, 11112.
194 S. Tenney, W. He, J. Ratliff, D. Mullins, D. Chen, *J. Phys. Chem. C,* 2010, **114**, 21652.
195 J. R. Croy, B. R. *Cuenya, Appl. Catal. A*, 2008, **350**, 207.
196 B. R. Cuenya, W. Keune, *Appl. Phys. Lett.*, 2009, **95**, 143103.
197 B. R. Cuenya, W. Keune, *Phys. Rev. B* 2009, **80**, 125412.
198 A. Naitabdi, B. R. A. Cuenya, *J. Phys. Chem. C*, 2009, **113**, 1433.
199 T. Toda, M. Watanabe, *J. Electrochem. Soc.*, 1998, **145**, 4185.
200 I. E. L. Stephens, A. S. Bondarenko, L. Bech, I. Chorkendorff, *Chem. Catal. Chem.,* 2012, **4**, 341.
201 V. Stamenkovic, N. M. Markovic, *J. Am. Chem. Soc.,* 2006, **128**, 8813.
202 C. Wang, V. Stamenkovic, *J. Am. Chem. Soc.*, 2011, 133, 14396.
203 J. Durst, F. Maillard, *J. Phys. Chem. Lett*., 2014, **5**, 434.
204 K. J. Andersson, J. Rossmeisl, I. Chorkendorff, *J. Am. Chem. Soc.*, 2009, 131, 2404.
205 F. Tao, G. A. Somorjai, *Science*, 2008, **322**, 932.
206 B. Hammer, J. K. Nørskov, *Adv. Catal.,* 2000, **45**, 71.
207 K. J. J. Mayrhofer, M. Arenz, *Angew. Chem., Int. Ed.*, 2009, **48**, 3529.
208 K. Lee, J. H. Jang, *J. Phys. Chem. C,* 2013, **117**, 9164.
209 S. Xie, Y. Xia, *Nano Lett.* 2014, **14**, 3570.
210 C. Yu, P. Strasser, *Faraday Discuss.*, 2009, **140**, 283.
211 V. S. Bagotsky, *Fuel Cells: Problems and Solutions*, Wiley: New York, 2009.
212 Y. Chung, C. Pak, Y. Lee, D. Seung, *J. Phys. Chem. C* 2008, **112**, 313.
213 G. S. Park, C. Pak, Y. Lee, D. Seung, *J. Power Sources*, 2008, **176**, 48.
214 Y. Shao-Horn, D. Morgan, *Top. Catal.*, 2007, **46**, 285.
215 E. Antolini, E. R. Gonzalez, *Solid State Ionics*, 2009, **180**, 746.
216 C. V. Subban, F. T. Wagner, F. J. DiSalvo, *J. Am. Chem. Soc.*, 2010, 132, 17531.
217 S. Y. Huang, P. Ganesan, S. Park, B. N. Popov, *J. Am. Chem. Soc.,* 2009, **131**, 13898.
218 S. E. Jang, H. Kim, *J. Am. Chem. Soc.*, 2010, **132**, 14700.
219 S. Sun, J. P. Dodelet, *Adv. Mater.,* 2008, **20**, 571.
220 C. Koenigsmann, R .R. Adzic, S. S. Wong, *Nano Lett.*, 2010, **10**, 2806.
221 Z. Chen, Y. Yan, *Angew. Chem., Int. Ed.*, 2007, **46**, 4060.
222 S. M. Alia, G. Zhang, Y. S. Yan, *Adv. Funct. Mater,*. 2010, **20**, 3742.
223 Y. J. Song, J. A. Shelnuttt, *Chem. Mater.* 2006, **18**, 2335.
224 Y. Song, J. A. Shelnutt, *Nano Lett.*, 2009, **9**, 1534.
225 H. W. Liang, S. H. Yu, *Adv. Mater.* 2011, **23**, 1467.
226 B. Lim, Y. Xia, *Science*, 2009, **324**, 1302.
227 Z. H. Lin, M. H. Lin, H. T. Chang, *Chem. Eur. J.* 2009, **15**, 4656.
228 S. M. Alia, B. S. Pivovar, *ACS Catal.* 2014, **4**, 1114.
229 B. Xia, X. Wang, X. Lou, *Angew. Chem. Int. Ed.*, 2012, **51**, 7213.
230 J. Zhang, K. Sasaki, E. Sutter, R. R. Adzic, *Science*, 2007, 315
231 A. C. Ferrandez, P. Buvat, C. Coutanceau, *Chem. Mater.*, 2013, **25**, 3797.
232 K. Miyabayashi, M. Miyake, Langmuir, 2014, **30**, 2936.
233 J. Snyder, K. Livi , J. Erlebacher, *Adv. Funct. Mater.*, 2013, **23**, 5494.
234 Z. Z. Jiang, Z. Wang, *Chem. Commun.*, 2010, **46**, 6998.
235 S. Takenaka, H. Miyamoto, *J. Phys. Chem. C*, 2014, **118**, 774.
236 S. Takenaka, H. Miyamoto, *J. Phys. Chem. C*, 2007, *111*, 15133.
237 S. Chen, Z. Wei, L. Wan, *J. Am. Chem. Soc.*, 2012, **134**, 13252.
238 L. Li, Y. Xue, M. R. Xia, S. G. Chen, Z. D. Wei, SCIENTIA SINICA Chimica, 2013, 43, 1566.
239 Y. Nie, S. Chen, Z. Wei, *Chem. Commun.*, 2014, **50**, 15431.
240 Y. J. Tong, *Chem. Soc. Rev.*, 2012, 41, 8195.
241 M. E. Escribano, A. Cuesta, *Chem. Phys. Chem*., 2011, **12**, 2230.
242 D. Strmcnik, M. E. Escribano, K. Kodama, V. R. Stamenkovic, A. Cuesta, N. M. Markovic, Nat. Chem., 2010, **2**, 880.
243 B. Genorio, R. Subbaraman, D. Strmcnik, D. Tripkovic, V. R. Stamenkovic, N. M. Markovic, *Angew. Chem. Int. Ed.,* 2011, **50**, 5468.
244 Z. B. Wang, G. P. Yin, *J. Phys. Chem. C* 2010, **114**, 672.
245 B. Fang, N. K. Chaudhari, J. S. Yu, *J. Am. Chem. Soc.*, 2009, **131**, 15330.
246 C. Hartnig, T. J. Schmidt, *J. Power Sources*, 2011, **196**, 5564;
247 K. Kinoshita, J. T. Lundquist, P. Stonehart, *J. Electroanal. Chem. interfacial electrochem.*, 1973, **48**, 157;
248 J. C. Meier, C. Galeano, I. Katsounaros, A. A. Topalov, A. Kostka, F. Schüth, K. J. J. Mayrhofer, *ACS Catal.*, 2012, **2**, 832.
249 T. J. Schmidt, J. Baurmeister, *J. Power Sources*, 2008, **176**, 428;
250 H. Tang, Z. Qi, M. Ramani, J. F. Elter, *J. Power Sources*, 2006, **158**, 1306.
251 S. Donthu, M. Cai, M. Ruthkosky, I. Halalay, *Chem. Commun.*, 2009, **4**, 4203;
252 Y. Liu, W. E. Mustain, *ACS Catal.*, 2011, 1, 212.
253 M. F. Mathias, P. T. Yu, *Electrochem. Soc. Interface*, 2005, **14**, 24.
254 Yu, X.; Ye, S. J. Power Sources 2007, 172, 145.
255 F. Coloma, *Catal.*, 1995, **154**, 299.
256 N. T. Cuong, *Phys. Status Solidi,* 2006, **13**, 3472.
257 D. Banham, V. Briss, *J. Mater. Chem.*, 2012, **22**, 7164.
258 B. Fang, J.-S. Yu, *Chem. Mater.*, 2009, **21**, 789.
259 K. P. Johnston*, J. Phys. Chem. C,* 2010, **114**, 10796.
260 K. J. J. Mayrhofer, F. Schüth*, J. Am. Chem. Soc.*, 2012, 134, 20457.
261 S. Chen, Z. Wei, P. Shen, *Chem. Commun.*, 2011, **47**, 10984.
262 L. Li, S. G. Chen, Z. D. Wei, X. Q. Qi, M. R. Xia, Y. Q. Wang, *Phys. Chem. Chem. Phys.*,2012, 14,16581.
263 T. Kim, Y. Kim, *Chem. Commun.*, 2014, **50**, 596.
264 S. Park, D. Kim, T. Kim, Y. Kim, ACS Catal. 2013, **3**, 3067.
265 L. Cuo, Z. Wei, *J. Power Sources,* 2013, **247**, 360.
266 Y. Y. Shao, J. Liu, Y. Wang , Y. H. Lin, *J. Mater. Chem*., 2009, **19**, 46.
267 S. Sharma, B. G. Pollet, *J. Power Sources,* 2012, **208**, 96.
268 Y. Liu, S. Shrestha, W. E. Mustain, *ACS Catal*., 2012, **2**, 456.
269 X. Cui, J. Shi, H. Chen, L. Zhang, *J. Phys. Chem. B* 2008, **112**, 12024.
270 J. Rajeswari, B. Viswanathan, T. K. Varadarajan, *Mater. Chem. Phys.* 2007, **106**, 168.
271 S. Huang, P. Ganesan, B. N. Popov, ACS Catal., 2012, 2, 825.
272 C. H. Yao, F. Li, X. Li, *J. Mater. Chem.*, 2012, **22**, 16560.
273 K. Senevirathne, R. Hui, S. Campbell , *Electrochim. Acta.*, 2012, **59**, 538.
274 H. Liu, F. Wang, Y. Zhao, H. Fong, Nanoscale, 2013, **5**, 3643.
275 Y. Liu, W. E. Mustain, *J. Am. Chem. Soc.*, 2013, **135**, 530.
276 H. Chhina, S. Campbell, *J. Power Sources,* 2006, **161**, 893.
277 C. P. Lo, V. Ramani, *ACS Appl. Mater. Interfaces,* 2012, **4**, 6109.
278 E. Toyoda, R. Jinnouchi, *Angew. Chem. Int. Ed.,* 2013, **52**, 4137.
279 J. A. Horsley, *J. Am. Chem. Soc.* 1979, **101**, 2870.
280 V. Thanh Ho, B. Hwang, *J. Am. Chem. Soc.*, 2011, **133**, 11716.
281 X. Xie, S. Chen, Z. Wei, *Chem. Commun.*, 2013, **49**, 10112.
282 X. Xie, Y. Xue, L. Li, Z. Wei, *Nanoscale*, 2014, **6**,11035.
283 K. Jukk, N. Alexeyeva, P. Ritslaid, J. Kozlova, V. Sammelselg, K. Tammeveski, *Electrocatalysis*, 2013, **4**,42.
284 J. Qiao, R. Lin, B. Li, J. Ma, J. Liu, *Electrochim. Acta,* 2010, **55**, 8490.
285 V. I. Zaikovskii, K. S. Nagabhushana, V. V. Kriventsov, K. N. Loponov, S. V. Cherepanova, R. I. Kvon, D. I. Kochubey, E. R. Savinova, *J. Phys.Chem. B*, 2006, **110**, 6881.
286 R. Zhou, S. Qiao, *Chem. Mater.*, 2014, **26**, 5868.
287 M. H. Shao, R. R. Adzic, *Langmuir* 2006, **22**, 10409.
288 Y. G. Suo, L. Zhuang, *Angew. Chem., Int. Ed.*, 2007, **46**, 2862.
289 L. Xiao, L. Zhuang, *J. Am. Chem. Soc.*, 2009, **131**, 602.
290 M. Shao, *J. Power Sources,* 2011, **196**, 2433.
291 M. Shao, K. Sasaki, R. R. Adzic, *J. Am. Chem. Soc.*, 2006, **128**, 3526.
292 Y. C. Wei, C. W.Liu, K. W. Wang, *Chem. Commun.*, 2011, **47**, 11927.
293 W. Tang, G. Henkelman, *J. Chem. Phys.* 2009, **130**, 194504.
294 S. Guo, X. Zhang, G. Lu, S. Sun, *J. Am. Chem. Soc.*, 2014, **136**, 15026.
295 C. Koenigsmann, E. Sutter, T. A. Chiesa, R. R. Adzic, S. S. Wong, Nano Lett., 2012, **12**, 2013.

296 S. Kondo, M. Nakamura, N. Maki, N. Hoshi, *J. Phys. Chem. C*, 2009, **113**, 12625.
297 L. Xiao, L. Zhuang, Y. Liu, J. Lu, H. D. Abruna, *J. Am. Chem. Soc.*, 2008, **131**, 602.
298 M. Shao, X. Xia, *Chem. Commun.*, 2011, **47**, 6566.
299 Y. Lu, Wei Chen, *J. Am. Chem. Soc.*, 2014, 136, 11687.
300 W. Ding, M. Xia, Z. Wei, L. Wan, *Chem. Commun.*, 2014, **50**, 6660.
301 F. T. Wagner, *J. Phys. Chem. Lett.* 2010, 1, 2204.
302 C. W. B. Bezerra, L. Zhang, K. Lee, H. Liu, A. L. B. Marques, E. P. Marques, H. Wang, J. Zhang, Electrochim. Acta, 2008, **53**, 4937.
303 R. Jasinski, Nature, 1964, **201**, 1212.
304 E. Yeager, *Electrochim. Acta.,* 1984, **29**, 1527.
305 H. Liu, C. Song, Y. Tang, J. Zhang, *Electrochim. Acta.*, 2007, **52**, 4532.
306 D. H. Lee, W. J. Lee, W. J. Lee, S. O. Kim, Y. H. Kim, *Phys. Rev. Lett.*, 2011, 106.
307 M. Lefèvre, E. Proietti, F. Jaouen, J. P. Dodelet, *Science*, 2009, **324**, 71.
308 D. Deng, L. Yu, X. Chen, G. Wang, L. Jin, X. Pan, J. Deng, G. Sun, X. Bao, *Angew. Chem., Int. Ed.*, 2013, 52, 371.
309 Q. Shi, F. Peng, S. Liao, H. Wang, H. Yu, Z. Liu, B. Zhang, D. Su, *J. Mater. Chem. A*, 2013, 1, 14853.
310 E. Proietti, F. Jaouen, M. Lefèvre, N. Larouche, J. Tian, J. Herranz J. P. Dodelet, *Nat. Commun.*, 2011, **2**, 416.
311 H. Xiao, Z. G. Shao, G. Zhang, Y. Gao, W. Lu, B. Yi, *Carbon*, 2013, **57**, 443.
312 S. A.Wohlgemuth, T. P. Fellinger, M. Antonietti, *J. Mater. Chem. A*, 2013, **1**, 4002.
313 P. Su, H. Xiao, J. Zhao, Y. Yao, Z. Shao, C. Li, Q. Yang, *Chem. Sci.*, 2013, **4**, 2941.
314 G. Wu, K. L. More, C. M. Johnston, P. Zelenay, *Science*, 2011, **332**, 443.
315 P. Zhang, F. Sun, Z. Xiang, Z. Shen, J. Yun, D. Cao, *Energy Environ. Sci.*, 2014, **7**, 442.
316 Z. S. Wu, L. Chen, J. Liu, K. Parvez, H. Liang, J. Shu, H. Sachdev, R. Graf, X. Feng, K. Müllen, *Adv. Mater.*, 2013, **26**, 1450.
317 J. S. Lee, G. S. Park, S. T. Kim, M. Liu, J. Cho, *Angew. Chem. Int. Ed.*, 2013, **52**, 1026.
318 G. Wu, C. M. Johnston, N. H. Mack, K. Artyushkova, M. Ferrandon, M. Nelson, J. S. Lezama-Pacheco, S. D. Conradson, K. L. More, D. J. Myers, P. Zelenay, *J. Mater. Chem.*, 2011, **21**, 11392.
319 K. Ai, Y. Liu, C. Ruan, L. Lu , G. Lu, *Adv. Mater.*, 2013, **25**, 998.
320 G.Wu, Z. W. Chen, K. Artyushkova, F. H. Garzon, P. Zelenay in Proton Exchange Membrane Fuel Cells 8, Parts 1 and 2, Vol. 16 (Eds. : T. Fuller, K. Shinohara, V. Ramani, P. Shirvanian, H. Uchida, S. Cleghorn, M. Inaba, S. Mitsushima, P. Strasser, H. Nakagawa, H. A. Gasteiger, T. Zawodzinski, C. Lamy), Electrochemical Society Inc, Pennington, 2008, pp. 159.
321 K. Wiesener, *Electrochim. Acta*., 1986, **31**, 1073.
322 R. Franke, D. Ohms, K.Wiesener, J. *Electroanal. Chem.*, 1989, **260**, 63.
323 G. Liu, X. Li, P. Ganesan ,B. N. Popov, *Appl. Catal. B*, 2009, 93, 156.
324 E. J. Biddinger, U. S. Ozkan, *J. Phys. Chem. C*, 2010, *114*, 15306.
325 J. A. R. van Veen, H. A. Colijn, J. F. van Baar, *Electrochim. Acta*, 1988, **33**, 801.
326 A. L. B. Wijnoltz, W. Visscher, J. A. R. van Veen, E. Boellaard, A. M. Van der Kraan, S. C. Tang, *J. Phys. Chem. B*, 2002, **106**, 12993.
327 M. Bron, J. Radnik, M. Fieber-Erdmann, S. Fiechter, *J. Electroanal. Chem.*, 2002, **535**, 113.
328 H. Schulenburg, S. Stankov, V. Schunemann, J. Radnik, I. Dorbandt, S. Fiechter, H. Tributsch, *J. Phys. Chem. B*, 2003, 1**07**, 9034.
329 M. Ferrandon, *J. Phys. Chem. C* 2012, **116**, 16001.
330 G. Wu, P. Zelenay, *ACS Nano*, 2012, **6**, 9764.
331 Y. Hu, C. Liu, W. Xing, *J. Power Sources* 2013, **225**, 129.
332 Q. Li, J. Cho, G. Wu, *Adv. Energy Mater.,* 2014, **4**, 1301415.
333 D. Ohms, S. Herzog, R. Franke, V. Neumann, K. Wiesener, S. Gamburcev, A. Kaisheva, I. Iliev, *J. Power Sources* 1992, **38**, 327.
334 V. Nallathambi, J. W. Lee, S. P. Kumaraguru, G. Wu, *J. Power Sources,* 2008, **183**, 34 .
335 X. Chen, S. Sun, D. Xia, *J. Phys. Chem. C,* 2012, **116**, 22737.
336 H. W. Liang, X. Feng, K. Müllen, *J. Am. Chem. Soc.* 2013, **135**, 16002.
337 G. Faubert, R. Cote, J. P. Dodelet, M. Lefèvre, P. Bertrand, *Electrochim. Acta*., 1999, **44**, 2589.
338 F. Zhang, X. Pan, Y. Hu, L. Yu, X. Chen, P. Jiang, H. Zhang, S. Deng, J. Zhang, T. B. Bolin, S. Zhang, Y. Huang, X. Bao, *Proc. Natl. Acad. Sci. USA* 2013, **110**, 14861.
339 W. Chen, Z. Fan, X. Pan, X. Bao, *J. Am. Chem. Soc.* 2008, **130**, 9414.
340 Y. Hu, W. Xing, Q. Li, *Angew. Chem. Int. Ed.* 2014, **53**, 3675.
341 G. Wu, N. Li, D. R. Zhou, *J. Solid State Chem.*2004, 177, 3682.
342 Y. Liang, H. Dai, *Nature Materials*, 2011, **10**, 780.
343 Y. Liang, H. Dai, *J. Am. Chem. Soc.*, 2012, *134*, 3517.
344 F. Cheng, T. Zhang, Y. Zhang, J. Du, X. Han, J. Chen, *Angew. Chem. Int. Ed.*, 2013, **52**, 2474.
345 J. Lee, G. Park, H. Lee, S. Kim, R. Cao, M. Liu, J. Cho, *Nano Lett.*, 2011, **11,** 5362.
346 L. Mao, D. Zhang, T. Sotomura, K. Nakatsu, N. Koshiba, T. Ohsaka, *Electrochim. Acta*, 2003, **48**, 1015.
347 F. Cheng, Y. Su, J. Liang, Z. Tao, *J. Chen, Chem. Mater.*, 2010, **22**, 898.
348 F. Lima, M. Calegaro, E. Ticianelli, *J. Electroanal. Chem.*, 2006, **590**, 152.
349 Y. Tan, C. Xu, G. Chen, X. Fang, N. Zheng, Q. Xie, *Adv. Funct. Mater.*, 2012, **22**, 4584.
350 E. J. M. Yeager, *Catal.*, 1986, **38**, 5.
351 T. J. Ohsaka, *Electrochem. Soc.,* 2006, **153**, A1365.
352 Y. Gorlin, T. Jaramillo, *J. Am. Chem. Soc.*, 2010, **132**, 13612.
353 Y. Zhang, Y. Hu, S. Li, J. Sun, B. Hou, *J. Power Sources* 2011, **196**, 9284.
354 J. Lee, G. Park, H. Lee, S. Kim, R. Cao, M. Liu, J. Cho, *Nano Lett*., 2011, **11**, 5362.
355 Z. Yang, X. Zhou, H. Nie, Z. Yao, S. Huang, *ACS Appl. Mater. Interfaces*, 2011, **3**, 2601.
356 Y. Gorlin, C. Chung, D. Nordlund, B. Clemens, T. Jaramillo, *ACS Catal.*, 2012, **2**, 2687.
357 Y. Liang, H. Dai, *J. Am. Chem. Soc.*, 2012, **134**, 15849.
358 M. Hamdani, R. N. Singh, P. Chartier, *Int. J. Electrochem. Sci*., 2010, **5**, 556.
359 B. Marsan, *Electrochim. Acta,* 2008, **53**, 7012.
360 H. Zhu, S. Sun, *Nano Lett.*, 2013, **13**, 2947.
361 G. Wu, P. Zelenay, *Chem. Commun.*, 2010, **46**, 7489.
362 K. Sasaki, R. R. Adzic, *Phys. Chem. Chem. Phys.*, 2008, **10**, 159.
363 H. Imai, *Appl. Phys. Lett.,* 2010, **96**, 191905.
364 D. B. Meadowcroft, *Nature* 1970, **226**, 847.
365 R. F. Savinell, *Nat. Chem.*, 2011, **3**, 501.
366 J. Suntivich, H. A. Gasteige, N. Yabuuchi, H. Nakanishi, J. B. Goodenough, Y. Shao-Horn, *Nat. Chem.*, 2011, **3**, 546.
367 E. Bucher, A. Egger, P. Ried, W. Sitte, P. Holtappels, *Solid State Ionics*, 2008, **179**, 1032.
368 J.-I. Jung, D. D. Edwards, *J. Eur. Ceram. Soc.,* 2012, **32**, 3733.
369 M. Cheriti, A. Kahoul, *Mater. Res. Bull.*, 2012, **47,** 135.
370 X. X. Li, W. Qu, J. J. Zhang, H. J. Wang, *J. Electrochem. Soc.*, 2011, **158**, A597.
371 S. Malkhandi, P. Trinh, A. K. Manohar, K. C. Jayachandrababu, A. Kindler, G. K. Surya Prakash, S. R. Narayanan, *J. Electrochem. Soc.,* 2013,**160**, F943.
372 T. Poux, F. S. Napolskiy, T. Dintzer, G. Kerangueven, S. Y. Istomin, G. A. Tsirlina, E. V. Antipov, E. R. Savinova, *Catal. Today*, 2012, **189**, 83.
373 E. Fabbri, *ChemElectroChem*, 2014, **1**, 338.
374 M. Risch, Y. S. Horn, *J. Am. Chem. Soc.,* 2014, **136,** 5229.
375 H. Wang, H. Dai, *Angew. Chem. Int. Ed.,* 2011, **50**, 10969.
376 G. Wu, Piotr Zelenay, *ECS Transactions*, 2011, **41**, 1709.
377 R. A. Sidik, A. B. Anderson, *J. Phys. Chem. B* 2006, **110**, 936.
378 Y. Feng, N. A. Vante, *Chem. Mater.,* 2008, **20**, 26.
379 Yu. Zhou, S. Yu, *Chem. Eur. J.*, 2010, **16**, 12000.
380 Y. J. Feng, N. A. Vante, *Fuel Cells,* 2010, **10**, 77.
381 D. J. Ham, J. S. Lee, *Energies*, 2009, **2**, 873.
382 H. X. Zhong, H. M. Zhang, G. Liu, Y. M. Liang, J.W. Hu, B. L. Yi, *Electrochem. Commun.* 2006, **8**, 707.
383 D. G. Xia, S. Z. Liu, Z. Y. Wang, G. Chen, L. J. Zhang, L. Zhang, S. Q. Hui, J. J. Zhang, *J. Power Sources*, 2008, **177**, 296.

384 S. Doi, A. Ishihara, S. Mitsushima, N. Kamiya, K. I. Ota, *J. Electrochem. Soc.* 2007, **154**, B362.
385 A. Ishihara, K. Lee, S. Doi, S. Mitsushima, N. Kamiya, M. Hara, K. Domen, K. Fukuda, K. Ota, *Electrochem. Solid-State Lett.*, 2005, **8**, A201.
386 T. Ando, S. Izhar, H. Tominaga, M. Nagai, *Electrochim. Acta* 2010, **55**, 2614.
387 B. Cao, P. G. Khalifah, *Angew. Chem. Int. Ed.,* 2013, **52**, 10753.
388 Y. Wang, J. Zhang, *Chem.Soc.Rev.*, 2013, **42**, 5768.
389 D. S. Yu, E. Nagelli, F. Du, L. M. Dai, *J. Phys. Chem. Lett.*, 2010, **1**, 2165.
390 L. Yang, Y. Ma, Z. Hu, *Angew. Chem.*, 2011, **123**, 7270.
391 K. P. Gong, L. M. Dai, *Science* 2009, **323**, 760.
392 L. T. Qu, L. M. Dai, *ACS Nano,* 2010, **4**, 1321.
393 S. S. Yu, L. M. Dai, *J. Am. Chem. Soc.*, 2010, **132**, 15127.
394 Z. H. Sheng, X. H. Xia, *ACS Nano* 2011, **5**, 4350.
395 R. L. Liu, K. Müllen, *Angew. Chem., Int. Ed.*, 2010, **49**, 2565.
396 C. Xiong, Z. Wei, *Journal of Power Sources,* 2012, 215, 216.
397 Z. Yang, S. Huang, *Acs,Nano*, 2012, **6**, 205.
398 D. Yang, J. Yu, *J. Am. Chem. Soc.*, 2012, **134**, 16127.
399 Z. Liu, F. Peng, *Angew. Chem. Int. Ed.*, 2011, **50**, 3257.
400 X. Sun, W. Xu, W. Xing, *ACS Catal.*, 2013, **3**, 1726.
401 C. H. Choi, S. Woo, *J. Mater. Chem.*, 2012, **22**, 12107.
402 J. Liang, S. Z. Qiao, *Angew. Chem. Int. Ed.*, 2012, **51**, 11496;
403 Y. Zheng, S. Z. Qiao, *Angew. Chem. Int. Ed.*, 2013, **52**, 3110.
404 S. Wang, L. Dai, *Angew. Chem. Int. Ed.*, 2012, **51**, 4209.
405 Z. Jin, J. Yao, C. Kitrell , J. M. Tour, *ACS Nano*, 2011, **5**, 4112.
406 T. Shari, G. Hu, X. Jia, T. Wagberg, *ACS Nano*, 2012, **6**, 8904.
407 K. R. Lee, K. U. Lee, J. W. Lee, B. T. Ahn, S. I. Woo, *Electrochem. Commun.*, 2010, **12**, 1052.
408 N. P. Subramanian, X. Li, V. Nallathambi, S. P. Kumaraguru, H. C. Mercado, G. Wu, J. W. Lee, B. N. Popov, *J. Power Sources*, 2009, **188**, 38.
409 Z. Luo, S. Lim, Z. Tian, J. Shang, L. Lai, B. MacDonald, C. Fu, Z. Shen, T. Yu, J. Lin, *J. Mater. Chem.*, 2011, **21**, 8038.
410 H. Niwa, K. Horiba, Y. Harada, M. Oshima, T. Ikeda, K. Terakura, J. Ozaki, S. Miyata, *J. Power Sources*, 2009, **187**, 93
411 H. Kim, K. Lee, S. I. Woo, Y. Jung, *Phys. Chem. Chem. Phys.*, 2011, **13**, 17505.
412 C. H. Choi, S. H. Park and S. I. Woo, *ACS Nano*, 2012, **6**, 7084.
413 D. Wei, G. Yu, *Nano Lett.*, 2009, **9**, 1752.
414 A. L. M. Reddy, P. M. Ajayan, *ACS Nano* 2010, **4**, 6337.
415 Z. Jin, J. M. Tour, *ACS Nano,* 2011, **5**, 4112.
416 X. Wang, H. Dai, *Science* 2009, **324**, 768.
417 F. Gao, J. J. Spivey, *J. Am. Chem. Soc.*, 2012, **135**, 3315.
418 Y. Zheng, S. Z. Qiao, *J. Am. Chem. Soc.,* 2011, **133**, 20116.
419 J. S. Lee, J. Cho, *Angew. Chem. Int. Ed.*, 2013, **52**, 1026.
420 Y. Zhao, K. Hashimoto, *J. Am. Chem. Soc.*, 2012, **134**, 19528.
421 M. Zhong, T. Kowalewski, *J. Am. Chem. Soc.*, 2012, **134**, 14846.
422 G. Goenaga, S. Ma, S. Yuan, D. J. Liu, *ECS Trans.*, 2010, **33**, 579.
423 D. Zhao, J. L. Shui, C. Chen, X. Chen, B. M. Reprogle, D. Wang, D. J. Liu, *Chem. Sci.*, 2012, **3**, 3200.
424 S. Ma, G. A. Goenaga, A. V. Call, D. J. Liu, *Chem.Eur. J.*, 2011, **17**, 2063.
425 Q. Yang, P. Su, H. Xiao, J. Zhao, Y. Yao, Z. G. Shao, C. Li, *Chem. Sci.*, 2013, **4**, 2941.
426 P, Zhang, D, Cao, *Energy Environ Sci.*, 2014, **7,** 442
427 X. B. Wang, Y. Q. Liu, D. B. Zhu, L. Zhang, H. Z. Ma, N. Yao, B. L. Zhang, *J. Phys. Chem. B,* 2002, **106**, 2186
428 G. Gastone, B. Valerio, B. Fabrizio, F. Valeria, J. *Am. Chem. Soc.* 1986, **108**, 2420 .
429 W. Ding, Z. Wei, *Angew. Chem. Int. Ed.*, 2013, **52**, 1.
430 G. Xia, G. Wu, *ACS Appl. Mater. Interfaces,* 2013, **5**, 8607.
431 W. Jiang, J. Hu, Z. Wei, L. Wan, *J. Mater. Chem. A,* 2014, **2**, 10154.
432 Y. Zheng, S. Qiao, *Small,* 2012, **8**, 3550.
433 G. Tian, F. Wei, *Small*, 2014, **10**, 2251.
434 C. Choi, S. Woo, *Applied Catalysis B:Environmental*, 2014, **44**, 760.
435 J. Masa, A. Zhao, W. Xia, Z. Sun, B. Mei, M. Muhler, W. Schumann, *Electrochem. Commun.*, 2013, **15**, 113.
436 W. S. Hummers, R. E. Offeman, *J. Am. Chem. Soc.,* 1958, **80**, 1339.
437 S. Liu, C. R. Loper, *Carbon*, 1991, **29**, 1119.
438 H. K. Mayer, Elemental Analysis of Graphite, Proceedings 24th Biennial Conference of theAmerican Carbon Society, 1999.
439 Y. Koshino, A. Narukawa, *Analyst*, 1993, **118**, 827.
440 K. Zaghib, X. Song, A. Guerfi, R. Rioux, K. Kinoshita, *J. Power Sources*, 2003, **119**,8.
441 D.W. McKee, *Carbon*, 1974, **12**, 453.
442 E. A. Heintz, W. E. Parker, *Carbon*, 1966, **4**, 473.
443 http://graphites-carbons.superiorgraphite.com.
444 http://www.cocangraphite.com.
445 http://www.famousminerals.com.
446 X. Dai, G. G.Wildgoose, R. G. Compton, *Analyst* 2006, **131**, 901.
447 C. B. McAuley, G. G. Wildgoose, R. G. Compton, L. D. Shao, M. L. H. Green, *Sens. Actuators B* 2008, **132**, 356.
448 K. Jurkschat, X. Ji, A. Crossley, R. G. Compton, C. E. Banks, *Analyst*, 2007, **132**, 21.
449 X. Dai, G. G. Wildgoose, C. Salter, A. Crossley, R. G. Compton, *Anal. Chem.*, 2006, **78**, 6102.
450 C. H. A. Wong, C. K. Chua, B. Khezri, R. D. Webster, M. Pumera, *Angew. Chem.*, 2013, **125**, 8847.
451 L. Wang, M. Pumera, *Angew. Chem.* 2013, **125**, 1.

